La laser : un outil de contrôle et de mesure en photochimie

Par
François Légaré

thèse présentée au département de chimie en vue
de l'obtention du grade de docteur ès sciences (Ph.D.)

FACULTE DES SCIENCES
UNIVERSITE DE SHERBROOKE

Sherbrooke, Québec, Canada, juillet 2004

SOMMAIRE

Durant ma thèse, j'ai travaillé sur trois projets de recherches distincts. Ils ont en commun l'utilisation d'impulsions lasers. Deux de ces projets ont le même objectif malgré une approche très différente : suivre temporellement la structure des molécules lors de processus photochimiques femtosecondes (et attosecondes). Enfin, le troisième projet propose deux nouveaux schémas de contrôle laser lors d'inversion de population vers un état d'énergie doublement dégénéré.

Tout d'abord, nous avons étudié expérimentalement le processus de collision électron-molécule induit par une impulsion laser intense. Le paquet d'onde électronique éjecté par l'ionisation oscille sous l'action de la composante électrique du champ laser et revient à l'ion parent sous la forme d'un train d'impulsions attosecondes. Pour pouvoir caractériser temporellement ce train d'impulsions électroniques, il nous faut une horloge ayant une précision sub-femtoseconde (fs). « L'horloge moléculaire » peut offrir une telle résolution temporelle : cette méthode consiste à utiliser les vibrations de l'ion moléculaire généré lors de l'ionisation pour déterminer le temps écoulé entre l'émission d'un électron dans le continuum et le retour de cet électron à l'ion parent. Ce concept a été démontré expérimentalement avec la molécule d'hydrogène. Ceci nous a permis de confirmer la structure temporelle du train d'impulsions électroniques. Ces impulsions peuvent à leur tour être utilisées pour étudier la dynamique moléculaire suivant l'ionisation. Nous avons utilisé cette approche pour étudier la dynamique de l'ion D_2^+. Nous obtenons une résolution temporelle de 200 attosecondes et une résolution spatiale de l'ordre de 0.05 Å. Ces résultats sont présentés aux chapitres 1 et 2.

Ensuite, nous avons étudié l'explosion coulombienne induite par une impulsion laser à quelques cycles optiques. Nous avons tout d'abord étudié expérimentalement la double ionisation de D_2. Nous mesurons la structure de D_2 avec une résolution de 0.3 Å. En utilisant le concept d'horloge moléculaire développé au chapitre 1, nous montrons que le temps moyen pour que la double ionisation soit complète est de 4 fs lorsque l'impulsion

laser a une durée de 8.6 fs et une intensité avoisinant 10^{15} W/cm^2. Ce temps est suffisament court pour penser utiliser l'explosion coulombienne laser comme sonde dans des expériences de dynamique moléculaire. En utilisant la spectroscopie de coincidence et des impulsions lasers sub-8 fs, nous avons étudié l'explosion coulombienne de D_2O via $D_2O^{4+} \rightarrow D^+ + O^{2+} + D^+$ et celle de SO_2 via $SO_2^{7+} \rightarrow O^{2+} + S^{3+} + O^{2+}$. Nous montrons qu'il est possible de mesurer la structure de petites molécules avec une résolution spatiale similaire à D_2. Enfin, nous avons réalisé deux expériences pompe-sonde avec nos impulsions sub-8 fs. La pompe, moins intense, démarre la dynamique par ionisation multiphotonique. La sonde mesure la structure moléculaire à différents délais par explosion coulombienne. En utilisant l'ion D_2^+, nous confirmons une résolution temporelle d'environ 5 fs. Enfin, nous montrons qu'il est possible de distinguer si une dissociation est symétrique ou assymétrique en sondant $SO_2^{3+} \rightarrow O^+ + S^+ + O^+$, $SO_2^{2+} \rightarrow O^+ + S^+ + O$ et $SO_2^{2+} \rightarrow SO^+ + O^+$ par explosion coulombienne via l'état $SO_2^{7+} \rightarrow O^{2+} + S^{3+} + O^{2+}$. Nous montrons que le canal $SO_2^{2+} \rightarrow O^+ + S^+ + O$ n'a aucun intermédiaire SO^{2+}. Ces résultats sont présentés aux chapitres 3 à 5.

Enfin, je propose deux schémas de contrôle laser. Le transfert de population entre états quantiques est un sujet qui a été grandement étudié dans la littérature. Plusieurs techniques optiques ont été proposées mais aucune lorsque l'état final est doublement dégénéré. J'étudie ce cas par simulation numérique de l'équation de Schrödinger dépendante du temps pour un système à 4 niveaux. Le contrôle est possible en utilisant l'effet Stark et en modulant temporellement la fréquence de l'impulsion laser qui effectue le transfert de population. Je confirme les résultats de mes simulations par un modèle analytique.

> *« Lasers have been discovered by the wrong people; namely, by physicists. The result is that the chemists haven't grabbed it to the extent they should. In actual fact, in every laser process, whether it starts with physics or goes through chemistry, much of it will pure become chemistry. The only people who can make real progress are the chemists. »*
>
> Edward Teller, 1972

REMERCIEMENTS

Tout d'abord, je tiens à remercier André D. Bandrauk pour m'avoir accueilli dans son laboratoire de chimie théorique en 1999 comme étudiant graduée. J'y ai fait ma maîtrise et c'est lui qui m'a suggéré de faire mon doctorat en co-direction avec Paul B. Corkum. Ces trois dernières années seront inoubliables. La stimulation intellectuelle y était à chaque jour et j'ai vraiment découvert à quel point la science était ma passion. C'est une chance d'avoir travailler avec toi Paul, merci. J'espère avoir encore la chance de vivre cette expérience fantastique. Nos nombreuses discussions ont été très enrichissantes. Je tiens à les remercier tous les deux pour leur soutien et leur encouragement. Enfin, je les remercie d'avoir mis à ma disposition des ressources financières et techniques pour la mise en œuvre de cette thèse en collaboration avec l'Université de Sherbrooke et le Conseil National de Recherches Canada. Je tiens à remercier les organismes subventionnaires suivants : les Fonds de recherche sur la nature et les technologies, le Conseil de recherches en sciences naturelles et en génie du Canada, l'Institut canadien pour les innovations en photonique et le Conseil National de Recherches Canada

Merci à tous les membres du laboratoire de chimie théorique et à ceux du Conseil National de Recherches Canada. Plusieurs d'entre eux sont devenus de très bon amis. Je tiens à remercier particulièrement David M. Villeneuve. Grâce à lui, les lasers sont maintenant mes jouets préférés. Tes encouragements et tes conseils ont grandement aidé à diminuer mon niveau de nervosité.

Merci à tous les membres de ma famille et à la famille de mon épouse pour vos encouragements. Merci Josée pour l'appui que tu m'offres. Durant toutes ces années, tu as accepté beaucoup de compromis pour faire en sorte que je puisse réaliser ma passion. Merci à mon fils, Charles. Ma vie est maintenant comblée. Enfin, je remercie mes parents. Depuis que je suis haut comme trois pommes, vous m'avez encouragé et motivé à faire le meilleur de moi-même.

TABLE DES MATIÈRES

LISTE DES FIGURES

CHAPITRE 1

Figures tirées de Niikura *et al.* Nature **417**, 917 (2002).

CHAPITRE 4

Figures tirées de Légaré *et al.* Soumis à Physical Review Letters (2004).

CHAPITRE 5

Figures tirées de Légaré *et al.*, En préparation.

CHAPITRE 6

Figures tirées de François Légaré, Physical Review A **68**, 063403 (2003).

INTRODUCTION

La terre sur laquelle nous vivons est principalement moléculaire et la lumière est l'énergie motrice à plusieurs réactions chimiques. Cette science est appelée la photochimie. Lors d'une réaction photochimique, l'espèce moléculaire absorbe des photons et il peut y avoir modification de la structure moléculaire. Plusieurs réactions photochimiques sont complètes en moins d'une picoseconde (1 ps = 10^{-12} s.). Certaines, comme le transfert de proton dans de petites molécules, prennent moins de 100 femtosecondes (1 fs = 10^{-15} s.) [1]. Avec le développement de la technologie laser femtoseconde, il est possible de mesurer la dynamique associée aux réactions photochimiques par la technique pompe-sonde. Ceci a valu le prix Nobel de chimie 1999 au Dr. A.H. Zewail [2]. La pompe, généralement une impulsion laser UV, démarre une réaction photochimique. La sonde, retardée en temps, mesure un signal qui dépend du délai entre la pompe et la sonde. Plusieurs processus photochimiques ont été étudiés : le transfert de charge [3], la photodissociation [4] et des réarrangements moléculaires comme l'isomérisation [5] et le transfert de proton [6].

Dans une expérience pompe-sonde, le signal qui dépend du temps est dû à un changement de structure. Le rêve des spectroscopistes est d'être capable de mesurer directement cette structure moléculaire. Lorsque celle-ci ne dépend pas du temps, la diffraction d'électrons [7] et de rayons-X [8] sont des techniques standards. Pour pouvoir utiliser ces techniques comme sonde dans des expériences femtosecondes, if faut trouver une façon de produire des impulsions d'électrons ou de rayons-X femtosecondes. En phase gazeuse, une technique moins connue, l'explosion coulombienne induite par collision, permet de mesurer la structure de petites molécules [9].

Pour les électrons, l'utilisation d'une photocathode et d'impulsions lasers femtosecondes permet de générer des impulsions d'électrons de quelques centaines de femtosecondes [10,11]. Pour la génération d'impulsions rayons-X, trois techniques sont proposées. La première

utilise la génération d'un plasma. Celui-ci est induit par une impulsion laser intense femtoseconde. Des sources d'une durée de quelques centaines de femtosecondes sont disponibles et permettent des manipulations pompe-sonde [12,13]. Le désavantage de cette source est qu'il est diffile d'obtenir un grand flux de photons. La deuxième technique utilise les sources synchrotrons actuelles. Ces sources produisent des impulsions rayons-X d'une durée d'environ 100 picosecondes. Des mesures pompe-sonde sur des systèmes biologiques ont été réalisées avec de telles sources [14]. En utilisant un interupteur non-linéaire, il serait possible de produire des impulsions d'une centaine de femtosecondes avec ces sources [15]. Le désavantage est qu'un grand nombre de photons sera perdu. La troisième technique proposée pour produire des impulsions rayons-X est appelée laser à électrons libres [16]. L'avantage de cette source sera son grand flux de photons et la possibilité d'en changer la longueur d'onde du micron aux rayons-X. La durée de l'impulsion sera de quelques centaines de femtosecondes. Le désavantage de cette source est qu'elle sera excessivement dispendieuse, soit environ 500 millions US. Un projet à l'Université Stanford est en cours. Pour plusieurs processus moléculaires, 100 fs n'est pas suffisament court pour pouvoir observer clairement les changements structuraux lors d'expérience de dynamique moléculaire [1,6,17]. Des techniques connexes doivent-être développées.

L'explosion coulombienne consiste à enlever un grand nombre d'électrons à une molécule en une période de temps très courte [9]. Si la charge finale est assez élevée, l'interaction entre les atomes constituant la molécule est coulombien et il y a dissociation. En mesurant tri-dimensionnellement les vitesses asymptotiques des fragments atomiques, il est possible de recontruire la structure moléculaire. Le temps d'interaction détermine la qualité de l'image obtenue [18]. Lors de collision, l'interaction dure environ 500 attosecondes (1 as. = 10^{-18} s.), ce qui est suffisament court pour obtenir une image de grande qualité [19]. Les techniques d'explosion coulombienne induite par collision sont difficiles à intégrer dans une expérience pompe-sonde. Pour cette raison, ces techniques sont peu utilisées et elles ont eu un faible impact scientifique. Pouvoir faire la même chose avec des impulsions lasers permettrait d'étudier les changements structuraux lors d'expériences de dynamique moléculaire.

En 1985, Mourou et al. ont proposé une technique permettant d'amplifier considérablement les sources lasers [20]. Leur intensité devenait suffisante pour pouvoir enlever plusieurs électrons à un atome (ou une molécule). Ces sources lasers intenses ont une longueur d'onde située généralement dans l'infra-rouge et l'ionisation est multiphotonique. Lorsque l'intensité est élevée, le régime tunnel décrit le taux d'ionisation [21]. Au tournant des années 1990, la communauté des champs lasers intenses observait différents processus mal compris: le spectre obtenu lors de la génération d'harmoniques [22], l'ionisation non-séquentielle [23] et la production de photoélectrons ayant des énergies élevées [24]. En 1993, P.B. Corkum a publié un modèle classique permettant d'expliquer l'origine de ces processus [25]. Dans ce modèle, l'électron éjecté au pic de la composante électrique du champ laser peut revenir à la source. Au retour, ce que l'on appelle la recollision, il peut y avoir recombinaison, collision élastique ou enfin collision inélastique. La recombinaison produit des harmoniques élevées. La collision élastique change la trajectoire de l'électron et ceci permet de générer des photoélectrons de grande énergie. La collision inélastique excite électroniquement l'atome ce qui augmente la probabilité de double ionisation. De plus, il était prédit que ces mécanismes étaient très sensibles à la polarisation du champ laser. Lorsque celle-ci est circulaire, ces procesus doivent disparaître, ce qui fut confirmé expérimentalement en 1994 [26]. La génération des impulsions lasers attosecondes est due au contrôle temporelle de la recombinaison [27,28]. Des impulsions d'une durée de 250 attosecondes sont maitenant disponibles [29] mais l'intensité de celles-ci demeure encore trop faible pour pouvoir penser enlever un grand nombre d'électrons à un atome (ou une molécule).

Pour les molécules, il y a deux processus supplémentaires qui sont observés : la dissociation induite par le champ laser [30] et l'explosion coulombienne à une distance crititque [31]. La dissociation observée confirmait les hypothèses théoriques [32]. L'observation d'une distance critique à laquelle les molécules se fragmentent fut expliquer en 1995 [33,34]. Ce phénomène est appelée «l'ionisation exaltée». Des simulations numériques sur H_2^+ montre que le taux d'ionisation est augmenté considérablement lorsque la distance internucléaire est d'environ 3-4 Å. La distance d'équilibre de H_2 n'est que de 0.75 Å. Cette déviation est due à un délai temporelle entre la première ionisation et la deuxième, ce qui permet une dynamique

vibrationnelle sur les états perturbés de H_2^+ [35]. Le temps nécessaire pour que le paquet d'onde vibrationnel de H_2^+ se déplace de 0.75 à 3-4 Å est inférieur à 20 fs. Avant 1997, les impulsions lasers intenses avaient une durée minimale de 20-30 fs, temps supérieur à celui nécessaire pour atteindre la distance critique. Une expérience pompe-sonde sur l'iode proposait que l'explosion coulombienne induite par une impulsion laser pouvait sonder en temps réel la position relative des atomes dans une molécule lors d'une réaction photochimique [36]. Pour des molécules plus légères, comme H_2, il fallait attendre la venue d'impulsions lasers plus courtes. Des calculs montrent que l'explosion coulombienne laser peut mesurer l'amplitude carrée d'une fonction d'onde [37] ou d'un paquet d'onde [38].

La technologie titanium saphire (λ = 800 nm) permet de générer des impulsions lasers intenses d'environ 20 fs. En 1996, Nisoli et al. proposait une technique permettant de générer des impulsions lasers sub-10 fs [39]. Elle utilise la propagation d'impulsions lasers intenses dans une fibre creuse remplie d'argon. Ceci permet d'ajouter des composantes spectrales par modulation temporelle de la phase. À la sortie de la fibre, la transformée de fourier du spectre permet la production d'impulsions lasers à quelques cycles optiques. Pour y arriver, il faut en contrôler la phase spectrale. Avec le développement récent des miroirs multicouches, il est maintenant possible de générer des impulsions lasers sub-5 fs [40]. Avec ces impulsions, il n'y a qu'une seule recollision. C'est cette technologie qui a permis la génération des impulsions lasers d'une durée de 250 attosecondes [29].

Les chapitres 1 à 5 proposent deux différentes techniques permettant de mesurer la structure des molécules. La première, présentée au premier et au deuxième chapitre utilise la recollision tandis que la seconde utilise l'explosion coulombienne induite par une impulsion laser à quelques cycles optiques. Les résultats d'explosion sont présentés aux chapitres 3 à 5. Au chapitre 1, nous confirmons expérimentalement la structure temporelle du paquet d'onde électronique qui revient à la source lors d'expérience d'ionisation non-séquentielle. En utilisant des impulsions lasers à 800 nm, d'une durée de ~50 fs et d'une intensité avoisinant les $2x10^{14}$ W/cm^2, nous montrons que l'électron éjecté par ionisation revient à la source sous

un train d'impulsions attosecondes [41]. Au chapitre 2, en utilisant le fait que le temps de retour dépend de la longueur d'onde du champ laser, nous confirmons qu'il est possible d'utiliser la première recollision pour faire des mesures ayant une précision de quelques centaines d'attosecondes sans pour autant avoir à générer de telles impulsions lasers [42].

Au chaptire 3, nous étudions la double ionisation de D_2 (explosion coulombienne) avec des impulsions lasers ultra-brèves. Nous montrons que la double ionisation de D_2 est complétée dans un temps moyen de ~4 fs lorsque l'impulsion laser a une durée de 8.6 fs et une intensité avoisinant les 10^{15} W/cm^2 [43]. Au chapitre 4, nous utilisons la spectroscopie de coincidence et des impulsions lasers sub-8 fs pour mesurer la structure de D_2O et de SO_2 lorsque nous explosons celles-ci via l'état $D_2O^{4+} \rightarrow D^+ + O^{2+} + D^+$ et l'état $SO_2^{7+} \rightarrow O^{2+} + S^{3+} + O^{2+}$ [44]. L'explosion coulombienne laser permet de mesurer la structure de petites molécules avec une précision inférieure à 0.3 Å. Au chapitre 5, nous utilisons l'explosion coulombienne laser comme sonde à réaction photochimique. La dynamique moléculaire est démarrée par ionisation multiphotonique. Notre pompe et notre sonde sont des impulsions lasers sub-8 fs. Nous montrons une résolution temporelle de l'ordre de 5 fs. Une expérience sur SO_2 montre qu'il est possible d'observer en temps réel les différents modes vibrationnels lors de processus photodissociatifs.

Du chapitre 1 à 5, nous avons étudié la possibilité d'utiliser des champs lasers intenses comme appareil photo à réaction photochimique. Le second rêve des photochimistes est d'être capable de contrôler l'absorption de la lumière. Le but est d'être capable de transférer efficacement et sélectivement des populations entre états quantiques. Dans un système à deux niveaux, le transfert efficace de population de l'état fondamental vers l'état excité peut se faire en utilisant des impulsions lasers π ou en modulant temporellement la fréquence du champ laser [45,46]. Pour des systèmes simples, il est possible d'imaginer des schémas de contrôle. Leurs hamiltoniens sont connus ce qui permet d'imaginer une perturbation dépendante du temps qui contrôlera l'absorption de lumière. Les systèmes à quelques niveaux [47-49] et les molécules diatomiques [50-56] ont été largement étudiés. Ces études ont eu un impact

considérable en optique quantique [57,58]. Pour des systèmes plus complexes, l'hamiltonien n'est pas connu et il est difficile d'utiliser le contrôle cohérent. Par manipulation optique, l'amplitude, la phase et la polarisation du champ laser peuvent être contrôlées [59-60]. Un algorythme d'optimisation permet de trouver l'impulsion optimale pour le processus désiré [61-63]. Au chapitre 6, j'utilise le contrôle cohérent pour le transfert efficace et sélectif de population dans un système où l'état final est doublement dégénéré. Par algèbre de Lie, Shah et al. ont montré qu'il faut au minimum 4 niveaux pour être capable de transférer efficacement la population dans un seul état [64]. Ils solutionnaient le prolème par contrôle optimal. Je propose deux schémas de contrôle simples permettant le transfert de population dans un tel système [65]. Deux impulsions lasers sont utilisées dans ces schémas, l'une produisant un effet Stark tandis que la seconde exécute le transfert de population entre les états quantiques.

CHAPITRE 1

CARACTÉRISATION D'UN TRAIN D'IMPULSIONS ÉLECTRONIQUES ATTOSECONDES

Dans l'article associé à ce chapitre (Niikura *et al.* Nature **417**, 917 (2002)), nous étudions temporellement le processus de recollision électron-molécule (ou atome). Lorsqu'un atome/molécule est ionisé par une impulsion laser intense polarisée linéairement, l'électron éjecté oscille sous l'action de la composante électrique du champ laser et retourne à l'ion parent sous la forme d'un train d'impulsions électroniques attosecondes (1 as = 10^{-18}s.). Lors du retour, des collisions élastiques et inélastiques peuvent avoir lieu, de même que l'émission d'harmoniques élevées. C'est à partir de ces harmoniques que les impulsions attosecondes sont générées. Pour confirmer si un processus est induit par la recollision, il suffit de changer la polarisation du champ laser de linéaire à circulaire. Les processus collisionnels sont rapidement supprimés lorsque la polarisation devient elliptique parce que la trajectoire du paquet d'onde électronique ne passe plus alors par l'ion.

Des calculs classiques prédisent que si l'impulsion laser a une longueur d'onde de 800 nm, le premier paquet d'onde passera ~1.8 fs dans le continuum avant son retour à l'ion parent. La durée temporelle du train est d'environ 10 fs pour une impulsion laser ayant une durée supérieure à 20 fs. Pour pouvoir caractériser temporellement ce train d'impulsions électroniques, il faut trouver une horloge ayant une précision sub-fs. L'ion moléculaire H_2^+ est l'horloge que nous avons choisie. Sa période vibrationnelle est de l'ordre de 10 fs.

Lorsque H_2 est ionisé vers H_2^+, deux paquets d'ondes sont générés et ils sont corrélés, l'un est vibrationnel et l'autre électronique. L'ionisation prends moins de 500 attosecondes lorsque la longueur d'onde du champ laser est de 800 nm. Nous sommes en mesure de simuler la propagation temporelle de ces paquets. Le paquet vibrationnel se déplace sur la surface

fondamentale de H_2^+ ($X\ ^2\Sigma_g^+$) pendant que le paquet d'onde électronique oscille dans le continuum sous l'action de la composante électrique du champ laser. Lorsque l'électron retourne à la source, le paquet d'onde vibrationnel a bougé et une collision inélastique peut provoquer la dissociation de l'ion. La mesure du spectre d'énergie cinétique des fragments H^+ nous permet de confirmer le profil temporel du train d'impulsions électroniques. La conclusion importante de cet article est que près de 50 % de la population électronique revient lors de la première collision et que la durée temporelle de ce paquet est d'environ 1 fs (1000 attosecondes).

Ma contribution personnelle à cet article s'est limitée aux simulations numériques de l'équation de Schrödinger. La Dr. R. Hasbani a pour sa part simulé la propagation du paquet d'onde électronique dans le continuum. En combinant les connaissances acquises de nos simulations, nous avons pu expliquer et confirmer les résultats expérimentaux du Dr. H. Niikura. Ils représentent une innovation majeure dans le domaine de la photophysique attoseconde. Nous avons établi que des mesures attosecondes peuvent être faites sans l'utilisation d'impulsions lasers de cette durée.

L'expérience montre que la possibilité de faire des mesures sous n'importe quelle échelle temporelle permet l'étude de nouveaux domaines en science. Présentement, des sondes optiques attosecondes (10^{-18}–10^{-15} s) sont disponibles. L'approche utilisée pour générer celles-ci est l'ionisation des atomes avec des impulsions lasers intenses de quelques cycles optiques. Ce processus non-linéaire permet la production d'harmoniques élevées lors de la collision entre l'électron et l'ion parent. Le mécanisme permettant la production d'impulsions attosecondes implique que l'électron est contrôlé avec une telle précision. Nous proposons que l'électron peut être lui-même utilisé pour des mesures ultra-brèves. Nous utilisons une horloge moléculaire pour montrer que l'électron qui entre en collision avec l'atome ionisée revient avec une densité de courant élevée, et sous un train d'impulsions ayant chacune une durée d'environ 1 femtoseconde (10^{-15} s.). Cette horloge est basée sur la propagation d'un

paquet d'onde vibrationnel dans H_2^+. Enfin, nous utilisons l'horloge moléculaire pour étudier la dynamique associée à la double ionisation non-séquentielle.

Sub-laser-cycle electron pulses for probing molecular dynamics

Hiromichi Niikura*, F. Légaré*†, R. Hasbani*, A. D. Bandrauk†, Misha Yu. Ivanov*, D. M. Villeneuve* & P. B. Corkum*

*National Research Council of Canada, 100 Sussex Drive, Ottawa, Ontario K1A OR6, Canada

†Université de Sherbrooke, Sherbrooke PQ, Canada

Abstract

Experience shows that the ability to make measurements in any new time regime opens new areas of science. Currently, experimental probes for the attosecond time regime (10^{-18}–10^{-15} s) are being established. The leading approach is the generation of attosecond optical pulses by ionizing atoms with intense laser pulses. This nonlinear process leads to the production of high harmonics during collisions between electrons and the ionized atoms. The underlying mechanism implies control of energetic electrons with attosecond precision. We propose that the electrons themselves can be exploited for ultrafast measurements. We use a 'molecular clock', based on a vibrational wave packet in H_2^+ to show that distinct bunches of electrons appear during electron–ion collisions with high current densities, and durations of about 1 femtosecond (10^{-15} s). Furthermore, we use the molecular clock to study the dynamics of non-sequential double ionization.

A substantial effort is under way to develop single attosecond optical pulses[1–3], or trains of attosecond pulses[4–6], using the physical processes occuring in high-harmonic generation[7]. High harmonics are produced during the electron–ion collisions induced by strong-field laser ionization, usually referred to as 'recollision'. Within one optical period an electron is removed from the atom, is driven back when the laser field reverses its direction, and collides with the parent ion. The duration of the electron–ion recollision largely determines the duration of the attosecond photon pulse.

Here we study the recollision electron wave packet, measuring both the probability of recollision and its time structure. Although only one electron is involved in the electron–ion recollision, we adopt the language of electron beams to indicate the potential applications of recollision electrons. These applications are the topic of the final section of this Article.

We characterize the unusually large current density and its time structure as seen by the ion following ionization. To do this, we use H_2 molecules in a low-density gas as a molecular clock. As ionization simultaneously forms two wave packets — one a vibrational wave packet moving on the H_2^+ ($X^2\Sigma_g^+$) surface; the other, the electron wave packet that we wish to study — ionization starts the vibrational clock in H_2^+. We choose H_2 as the molecular clock because of the speed of its vibrational wave packet, and because all excited states of H_2^+ directly dissociate. By choosing the molecular axis perpendicular to the laser electric field, we decouple the $X^2\Sigma_g^+$ and $A^2\Sigma_u^+$ surfaces in H_2^+; ensuring that the clock remains accurate in the presence of the field. To read the clock, we observe the kinetic energy of the protons produced by inelastic scattering when the electron recollides with the parent ion. The kinetic energy distribution measures the position of the vibrational wave packet at the time of recollision, and therefore the recollision time. In our experiment the time resolution is ~1 fs.

Next, we apply the molecular clock to follow the subcycle correlated electron dynamics. Non-sequential double ionization (two-electron ionization that cannot be described by two sequential single-electron ionization processes) is a common occurrence during strong-field ionization of atoms or molecules containing two or more electrons[7–13]. We distinguish the double ionization due to recollision from instantaneous double ionization by using the molecular clock, and find that electron recollision dominates others by at least two orders of

magnitude. We confirm that the most important route to non-sequential ionization is through the production of excited states by recollision that can later ionize in the strong laser field.

Finally, we compare the double-ionization yield due to recollision in H_2 and helium[8,11,13]. We find that double ionization (excitation) is about ten times more probable in hydrogen molecules than in helium[11,13].

Selecting the fragmentation channel

We now proceed to fully characterize the current density using H_2 double ionization (excitation) for all aspects of the measurement. (For convenience, we will use 'double-ionization' when referring to either the non-sequential emission of two electrons, or the emission of one and the correlated excitation of the other.)

First, we identify collision-induced excitation or double ionization through the previously observed[14,15] high kinetic energy of the fragment protons that are produced. We show that recollision is responsible for these energetic protons by comparing the kinetic energy spectrum measured with linear and elliptically polarized light[16]. Second, the ellipticity dependence of the proton yield measures the initial velocity spread of the electron wave packet. With this input, we calculate the current density seen by the newly ionized ion. Third, we confirm the predicted temporal structure by comparing the calculated and measured kinetic-energy spectrum. Finally, we confirm the magnitude of the current density by comparing the calculated and measured probability of double ionization.

Figure 1 plots the potential-energy surfaces of molecular hydrogen and its ions. Single ionization (represented as the solid vertical arrow in Fig. 1) results in the formation of two correlated wave packets. One is the electron wave packet that we wish to characterize. The other is a vibrational wave packet moving (horizontal arrow) on the field-modified Σ_g potential-energy surface until electron re-collision occurs.

When the electron wave packet returns to the ion it can inelastically scatter, producing excited states of H_2^+ or further ionizing the ion (dotted arrow in Fig. 1). All excited states of H_2^+ lead to dissociation of the molecular ion. They can be identified through the kinetic-

energy spectrum of the protons, provided that the laser field does not further ionize them. To avoid further ionization we keep the light intensity low, and we exploit two additional effects: that ionization is not enhanced for perpendicular orientation[17], and that ionization is suppressed for anti-symmetric states[18]. The kinetic energy spectrum gives us a relatively uncomplicated 'time history' of the recollision dynamics. The channel of interest produces fragments with kinetic energy in the range 1–10 eV.

We performed the experiment in a time-of-flight mass spectrometer containing H_2 molecules at a pressure of 10^{-6} torr. We apply a uniform electric field across two parallel electrodes separated by 3 cm. A 1-mm-diameter hole in one electrode allows us to observe protons only from those molecules whose axis lies close to parallel with respect to the time-of-flight axis. The signal is measured on a microchannel plate detector.

Although we could observe molecules with any orientation, we concentrate on those that are oriented perpendicular to the laser polarization. H_2^+ cannot change its orientation[19] in the brief interval between ionization, recollision and dissociation. The collection half-angle depends on the dissociation velocity of the fragments and the applied electric field. For our experimental conditions, the half angle was 8^0 at 10 eV with the angle increasing with the inverse of the velocity.

H_2 molecules are ionized by a 50-fs light pulse of 800 nm wavelength, propagating perpendicular to the time-of-flight axis and focused to a peak laser intensity of (1.5±0.5) X 10^{14} Wcm^{-2}. The intensity is calibrated against the ionization of xenon[20]. At this intensity the recollision electron should have maximum collision energy of ~30 eV, sufficient only to excite $X^2\Sigma_g^+ \rightarrow A^2\Sigma_u^+$ in the molecular ion. To change the ellipticity of the laser light we rotate a half-wave plate that is placed before a fixed quarter-wave plate. This procedure preserves the direction of the major axis as the ellipticity changes. We now proceed to identify the signature of recollision in the kinetic-energy spectrum.

Confirming recollision

Figure 2 plots the measured kinetic energy spectrum of the protons. The main plot, shown on a very-much-expanded vertical scale, is for molecules oriented perpendicular to the field direction, whereas the inset is for molecules oriented in the parallel direction. Because of its scale, the main plot of Fig. 2 most clearly shows the low-probability events, namely the protons with high kinetic energy.

To identify the channel of interest, we must distinguish it from other dissociation channels that influence the kinetic-energy spectrum of the protons. Bond softening[21,22], which originates from the mixing of the Σ_g and Σ_u levels by the laser field, is responsible for the kinetic-energy peak near 0.5 eV, clearly seen in Fig. 2 inset. To eliminate bond-softened molecules, we select perpendicularly oriented molecules where Σ_g and Σ_u are decoupled. Enhanced ionization, which refers to the large and broad increase in ionization rate with the internuclear coordinate in the region where the bond breaks[17,23,24], is responsible for the peak in the ~2.5 eV region. Like bond softening, it is also eliminated for perpendicular molecules[18].

We confirm, by measuring the number of protons as a function of the ellipticity of the laser light[1,10,12,16], that recollision is responsible for the high-kinetic-energy protons. Processes caused by electron recollision are very sensitive to small deviations from linear polarization[7]. The inset in Fig. 3 illustrates the method that we use. In linearly polarized light, the laser field dominates the electron motion in the direction of the laser polarization. However, the quantum-mechanical uncertainty of the electron's velocity at the time of ionization causes the electron wave packet to have expanded significantly in the lateral direction by the time it re-collides with the ion (Fig. 3 inset). We can easily influence the electron trajectory by adding a small ellipticity to the laser pulse. The weak perpendicular field pushes the electron wave packet to the side so that recollision becomes impossible.

The sensitivity to ellipticity is seen in Fig. 2. The upper curve is obtained using linearly polarized light, and the lower curve is obtained using light with ellipticity of Ey/Ex = 0.3 (where Ey (Ex) is the laser electric field in the direction perpendicular (parallel) to the molecular axis). Ellipticities between 0 and 0.3 occupy the intermediate region, whereas the

lower curve is essentially unchanged for higher ellipticities. The difference of data counts between the upper and lower curves determines the kinetic-energy spectrum of protons produced by recollision, as we will show below. It is clear from Fig. 2 that our measurements should concentrate on kinetic energies above about 4 eV.

Figure 3 shows the ellipticity dependence of the recollision yield. All high kinetic-energy fragments have the same ellipticity dependence. At each ellipticity, we integrate the signal count in the kinetic energy range 4–9 eV. The three curves included in Fig. 3 are for argon and for H2 molecules aligned parallel and perpendicular to the laser polarization.

Lateral spread of the electron wave packet

The velocity that the electron acquires in the direction perpendicular to the laser field during ionization determines the expansion of the electron wave packet in the lateral direction. If the velocity is large, the wave packet that recollides is spread over a large area. We concentrate on the lateral velocity for molecules aligned perpendicular to the laser field.

As the laser ellipticity increases, the electron wave packet is pushed further from the ion core in the direction of the minor component of the laser field. When the electron wave packet returns to the ion core for the first time, at a time $\Delta t = 1.8$ fs after its birth, its displacement is given by $dx \approx 5.14\varepsilon E/m\omega^2$ (ref. 12), where ε is ellipticity, E is the strength of laser field, m is the electron mass and ω is the laser angular frequency. Our 1/e width $\varepsilon = 0.14$ yields a 1/e displacement dx = 7.7 Å. Because the effective collision cross-section is small (~1 $Å^2$), the displacement allows us to measure the spatial distribution of the electron wave packet when it returns to the ion core[12]. From this distribution, we determine that the initial velocity spread at the time of ionization is ~4.2 $Åfs^{-1}$. The observed ellipticity dependence shows a gaussian form, as predicted by tunnelling theory[25]. Argon is used as a reference that we can accurately calculate. For argon (open squares in Fig. 3) the same procedure yields ~5.6 $Åfs^{-1}$, in excellent agreement with 5.4 $Åfs^{-1}$ predicted by the atomic tunnelling theory[25].

Knowledge of both the expansion velocity of the electron wave packet and its shape provides the initial conditions for a semiclassical simulation of the electron dynamics

following ionization[13]. In the calculation, we follow many electron trajectories in two dimensions; each trajectory is characterized by different initial positions and velocities and by a weight ρ_I, which reflects the probability of that trajectory. We count the number of trajectories passing through the surface of a circle of radius r_0, where πr_0^2 is the inelastic cross-section (ref. 26 and <http://physics.nist.gov/PhysRef-Data/Ionization/Xsection.htmll> for the $\Sigma_g \rightarrow \Sigma_u$ transition in H_2^+; within a unit time. In the calculations, we correct the atomic tunnelling[27] rate to include the molecular structure. We also include the influence of the molecular ion's field on the free electron trajectories.

Figure 4 is a plot of the calculated current density experienced by the molecular ion. Only electrons with energy greater than the resonant energy between Σ_g and Σ_u are included in this plot. Otherwise, the current density includes all other electrons that pass through the collisional surface of area πr_0^2: Figure 4 shows that the recollision current consists of five micro-bunches. The current density rises in the second half-period after ionization, reaching $8 \times 10^{10} Acm^{-2}$. At later times, the amplitude decreases rapidly. Such high current densities are available only from very large accelerators such as SLAC.

Temporal structure of the electron wave packet

To confirm the time structure of the recollision, we turn our attention to the vibrational wave packet. The laser parameters place our experiment in the regime where ionization can be calculated by assuming that the electron tunnels through the barrier caused by the superposition of the laser field and the ion field[27,28]. Removing an electron from H_2 forms a vibrational wave packet on the ground Σ_g of H_2^+ that resembles the ground-state wavefunction. Ionization simultaneously releases the electron wave packet that we have been discussing. The distortion of the vibrational wave packet compared to the ground-state wavefunction of H_2 (ref. 29) owing to the dependence of the ionization rate on the internuclear separation is included in the calculation.

We follow the H_2^+ wave packet by solving Schrödinger's equation on the Σg molecular potential. By including the interaction of the laser field with the perpendicular induced dipole,

we confirm that, at this intensity, other states have a negligible effect on the motion of the wave packet. The proton kinetic-energy spectrum resulting from recollision is obtained by projecting the Σ_g wave packet onto the Σ_u continuum wavefunctions.

Figure 5 (solid line) shows the incoherent sum of the kinetic energy spectra of protons produced by all five micro-bunches weighted according to their relative probabilities as determined by the calculated time independent current density in Fig. 4, and weighted by the cross-section at the average internuclear separation[26] for each micro-bunch. We have used angle-averaged cross-sections because, to our knowledge, no cross-section data are available for oriented molecules. We show the individual contribution of the first and third recollision as dotted lines. Their time separation is 2.7 fs. It is clear from Fig. 5 that we can resolve contributions from an intermediate electron pulse.

The experimental kinetic energy spectrum (data points) is also plotted in Fig. 5. In the vertical direction, error bars are determined by shot-to-shot statistics. The error in the horizontal direction is only dependent on the measurement resolution (500 ps) of the time-of-flight mass spectrometer. The error is of the order of the spacing of the data points. To obtain the experimental data for Fig. 5, the kinetic-energy spectrum, measured with elliptically polarized light (Fig. 2, circles), was subtracted from the kinetic-energy spectrum measured with linearly polarized light (Fig. 2, squares). This procedure distinguishes the processes due to recollision from other sources.

The overlap between the calculation and the experiment in Fig. 5 is notable. We stress that our ability to measure the ~1-fs duration of the first micro-bunch is achieved because of the double correlation between the electronic and vibrational wave packets. We do not use either time-dependent polarization[1] or a few-cycle pulse[2,3].

Magnitude of the electron current density

In Fig. 5, we account for the relative magnitude of each recollision peak. The only free parameter is the overall normalization of the experimental kinetic-energy spectrum with respect to the theoretical one. Theoretically, using the current density in Fig. 4 and the angle-

averaged cross-section, we can predict the angle averaged probability that one single-ionization event will lead to inelastic excitation of Σ_u. At 1.5 X 10^{14}Wcm^{-2}, we calculate that 7% of all ionization events result in inelastic scattering. This establishes the vertical scale in Fig. 5 for the calculations. We now establish this experimentally.

The number of protons produced by recollision is plotted in Fig. 6 as a function of the alignment of the molecular axis with respect to the laser field. There are about 10 times more inelastic scattering events for molecules aligned parallel to the field than perpendicular. Were we able to align all molecules relative to the laser polarization, we could separate the influence of angle-dependent ionization rates and cross-sections. But owing to the small asymmetry in the polarizability and the large rotational constant, alignment is not possible.

Figure 7 shows the branching ratio between H_2^+ (circles), bond softening (0–0.9 eV, upward pointing triangles), enhanced ionization (0.9 – 4 eV, downward pointing triangles) and inelastic scattering (> 4 eV, squares). To obtain this branching ratio, we measure the probability of each product channel at 10^0 intervals. This establishes the probability as a function of angle. Then we integrate each channel over all 4π steradians. The branching ratio of each channel is obtained by dividing each probability by the sum of all channels. The experimental branching ratio into inelastically scattered fragments is ~2–3% at 1.5 X 10^{14} Wcm^{-2}. This establishes the vertical scale in Fig. 5 for the measurement. As with helium, double ionization is almost independent of the laser intensity[11,13].

Both the calculation and the measurement have a degree of uncertainty. By assigning a fragment kinetic energy >4 eV to inelastic scattering, we experimentally underestimate the true branching ratio into inelastic channels. We know that, at least for perpendicular molecules (Fig. 2), about 30% of all inelastic events lead to protons with kinetic energy in the 2–4 eV range. But if the molecule is oriented parallel to the internuclear axis, such events are overwhelmed by the enhanced ionization peak and we cannot accurately measure them. Theoretically, we overestimate the experimental branching ratio by using hard-sphere[13], angle-averaged cross-sections and two-dimensional trajectories. In view of these uncertainties, the experiment and calculation agree.

Strong-field non-sequential double ionization

Of the phenomena observed in the interaction between atoms/molecules and ultrashort intense laser pulses (high-harmonic generation[30,31], very-high-energy electron production[32,33], and nonsequential double ionization[8,10,11]), all but the last can be described with a single active electron[11]. Thus non-sequential double ionization gains a particular significance within strong-field physics, connecting it to multi-electron physics, a subject that is important in many other areas of science. There are a number of important issues in non-sequential double-ionization physics that our experiment allows us to comment on Multi-electron dynamics.

Although we have expressed our results in terms of the current density and concentrated on the electron that recollides, we obtain the current by measuring the correlatedelectron dynamics during strong-field ionization. Until recently, the basic mechanism responsible for double ionization was a subject of controversy[11]. Strong-field double ionization was initially thought to be caused by shake-off[8]—the departing electron causes the remaining electron to become unbound. It is now accepted that recollision is the main mechanism responsible for double ionization. However, previous experimental measurements were not precise enough to eliminate the possibility that shake-off (or other instantaneous double-ionization processes that are important for X-ray double ionization) plays a minor role.

The double correlation of vibrational and electron wave packet in H_2 allows instantaneous double ionization to be identified, as it would place the H_2^+ on an excited surface before any nuclear motion could occur in the Σ_g. Referring to Fig. 2, we do not observe protons with kinetic energy above ~9.5 eV. The lack of energetic protons with kinetic energy greater than 10 eV implies that, at an intensity of 1.5×10^{14} Wcm^{-2}, the branching ratio into instantaneous double ionization cannot exceed 10^{-4}.

However, we do resolve in time the decay of the electron–electron interaction in H_2 during ionization in a strong field. Following ionization, the interaction has the complex temporal structure similar to the electron current density in Fig. 4.

The role of excited states. The unique advantage of H_2 is that all excited states of H_2^+ are unstable. Therefore the kinetic-energy spectrum of the fragments can identify the dissociation channels. We find that excited states dominate H_2 double ionization in the intensity regime in which we work. At higher intensities, the Σ_u state would ionize during the laser pulse, making it an important pathway to double ionization. The role of excitation as a route to double ionization in atoms has been the subject of considerable speculation[13,34,35].

The significance of alignment in molecular ionization. The transverse velocity spread of the electron as it leaves the atom (molecule) determines the probability of all recollision processes (high-harmonic generation, double ionization and elastic scattering). The data in Fig. 3 allow us to make three important observations about the transverse velocity spread. First, for either alignment of the molecule with respect to the laser polarization, the ellipticity dependence shown in Fig. 2 is independent of the kinetic energy of the fragments in the range caused by recollision (4–9 eV), and is therefore independent of which micro-pulse leads to the excitation. Second, the ellipticity dependence is slightly different for the parallel and perpendicular orientation of the molecules. The transverse velocity spread perpendicular to the laser field therefore depends slightly on the molecular alignment with respect to the laser field. For molecules aligned parallel to the laser polarization, the l/e width of the velocity distribution is 5.0 $Åfs^{-1}$, while, for perpendicular aligned molecules, the l/e width of the velocity distribution is 4.2 $Åfs^{-1}$. Third, although Ar has almost the same ionization potential as H_2, the l/e width of the transverse velocity of Ar (~5.6 $Åfs^{-1}$) is larger than that for either orientation of H_2.

In contrast to atomic tunnelling theory[25], there have been no theoretical predictions of the electron wave packet spread in molecules. Qualitatively, in agreement with our measurements, we might expect a smaller spread from the broader tunnel that characterizes a perpendicular molecule. The probability of double ionization (excitation). Although both H_2 and helium have two electrons, the probability of double ionization or excitation is about 10 times higher for H_2 than for He (ref. 11). It is also significantly greater for H_2 than for neon[36], although neon has many more electrons.

Using attosecond electrons for probing

Implicit in our results is the potential to exploit recollision electrons in a number of subfields of gas-phase molecular science operating on all timescales. Currently it is assumed that attosecond science will be an extension of ultrashort-pulse science in a new time regime. However, extreme ultraviolet attosecond pulses are not generated in a laser system but in a very inefficient process involving 'free' electrons[2,3]. Focusing the attosecond extreme ultraviolet radiation onto another gas is also inefficient. In contrast, attosecond electron bunches are produced with ~100% efficiency, and have a high probability of interaction. It seems likely that attosecond science will use attosecond electron pulses and attosecond photon pulses equally. In addition, the technology needed for producing and using attosecond electron bunches is available in many laboratories. We have used a 50-fs laser to produce an electron micro-bunch that has a duration of ~1fs. This is possible because we exploit correlation—we probe only those molecules that undergo ionization.

If it is necessary to eliminate the weaker micro-bunches and reach individual bunches of electrons, we can borrow two approaches that have been proposed to reach single attosecond optical pulses. One approach uses a few-cycle visible pulse to confine the time of ionization, and to ensure that the driving pulse is terminated before a second recollision is likely[2,3]. The other approach exploits a fundamental pulse with time-dependent polarization to control the electron trajectory[1]. With time-dependent polarization, recollision is only possible for a fraction of the driving laser period, resulting in attosecond extreme ultraviolet pulses and attosecond recollisions.

But what are the implications for conventional femtosecond science? Conventional femtosecond science has no convenient short-wavelength source, although there is a great deal of interest in creating one using X-rays[37] or electrons[38]. Recollision electrons can play that role. Depending on the wavelength of the laser light that creates them, recollision electrons can have very high energies. These electrons are produced when and where they are needed. In effect, they are 'slaved' with attosecond precision to the optical beam that created them. Controlling the laser pulse controls the electrons, both their production and their subsequent motion[39,40].

As probes in femtosecond experiments, recollision electrons are expected to have unique advantages over laser photons. The most important advantage arises during elastic scattering. If the electrons are sufficiently energetic, an image of the structure of the molecule is impressed onto the diffracted electron distribution. Although the recollision electron probes the ion a few femtoseconds after ionization (for most molecules), there is no time for the structure of the neutral molecule to change. Therefore, although the ion is probed, the structure of the neutral molecule is imaged.

Even when time resolution is not an issue, recollision electrons will find applications. For example, in a gas that combines a mixture of excited and unexcited molecules, the intense laser field that is used to create the recollision electrons will preferentially ionize the excited molecules—exactly the molecules that we wish to observe. As the recollision electron probes only its parent, excited molecules will be preferentially imaged.

Few molecules will be needed for imaging, because the current densities are so large. In fact, there is a substantial effort under way to develop methods for single-molecule imaging or few-molecule imaging[40]. The very large current densities that characterize recollision events suggest that recollision electrons could contribute to this effort.

Acknowledgements

F.L. acknowledges financial support from Canada's Natural Science and Engineering Research Council, the Canadian Institute for Photonics Innovation and Québec's Fonds pour la Formation des Chercheurs et l'Aide à la Recherche.

References:

1. Corkum, P. B., Ivanov, M. Yu. & Burnett, N. H. Sub-femtosecond pulses. *Opt. Lett.* **19**, 1870–1872 (1994).

2. Drescher, M. et al. X-ray pulses approaching the attosecond frontier. *Science* **291**, 1923–1927 (2001).

3. Hentschel, M. et al. Attosecond metrology. *Nature* **414**, 509–513 (2001).

4. Antoine, P., L'Huillier, A.& Lewenstein,M. Attosecond pulse trains using high-order harmonics. *Phys.Rev. Lett.* **77**, 1234–1237 (1996).

5. Paul, P. M. et al. Observation of a train of attosecond pulses from high harmonic generation. *Science* **292**, 1689–1692 (2001).

6. Papadogiannis, N. A.,Witzel, B., Kalpouzous, C. & Charalambidis,D. Observation of attosecond light localization in higher order harmonic generation. *Phys. Rev. Lett.* **83**, 4289–4292 (1999).

7. Corkum, P. B. A plasma perspective on strong field multiphoton ionization. *Phys. Rev. Lett.* **71**, 1994–1997 (1993).

8. Fittinghoff, D. N., Bolton, P. R., Chang, B. & Kulander, K. C. Observation of nonsequential double ionization of helium with optical tunneling. *Phys. Rev. Lett.* **69**, 2642–2645 (1992).

9. Weber, Th. et al. Correlated electron emission in multiphoton double ionization. *Nature* **405**, 658–661 (2000).

10. Bhardwaj, V. R., Rayner, D. M., Villeneuve, D. M. & Corkum, P. B. Quantum interference effects in double ionization and fragmentation of C_6H_6. *Phys. Rev. Lett.* **87**, 253003-1–253003-4 (2001).

11. Walker, B. et al. Precision measurement of strong field double ionization of helium. *Phys. Rev. Lett.* **73**, 1227–1230 (1994).

12. Dietrich, P., Burnett, N. H., Ivanov,M. Yu. & Corkum, P. B. High harmonic generation and correlated two electron multiphoton ionization with elliptically polarized light. *Phys. Rev. A* **50**, 3585–3588 (1994).

13. Yudin, G. L. & Ivanov, M. Yu. Physics of correlated double ionization of atoms in intense laser fields: Quasistatic tunneling limit. *Phys. Rev. A* **63**, 033404-1–033404-14 (2001); erratum *Phys. Rev. A* **64**, 019902 (2001).

14. Trump, C., Rottke, H.& Sandner,W. Strong-field photoionization of vibrational ground-state H_2^+ and D_2^+ molecules. *Phys. Rev. A* **60**, 3924–2928 (1999).

15. Staudte, A. et al. Observation of a nearly isotropic, high energy Coulomb explosion group in the fragmentation of D_2 by short laser pulses. *Phys. Rev. A* **65**, 020703-1–02070-4 (2002).

16. Sakai, H. et al. Non-sequential double ionization of D_2 molecules with intense 20 fs pulses. *Phys. Rev. Lett.* (submitted).

17. Constant, E., Stapelfeldt, H. & Corkum, P. B. Observation of enhanced ionization of molecular ions in intense laser fields. *Phys. Rev. Lett.* **76**, 4140–4143 (1996).

18. Muth-Böhm, J., Becker, A. & Faisal, F. H.M. Suppressed molecular ionization for a class of diatomics in intense femtosecond laser fields. *Phys. Rev. Lett.* **85**, 2280–2283 (2000).

19. Ellert, Ch. & Corkum, P. B. Disentangling molecular alignment and enhanced ionization in intense laser fields. *Phys. Rev. A* **59**, R3170–R3173 (1999).

20. Hankin, S., Villeneuve, D. M., Corkum, P. B. & Rayner, D. M. Nonlinear ionization of organic molecules in high intensity laser fields. *Phys. Rev. Lett.* **84**, 5082–5085 (2000).

21. Zavriyev, A., Bucksbaum, P. H.,Muller, H. G. & Schumacher, D.W. Ionization and dissociation in H_2 in intense laser fields at 1.064μm, 532nm and 355 nm. *Phys. Rev. A* **42**, R5500–R5513 (1990).

22. Zavriyev, A., Bucksbaum, P. H., Squier, J. & Salin, F. Light-induced vibrational states in H_2^+ and D_2^+ in intense laser fields. *Phys. Rev. Lett.* **70**, 1077–1080 (1993).

23. Seideman, T., Ivanov, M. Yu. & Corkum, P. B. The role of electron localization in intense field molecular ionization. *Phys. Rev. Lett.* **75**, 2819–2822 (1995).

24. Zuo, T. & Bandrauk, A. D. Charge-resonance-enhanced ionization of diatomic molecular ions by intense lasers. *Phys Rev. A* **52**, R2511–R2514 (1995).

25. Delone, N. B. & Krainov, V. P. Energy and angular electron spectra for the tunnel ionization of atoms by strong low-frequency radiation. *J. Opt. Soc. Am. B* **8**, 1207–1212 (1991).

26. Peek, J.M. Inelastic scattering of electrons by the hydrogen molecular ion. *Phys. Rev.* **134**, A877–A883 (1964).

27. Ammosov, M. V., Delone, N. B. & Krainov, V. P. Tunnel ionization of complex atoms and of atomic ions in an alternating electromagnetic field. *Zh. Eksp. Teor. Fiz.* **91**, 2008–2013 (1986); *Sov. Phys. JETP* **64**, 1191–1194 (1989).

28. Keldysh, L. V. Ionization in the field of a strong electromagnetic wave. *J. Exp. Theor. Phys.* **47**, 1945–1957 (1964).

29. Dietrich, P., Ivanov, M. Yu., Ilkov, F. & Corkum, P. B. Two-electron dissociative ionization of H_2 and D_2 in infrared fields. *Phys. Rev. Lett.* **77**, 4150–4153 (1996).

30. Macklin, J. J., Kmetic, J. D. & Gordon, C. L. High-order harmonic generation using intense femtosecond pulses. *Phys. Rev. Lett.* **70**, 766–769 (1993).

31. Bartels, R. et al. Shaped-pulse optimization of coherent emission of high-harmonic soft X-rays. *Nature* **406**, 164–166 (2000).

32. Mohideen, U. et al. High intensity above-threshold ionization of He. *Phys. Rev. Lett.* **71**, 509–512 (1993).

33. Paulus, G. G., Nicklich, W., Xu, H., Lambropoulos, P. & Walther, H. Plateau in above threshold ionization spectra. *Phys. Rev. Lett.* **72**, 2851–2854 (1994).

34. Feuerstein, B. et al. Separation of recollision mechanisms in nonsequential strong field double ionization of Ar: The role of excitation tunneling. *Phys. Rev. Lett.* **87**, 043003–043007 (2001).

35. Becker, A. et al. Laser-induced inner shell vacancies in double ionized argon. *J. Phys. B* **33**, L547–L552 (2000).

36. Bhardwaj, V. R. et al. Few cycle dynamics of multiphoton double-ionization. *Phys. Rev. Lett.* **86**, 3522–3525 (2001).

37. Rischel, C. et al. Femtosecond time-resolved X-ray diffraction from laser-heated organic films. *Nature* **390**, 490–492 (1997).

38. Ihee, H. et al. Direct imaging of transient molecular structures with ultrafast diffraction. *Science* **291**, 458–462 (2001).

39. Ivanov, M. Yu., Corkum, P. B., Zuo, T. & Bandrauk, A. D. Routes to control of intense-field atomic polarizability. *Phys. Rev. Lett.* **74**, 2933–2937 (1995).

40. Neutze, R. et al. Potential for biomolecular imaging with femtosecond X-ray pulses. *Nature* **406**, 752–757 (2000).

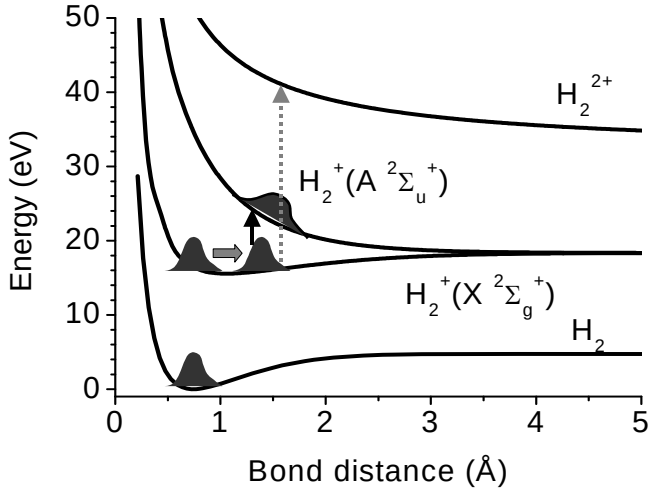

Figure 1 Important potential-energy curves for H_2 and its ions. Ionizing H_2 forms a dual wave packet. One is a vibrational wave packet on the ground (Σ_g) state of H_2. (shown). The other is an electron wave packet that moves in the laser field. The vibrational wave packet evolves until H_2^+ is excited by inelastic scattering caused by the returning electron wave packet.

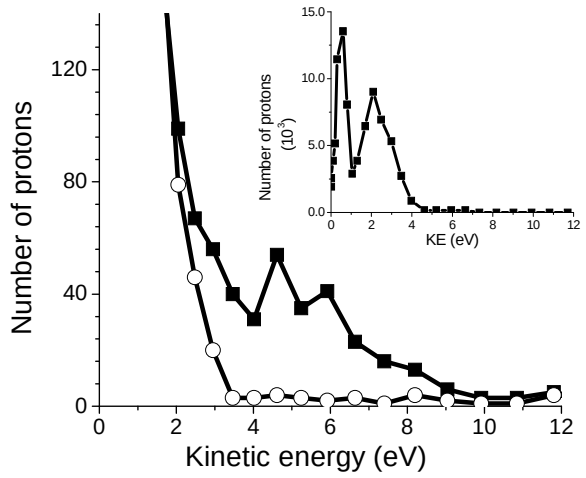

Figure 2 The number of protons measured per unit energy as a function of the proton kinetic energy. The upper curve is obtained with linear polarized light, whereas the lower curve is obtained with elliptically polarized light (ellipticity $E_y/E_x = 0.3$; E_x and E_y are defined in the text). Intermediate ellipticities fall between these curves. The main plot is for perpendicularly aligned molecules, the inset is for molecules aligned parallel to the laser field (KE, kinetic energy).

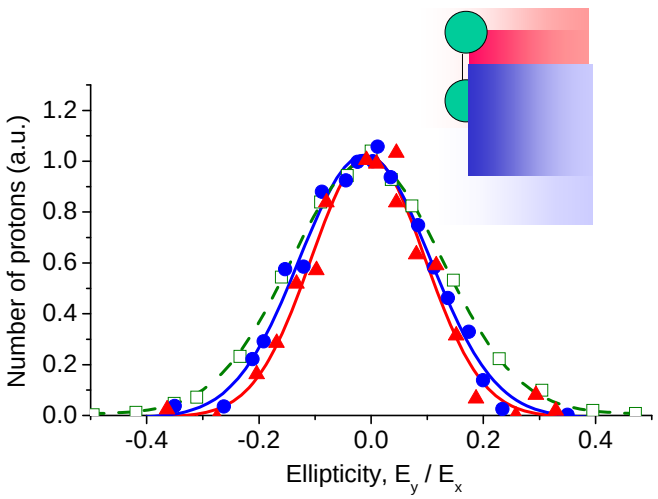

Figure 3 Ellipticity dependence of the number of energetic protons produced when an intense laser field ionizes H_2. Such narrow ellipticity dependence is characteristic of inelastic scattering between the recollision electron and the ion. The data is for H_2 aligned both parallel (blue filled circles) and perpendicular (red filled triangles) to the laser field. For comparison purposes, the ellipticity dependence of the double-ionization probability of argon, an atom with almost the same ionization potential, is shown (open green squares). The inset illustrates that elliptically polarized light can redirect the electron so that recollision becomes impossible (see text). (a.u., arbitrary units.)

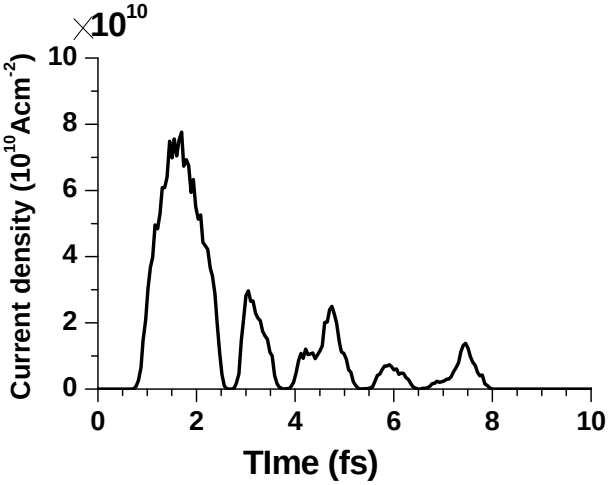

Figure 4 The calculated electron current density experienced by the ion as a function of time after ionization. Only electrons with sufficient energy for inelastic scattering are included.

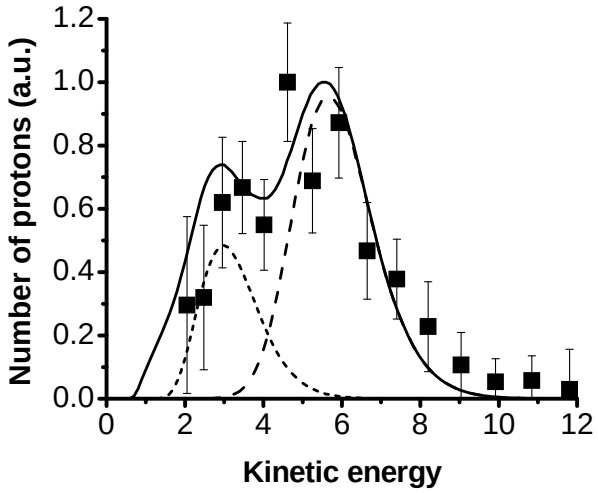

Figure 5 Observed (data points) and calculated (solid curve) kinetic-energy spectrum for the energetic protons caused by inelastic scattering. The agreement confirms the time dependence of the current density. The dashed lines show the contributions from the first (long dash) and third electron micro-bunch (short dash).

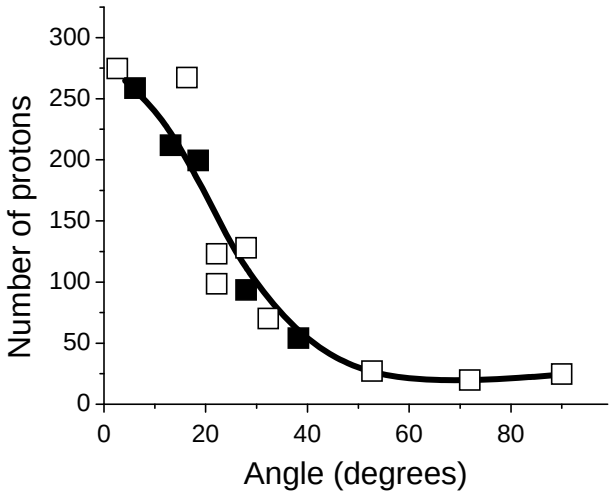

Figure 6 Angular dependence of the double-ionization (excitation) probability due to recollision. Data were taken from 40^o on one side of parallel to 90^o on the other side to ensure that the results were symmetric. All data points are included in the figure. Filled data points represent data on one side (0 to -40^o) and the open points represent the other side (0 to 90^o). Inelastic scattering is about 10 times more likely for a molecule aligned parallel to the field than for a molecule aligned perpendicular to the field.

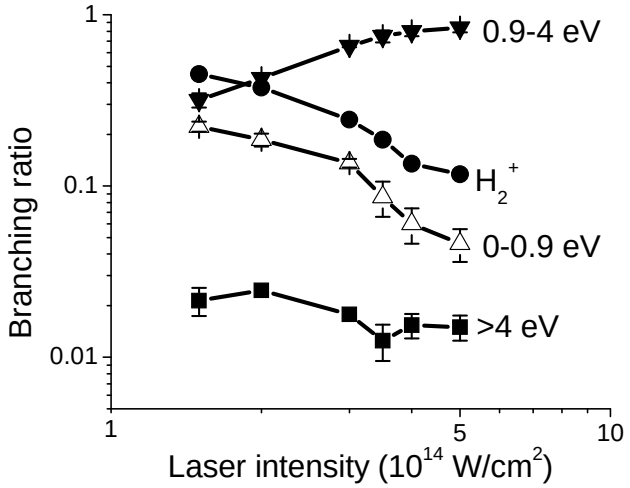

Figure 7 Intensity dependence of the double-ionization (excitation) probability. As with helium, the double-ionization probability (squares) is almost independent of the laser intensity in the non-sequential range. The other channels are bond softening (upwardpointing triangles), enhanced ionization (downward pointing triangles) and H_2^+ (circles).

CHAPITRE 2

DES MESURES ATTOSECONDES SANS IMPULSIONS LASERS ATTOSECONDES

Pour étudier la dynamique moléculaire, la technique pompe-sonde est très utilisée. La pompe démarre une réaction photochimique par inversion de population sur un état excité. Si l'état excité à une géométrie différente de l'état fondamental, un paquet d'onde vibrationnel est créé. La sonde permet de mesurer la dynamique associée à la propagation du paquet sur la surface potentiel de l'état excité. Le développement de sources lasers ultra-brèves permet de mesurer des dynamiques toujours plus rapides. Cette idée pousse les laseristes à produire des impulsions lasers toujours plus courtes. Des impulsions d'une durée de 250 attosecondes sont maintenant disponibles.

Dans l'article associé à ce chapitre (Niikura *et al.* Nature **421**, 827 (2003)), nous utilisons l'une des connaissances acquises au chapitre 1 : des mesures attosecondes sont possibles sans pour autant utiliser des impulsions lasers attosecondes. Ceci est possible lorsque deux paquets d'ondes sont corrélés par un processus attoseconde et que l'on contrôle l'une des paquets avec une précision attoseconde. Dans l'article associé au chapitre 1, nous avons montré que le paquet d'onde électronique généré par ionisation tunnel revient à sa source sous la forme d'un train d'impulsions attosecondes (la polarisation du champ laser doit-être linéaire). L'expérience nous montre que lorsque la longueur d'onde du champ laser est de 800 nm, près de 50 % de la population électronique revient à la source après avoir passé 1.8±0.5fs dans le continuum. Le reste de la population revient à de plus grand délai. C'est ce que l'on appelle la recollision. Des calculs classiques montrent que le temps de retour peut-être contrôlé en changeant la longueur d'onde du champ laser. Le délai entre l'ionisation et la première recollision est de 2/3 de la période optique. Pour ce qui est de la proportion de population électronique qui revient lors de la première collision, elle est insensible à la longueur d'onde. Nous contrôlons avec une précision de quelques centaines d'attosecondes le temps de retour

de ce paquet d'onde. Pour faire des mesures attosecondes, il faut corréler ce paquet à un autre. L'ionisation d'une molécule nous donne cette corrélation, un paquet d'onde vibrationnel est corrélé avec le paquet d'onde électronique.

En analogie avec la technique pompe-sonde, l'ionisation qui génère les deux paquets d'ondes corrélés est la pompe. La sonde est l'électron qui revient avec un délai d'environ 2/3 de la période optique. Changeant la fréquence du champ laser, nous pouvons varier le délai entre la pompe et la sonde. Dans cet article, nous mesurons le déplacement du paquet d'onde vibrationnel suivant l'ionisation de D_2 vers D_2^+ pour des délais entre 1.8 et 4.2 fs. Celui-ci se déplace sur l'état $X\ ^2\Sigma_g^+$. La recollision induit une collision inélastique qui excite D_2^+ vers ces états dissociatifs. Mesurant l'énergie cinétique des fragments D^+ en fonction de la fréquence du champ laser (équivaut au délai entre l'ionisation et la recollision), nous pouvons suivre avec une précision de quelques centaines d'attosecondes le déplacement du paquet d'onde vibrationnel. Nous comparons nos mesures expérimentales à des simulations numériques de l'équation de Schrödinger. En plus de réaliser ces simulations, j'ai aussi fait l'analyse des spectres expérimentaux. C'est le Dr. H. Niikura qui était responsable de l'expérience.

Pour pouvoir faire des mesures ultra-brèves, il est généralement accepté que des impulsions lasers d'autant plus brèves doivent être générées. Récemment, une étude temporelle de la relaxation suivant l'excitation électronique d'un électron de cœur du Krypton[1] a été rendu possible par l'utilisation d'impulsions attosecondes[2,3]. Une autre approche est possible pour sonder la dynamique ultra-brève, soit l'enchevêtrement, laquelle améliore la précision des mesures en optique quantique[4,5]. Dans cet article, nous utilisons cette approche pour observer le déplacement du paquet d'onde vibrationnel durant les premières femtosecondes suivant l'ionisation multiphotonique de D_2 vers D_2^+. Utilisant la corrélation entre le paquet d'onde vibrationnel et électronique produite lors de l'ionisation, nous obtenons une résolution temporelle d'environ 200 attosecondes et spatiale de 0.05 Angstrom. Une impulsion laser intense infra-rouge contrôle le paquet d'onde électronique, et la recollision de celui-ci avec la source[6-11] sonde le déplacement du paquet d'onde vibrationnel. Nos résultats montrent que la

durée de l'impulsion laser n'est pas un obstacle aux mesures spectroscopiques, pour autant que le processus étudié comprend des paquets d'onde corrélés et que l'un d'entre eux peut-être controlé. La résolution spatial n'est pas limitée à la taille du point focal ou à la longueur d'onde du champ laser.[P.S.]

[P.S.] Les références de ce paragraphe se retrouvent aux pages 44 et 45.

Probing molecular dynamics with attosecond resolution using correlated wave packet pairs

Hiromichi Niikura*, F. Légaré*†, R. Hasbani*, Misha Yu Ivanov*,
D. M. Villeneuve* & P. B. Corkum*
*National Research Council of Canada, 100 Sussex Drive, Ottawa, Ontario K1A 0R6, Canada
†Université de Sherbrooke, Sherbrooke PQ, Canada

Abstract

Spectroscopic measurements with increasingly higher time resolution are generally thought to require increasingly shorter laser pulses, as illustrated by the recent monitoring of the decay of core-excited krypton[1] using attosecond photon pulses[2,3]. However, an alternative approach to probing ultrafast dynamic processes might be provided by entanglement, which has improved the precision[4,5] of quantum optical measurements. Here we use this approach to observe the motion of a D_2 vibrational wave packet formed during the multiphoton ionization of D_2 over several femtoseconds with a precision of about 200 attoseconds and 0.05 Angstrom, by exploiting the correlation between the electronic and nuclear wave packets formed during the ionization event. An intense infrared laser field drives the electron wave packet, and electron recollision[6–11] probes the nuclear motion. Our results show that laser pulse duration need not limit the time resolution of a spectroscopic measurement, provided the process studied involves the formation of correlated wave packets, one of which can be controlled; spatial resolution is likewise not limited to the focal spot size or laser wavelength.

Our experiment is analogous to conventional pump–probe measurements[12], but the pump and probe occur within one optical cycle, a process that we call 'sub-laser-cycle molecular dynamics' (Fig. 1a). Ionization, which forms correlated wave packets around each peak of the laser field, is the pump. By removing one electron (creating an electron wave packet in the continuum), we weaken the force binding the protons and therefore launch a correlated vibrational wave packet (Fig. 1b). Because of its small mass, only the electron wave packet is influenced by the laser field. In linear polarization, the electron wave packet is first moved away from the parent ion but is pulled back by the laser field. The probability of electron re-collision with the parent ion reaches a maximum at a well-defined laser phase, about two-thirds of an optical period after the electron's transition to the continuum (Fig. 1a). Re-collision probes the vibrational wave packet (Fig. 1b). Changing the laser wavelength delays re-collision just as changing the position of a translation stage changes an optical pump–probe delay. (Neither re-collision nor the pump–probe analogy is essential: fast measurements are possible in their absence if both correlated partners are controlled, as discussed below.) Re-collision between an electron and its parent ion has long been known as a source of high-harmonics emission[7,8,13,14] and generation of high-energy electrons[7,9]. It is also responsible for correlated multi-electron ionization in strong laser fields[7,10,13], fragmentation in small molecules[11] and attosecond pulse generation[2,3,15]. For molecules, re-collision will also imprint the spatial structure of the ion on the harmonic emission spectrum[16] or on the photoelectron spectrum[6] in analogy with conventional electron diffraction (see, for example, ref. 17).

We use 40-fs laser pulses with an intensity of 1.5×10^{14} W.cm^{-2} tunable from 800 to 1,850 nm. Ionization induces vertical population transfer from the D_2 (X 1Sg.) potential energy surface to the D_2^+ ($X\ ^2\Sigma_g^+$) surface, with less than 10^{-6} of the population transferred to any other levels of D_2^+ (I. Litvinyuk, P. Dooley, D.M.V. and P.B.C., manuscript in preparation). Because the equilibrium internuclear separation is greater for D_2^+ (1.06 Å) than for D_2 (0.74 Å), ionization initiates a vibrational wave packet motion (Fig. 1b). For all wavelengths that we use, the instantaneous ionization rate[18] is sharply peaked near the instantaneous maxima of the oscillating field. The ionization bursts last 190–300 as (800 nm

to 1.85 μm). The nuclei are essentially frozen by their inertia on that timescale, ensuring that the pump stage is the same for all wavelengths.

We use electron–ion re-collision to observe motion on the D_2^+ ($X\ ^2\Sigma_g^+$) surface. Although the electron returns to the parent ion several times after ionization, the first return of the electron wave packet dominates[6] and can thus be used as a probe pulse with a duration of about 1 fs at 800 nm (ref. 6). The time delay between the creation of the correlated wave packets and their re-collision (pump–probe delay) is controlled by varying the laser wavelength. Our delay times range from 1.7 to 4.2 fs (about two-thirds of the period for l. 800–1,850 nm).

Inelastic scattering of the electron with the parent ion leads to excitation or double ionization, giving rise to the dissociative fragments of D^+. The kinetic energy of the fragments is determined by the internuclear separation at the time of electron re-collision. By using a small aperture in the time-of-flight apparatus, we observe only those fragments that originate from molecules aligned perpendicular to the laser polarization. This configuration eliminates laser-induced coupling between $X\ ^2\Sigma_g^+$ and $A\ ^2\Sigma_u^+$. Our choice of alignment ensures that the wave packet motion is simple, that it can be easily modelled and that $A\ ^2\Sigma_u^+$ is a good reference state. The existence of the well-understood reference state allows us to unequivocally interpret the kinetic energy spectrum and use it to measure the position of the vibrational wave packet. Figure 2 shows the kinetic energy spectrum of D^+ that is due to re-collision, for all wavelengths that we have studied. Although many dissociation pathways contribute to the observed kinetic energy spectra, we can isolate the Su state as particularly significant. This is because, among all inelastic scattering events from the Σ_g surface, excitation to Σ_u has the highest cross-section over the energy range examined here[19]. In addition, the Σ_u leads to fragments with the second-largest kinetic energy. Therefore this channel is easily identified in Fig. 2.We have labelled the data points that we associate with this channel with triangles. In Fig. 2 we see the motion of the wave packet reflected in the shift of this peak to lower energy with longer wavelength light.

To convert the measured kinetic energy spectrum to the vibrational wave packet on the Σ_g surface, we use the reflection principle[20]. The transformation includes the radial

dependence of the collision cross-section, and a self-consistent addition of the kinetic energy of the D_2^+ Σ_g. wave packet, assuming that the initial average wave packet velocity is zero and initial average kinetic energy is given by the zero-point energy of D_2. We then fit the wave packet with a gaussian. Its projection back to the kinetic energy spectrum yields the solid curves in Fig. 2. The gaussian fit on Σ_g determines the experimentally measured wave packet and the position of its peak. We emphasize that this is a fit to the experimental data, not a theoretical curve.

Figure 3 is a plot of the experimentally determined internuclear separation as a function of time. We represent the position of the vibrational wave packet by the peak position of the gaussian at each laser wavelength. At each wavelength, the re-collision time is defined by the mean time for the electron wave packet's first return. This establishes the experimental points in Fig. 3. The error bars are determined by the deviation of the fit. We determine the position and the velocity of the wave packet with sub-fs, sub-Å resolution.

Because we are demonstrating a new technique for ultrafast measurement, it is important to compare our measurement against a standard. The solid line in Fig. 3 is the result of a simulation of the motion of a vibrational wave packet on the Sg surface by solving the time-dependent Schrödinger equation. The discrepancy is within the error bars.

The portion of the kinetic energy distribution that is higher than that assigned to the Σ_u state in Fig. 2 corresponds to transitions to the $D2^{++}$ state. For 800nm the re-collision kinetic energy is insufficient to ionize $D2^+$, but at other wavelengths a contribution can be seen. The peak at lower kinetic energy is not clearly identified. It contains contributions of other excited states and of the electron's multiple returns[6]. These are also seen to move to lower kinetic energies as the re-collision time is delayed.

Our current measurement accuracy is limited by noise, but noise in our data is not a fundamental limit. Using three-dimensional imaging detectors instead of observing through a small pinhole would increase our signal strength by about two orders of magnitude. A high-density jet source and a laser with higher repetition rate could further increase our signal by orders of magnitude.

Our method is based on the principle of creating two correlated wave packets that could be formed on any crest of the laser field.We assert that these wave packets are actually entangled. A field crest occurs once during each half-period throughout the 40-fs pulse. Unless the electron and vibrational wave packet are entangled, the kinetic energy spectrum for D^+ must have a 3-eV modulation (for 800 nm light, 1.5 eV per deuteron). Such modulation is well known in strong-field single-particle processes such as high harmonics generated by ionizing atomic media[8,9,13,14].

In fact, there is no 1.5 eV modulation in the kinetic energy spectrum at 800nm in Fig. 2. We measured the spectrum with higher resolution to seek such modulation; none was observed. These experimental results are consistent with the vibrational and
electron wave packets being entangled. Entanglement arises because the departing electron contains information on the nuclear coordinate at the time of ionization and on the excited state of the D_2^+ formed in the re-collision. By observing only the deuterium ions, we integrate over all final states of other unseen, but entangled, partner particles. Such partial measurement eliminates the interference.

Regarding future applications, we note that the ultimate time resolution of correlated measurements is determined by the energy bandwidth of the electron bunch—many tens of electron volts in the present experiment. To obtain a resolution of 200 as will be a challenge similar to that of producing the shortest optical pulses[2].

Also, as long as both particles can be controlled, re-collision is unnecessary. For example, if two electrons are ejected into a field in a correlated fashion, the time difference between their ejection is mapped onto the final energy and angular spectra[10,15,21].

Correlated particles produced in a process with important dynamics to probe can always be measured as long as at least one of the pair can be controlled. Because of their low mass, electrons are easily controlled, and at progressively higher intensitites, muons,
protons, alpha particles and ions are also controllable. Applying correlation to nuclear dynamics requires a means of stimulating a process such that it will occur with high probability during the duration of the intense ultrashort pulse initiating it. Nuclear processes can be stimulated in an analogous manner to inelastic scattering in our experiment—by using a precursor molecule (such as HCl) and forcing ‘re-collision’ between a proton and the heavy

nucleus with an intense few-cycle optical pulse. To follow the subsequent dynamics, the relative trajectories of the correlated, charged nuclear fragments, as influenced by the field, can be measured.

Regarding the 'probe', we note that any method of observing the relative evolution of the correlated particles can be used for measurement. In molecular science, harmonic generation is one possible method[16] where phase matching eliminates the contribution from all but the first electron wave packet return, which occurs about two-thirds of a period following ionization. Elastic scattering is a second possible method[6], with diffraction determining the nuclear position at the time of re-collision.

Methods

Production and control of the electron wave packet

An optical parametric amplifier is used to shift the 40-fs output of a Ti:sapphire laser system to longer wavelengths. We use 800 nm, 1.2μm, 1.53μm and 1.85μm pulses. Each ionizes D_2 near the field maximum and provides a progressively longer time delay between ionization and re-collision. Taking the peak of the first electron microbunch to be the delay time, this corresponds to delay times of 1.7, 2.7, 3.4 and 4.2 fs. Changing the wavelength has other implications. The intensity and wavelength determine the maximum re-collision energy $3.17q^2E^2/(4m\omega^2)$ of the electron[7] (q and m are the electron mass and charge, ω and E are the laser pulse's angular frequency and electric field amplitude at the time of ionization). We use a light intensity of $1.5\text{x}10^{14}\text{W.cm}^{-2}$, calibrated against the ionization of xenon. Whereas at 800 nm the peak kinetic energy of the re-colliding electron is 30 eV, the ω^{-2} scaling of the kinetic energy means that at 1.85μm the energy of the peak re-colliding electron is about 160 eV.

Kinetic energy analysis

The kinetic energy spectrum of D^+ was measured with a time-of-flight (TOF) mass spectrometer filled with 10^{-6} torr of D_2. The TOF axis was perpendicular to the direction of propagation of the laser beam. A 1-mm-diameter hole in the electrode placed 1.5 cm from the laser focus selects only those D^+ ions resulting from dissociation of D_2^+ molecules that are aligned along the TOF axis. For the high-resolution results taken with 800-nm light (not shown), the extraction field was 133 V cm^{-1} and the acceptance angle of the TOF was 6 degrees at 8 eV. For the lower-resolution results, the extraction field was 400 V cm^{-1} giving an acceptance angle of 9 degrees at 8 eV.

Selection of the re-collision channel

Deuterium ions are produced by a number of processes during strong field ionization of D_2. We distinguish fragments resulting from inelastic scattering caused by the returning electron (Fig. 2) from those produced by any other process (such as sequential double ionization[22], bond softening[23] and enhanced ionization[24–27]) using the strong sensitivity of recollision phenomena to the ellipticity of the light polarization[6,7,13]. It only takes a small ellipticity to displace the electron laterally with respect to the parent ion so recollision is impossible7. In strong fields, the difference between the spectrum obtained with linear and elliptically polarized light is due to recollision.

Acknowledgements

We acknowledge discussions with A. Stolow, A. Sokolov, A. D. Bandrauk, S. Chelkowski and J. Marangos. The authors appreciate financial support from Canada's Natural Science and Engineering Research Council, the Canadian Institute for Photonics Innovation, and Le Fonds Québécois de la Recherche sur la Nature et les Technologies.

References:

1. Drescher, M. et al. Time-resolved atomic inner-shell spectroscopy. *Nature* **419**, 803–807 (2002).

2. Hentschel, M. et al. Attosecond metrology. *Nature* **414**, 509–513 (2001).

3. Paul, P. M. et al. Observation of a train of attosecond pulses from high harmonic generation. *Science* **292**, 1689–1692 (2001).

4. D'Ariano, G.M., Presti, P. L. & Paris, M. G. A. Using entanglement improves the precision of quantum measurements. *Phys. Rev. Lett.* **87**, 27040 (2001).

5. Resch, K. J., Lundeen, J. S. & Steinberg, A. M. Experimental observation of nonclassical effects on single-photon detection rates. *Phys. Rev. A* **63**, 020102 (2000).

6. Niikura, H. et al. Sub-laser-cycle electron pulses for probing molecular dynamics. *Nature* **417**, 917–922 (2002).

7. Corkum, P. B. Plasma perspective on strong field multiphoton ionization. *Phys. Rev. Lett.* **71**, 1994–1997 (1993).

8. Dietrich, P., Burnett, N. H., Ivanov,M. & Corkum, P. B.High harmonic generation and correlated twoelectron multiphoton ionization with elliptically polarized light. *Phys. Rev. A* **50**, 3585–3588 (1994).

9. Paulus, G. G., Nicklich, W., Xu, H., Lambropoulos, P. & Walther, H. Plateau in above threshold ionization spectra. *Phys. Rev. Lett.* **72**, 2851–2854 (1994).

10. Weber, Th. et al. Correlated electron emission with multiphoton double ionization. *Nature* **405**, 658–661 (2000).

11. Bhardwaj, V. R., Rayner, D. M., Villeneuve, D. M. & Corkum, P. B. Quantum interference in double ionization and fragmentation of C6H6 in intense laser fields. *Phys. Rev. Lett.* **87**, 253003 (2001).

12. Zewail, A. H. Femtosecond chemistry. *Science* **242**, 1645–1653 (1988).

13. Krause, J. L., Schafer, K. J. & Kulander, K. C. High-order harmonic generation from atoms and ions in the high intensity regime. *Phys. Rev. Lett.* **68**, 3535–3538 (1992).

14. Lewenstein,M., Balcou, Ph., Ivanov, M. Yu., L'Huillier, A. & Corkum, P. B. Theory of high-harmonic generation by low-frequency laser fields. *Phys. Rev. A* **49**, 2117–2132 (1994).

15. Ivanov, M., Corkum, P. B., Zuo, T. & Bandrauk, A. Routes to control of intense-field atomic polarizability. *Phys. Rev. Lett.* **74**, 2933–2936 (1995).

16. Lein,M., Hay, N., Velotta, R., Marangos, J. P. & Knight, P. L. Role of the intramolecular phase in highharmonic generation. *Phys. Rev. Lett*. **88**, 183903 (2002).

17. Hargittai, I. & Hargittai, M. *Stereochemical Applications of Gas-Phase Electron Diffraction* (VCH, New York, 1998).

18. Yudin, G. L. & Ivanov, M. Yu. Physics of correlated double ionization of atoms in intense laser fields: Quasistatic tunneling limit. *Phys. Rev. A* **63**, 033404 (2001); erratum 64, 019902 (2001).

19. Peek, J. M. Inelastic scattering of electrons by the hydrogen molecule ion. *Phys. Rev. A* **134**, 877–883 (1964).

20. Schinke, R. *Photodissociation Dynamics* 114–115 (Cambridge Univ. Press, Cambridge, UK, 1993).

21. Itatani, J. et al. Attosecond streak camera. *Phys. Rev. Lett.* **88**, 173903 (2002).

22. Lambropoulos, P. Mechanisms for multiple ionization of atoms by strong pulsed lasers. *Phys. Rev. Lett.* **55**, 2141–2144 (1985).

23. Zavriyev, A., Bucksbaum, P. H.,Muller, H. G. & Schumacher, D.W. Ionization and dissociation of H_2 in intense laser fields at 1.064mm, 532 nm, and 355 nm. *Phys. Rev. A* **42**, R5500–R5513 (1990).

24. Codling, K. & Frasinski, L. J.Dissociative ionization of small molecules in intense laser fields. *J. Phys. B* **26**, 783–809 (1993).

25. Seideman, T., Ivanov, M. Yu. & Corkum, P. B. Role of electron localization in intense-field molecular ionization. *Phys. Rev. Lett.* **75**, 2819–2822 (1995).

26. Zuo, T. & Bandrauk, A. D. Charge-resonance-enhanced ionization of diatomic molecular ions by intense lasers. *Phys Rev. A* **52**, R2511–R2514 (1995).

27. Constant, E., Stapelfeldt, H. & Corkum, P. B. Observation of enhanced ionization of molecular ions in intense laser fields. *Phys. Rev. Lett.* **76**, 4140–4143 (1996).

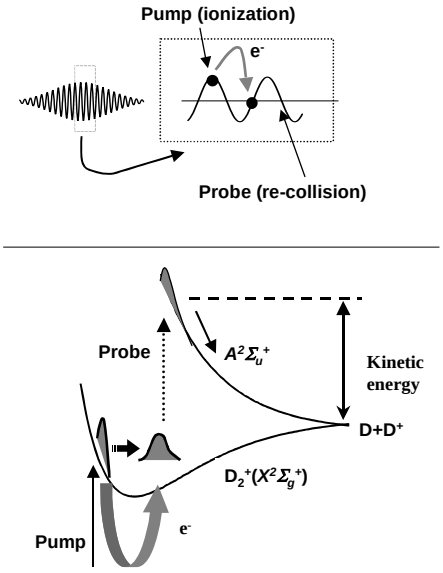

Figure 1 Processes probed and exploited with the sub-laser-cycle dynamics method using correlated wave packet pairs. a, Ionization forms correlated electronic and vibrational wave packets near each peak of the laser field. b, The vibrational wave packet moves on the D_2^+ ($X\ ^2\Sigma_g^+$) surface while the laser field causes the electron wave packet to re-collide (represented by a thick arrow in a and b). Inelastic scattering during re-collision probes the vibrational wave packet's position. We measure the kinetic energy of the D^+ fragments(b).

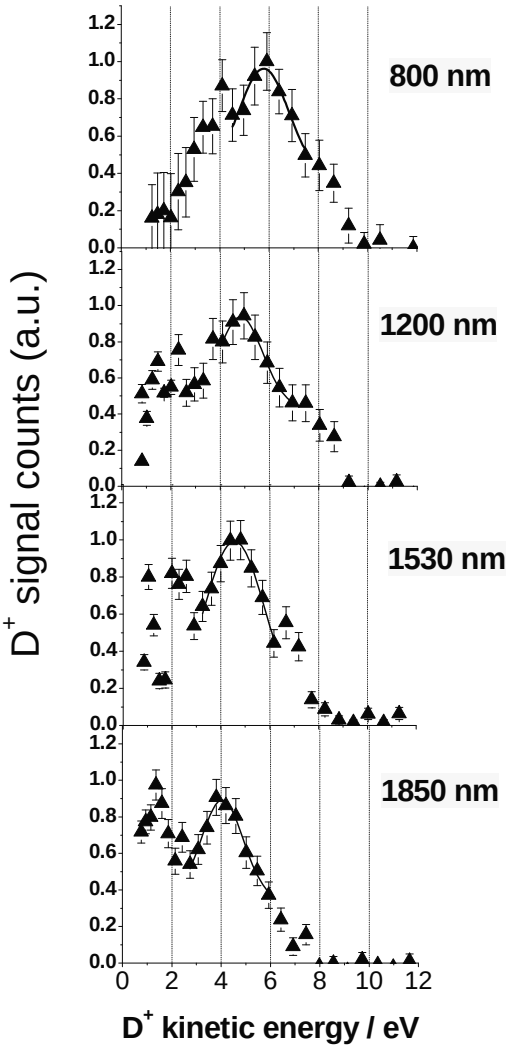

Figure 2 Kinetic energy distribution of D^+ at different pump–probe delay times. Shown is the experimental kinetic energy distribution of D^+ obtained using four different laser wavelengths, corresponding to different pump–probe delay times. Experimental error is estimated for each point by taking the square root of the signal counts. We identify the largest high-energy peak by the open data points with dissociation from D_2^+ ($A\ ^2\Sigma_u^+$). The curve is obtained by a fit to the data as described in the text.

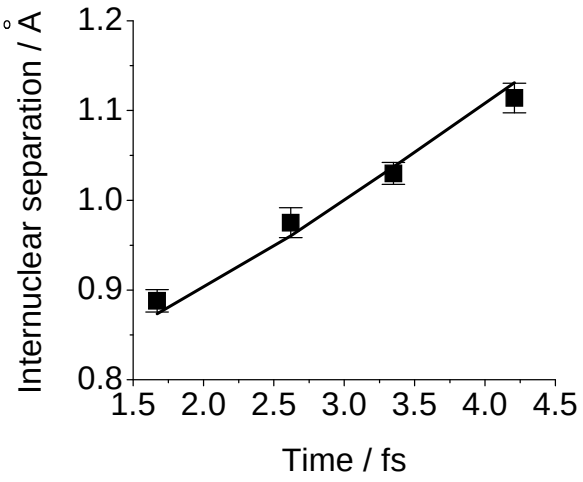

Figure 3 The measured wave packet position as a function of time. To associate the laser wavelength with the time of re-collision, we use the mean time of re-collision for the first electron micro-bunch at each laser wavelength. The position is determined from the peak of the fit in Fig. 2. The experimental error bars are determined by the error of the fit. The solid line is the calculated nuclear position as a function of time for a wave packet evolving on the D_2^+ ($X\ ^2\Sigma_g^+$) state. Because the time window that we measure is only about one-quarter of the full vibrational period of D_2^+ ($X\ ^2\Sigma_g^+$), the motion is almost linear.

CHAPITRE 3

ÉTUDE TEMPORELLE DE LA DOUBLE IONISATION DE D_2 INDUITE PAR UNE IMPULSION LASER ULTRA-BRÈVE

Ce chapitre et les deux prochains constituent le coeur de mon projet doctoral. Nous voulons étudier des processus moléculaires femtosecondes (fs) par explosion coulombienne. Pour la première fois, l'explosion coulombienne est étudiée avec des impulsions lasers à quelques cycles optiques. Chaque chapitre constitue une étape méthodologique.

Les impulsions lasers intenses et ultra-brèves (inférieures à 10 fs) sont générées en utilisant la propagation non-linéaire à l'intérieur d'une fibre creuse remplie d'argon. L'impulsion d'entrée a une durée de 45 fs centrée à 800 nm. À la sortie de la fibre, nous comprimons les impulsions à l'aide de mirroirs multicouches. À l'heure actuelle, nous générons des impulsions laser d'une durée de 8 fs (aussi à 800 nm). Nous mesurons le champ électrique de ces impulsions laser à l'aide de la technique SPIDER (*spectral phase interferometry for direct electric-field reconstruction*).

L'article associé à ce chapitre (Légaré *et al.* Physical Review Letters **91**, 093002 (2003)) étudie la double ionisation de D_2 à l'aide d'impulsions sub-10 fs. L'avantage d'étudier cette molécule est que nous pouvons simuler l'interaction laser-molécule et, en les comparant, comprendre en détails nos résultats expérimentaux.. L'état final est aussi purement coulombien ($D^+ + D^+$). Nous traitons l'ionisation en utilisant un modèle de type ADK tandis que la vibration de l'ion intermédiaire D_2^+ est résolue à l'aide de l'équation de Schrödinger dépendante du temps. En utilisant le concept d'horloge moléculaire développé au chapitre 1, nous pouvons déterminer le délai entre l'éjection du premier et du deuxième électron. Nous montrons que les processus complexes d'interaction laser-molécule sont beaucoup moins dominants lorsque des impulsions ultra-brèves (< 10 fs) sont utilisées. Ceci nous permet de conclure que l'explosion coulombienne laser est une technique permettant la mesure de la

structure moléculaire avec une résolution inférieure à l'Angstrom. Ils sont les tous premiers travaux expérimentaux étudiant l'interaction des molécules avec des impulsions aussi courtes et intenses.

La conclusion de ce chapitre est que l'ionisation utilisant des impulsion ultra-brèves est principalement séquentielle et semblable à l'ionisation d'un atome, ce que simplifie grandement l'analyse des résultats expérimentaux. Ceci est rendu possible grâce au développement d'impulsions lasers ultra-brèves, défi principal de mon projet doctoral. J'ai eu une aide appréciable de mon collègue Dr. F. Quéré avec qui j'ai implémenté la technique SPIDER. Mes collègues Dr. I.V. Litvinyuk et Dr. P.W. Dooley ont pour le part conçu la chambre d'interaction laser-molécule.

De plus, par des simulations numériques que j'ai effectuées, nous comprenons maintenant en détail les différents mécanismes d'ionisation des molécules. Ces simulations montrent que même avec une impulsion laser approchant les 0 fs, la nature de l'ionisation déforme l'image de la structure moléculaire. Pour D_2, nos simulations montrent une déformation d'environ 0.1 Å. Des conclusions générales sont émises dans cet article et peuvent être appliquées à des systèmes moléculaires plus complexes.

L'ionisation de D_2 prépare un paquet d'onde vivrationnel dans l'état électronique fondamental de D_2^+. L'éjection du deuxième électron place une paire d'ions D^+ sur un potentiel coulombien. La mesure de l'énergie cinétique des D^+ détermine le délai entre la première et la deuxième ionisation. Due à la diminution du potentiel d'ionisation et à l'augmentation rapide de l'intensité, le temps de vie de l'ion D_2^+ est inférieur à 5 fs lorsque l'impulsion laser intense a une durée de 8.6 fs. Nous simulons l'explosion coulombienne de l'état vibrationnel fondamental de D_2 avec une impulsion de 4 fs et comparons les résultats avec nos observations expérimentales.

Time-Resolved Double Ionization with Few Cycle Laser Pulses

F. Légaré[1,2], I.V. Litvinyuk[1], P.W. Dooley[1,3], F. Quéré[1], A.D. Bandrauk[2],
D.M. Villeneuve[1], and P. B. Corkum[1]

[1]*National Research Council of Canada, Ottawa, Ontario, Canada K1A 0R6*

[2]*Département de Chimie, Université de Sherbrooke, Sherbrooke, Québec, Canada*

[3]*Department of Physics & Astronomy, McMaster University, Hamilton, Ontario, Canada*

Ionization of D_2 launches a vibrational wave packet on the ground state of D_2^+. Removal of the second electron places a pair of D^+ ions onto a Coulombic potential. Measuring the D^+ kinetic energy determines the time delay between the first and the second ionization. Caught between a falling ionization and a rapidly rising intensity, the typical lifetime of the D_2^+ intermediate is less than 5 fs when an intense 8.6 fs laser pulse is used. We simulate Coulomb explosion imaging of the ground state wave function of D_2 by a 4 fs optical pulse and compare with our experimental observations.

Femtosecond pump-probe spectroscopy is an extremely powerful technique for studying molecular dynamics [1]. However, inferring mechanisms responsible for the dynamics from these measurements is difficult. Imaging molecular structure would be much more direct and intuitive. We show that laser induced Coulomb explosion for direct imaging of molecular structure is within reach.

Accurate Coulomb explosion imaging of molecular structure requires that the molecule reach a sufficiently high charge state for the inter-ionic potential to be approximated by Coulomb's law [2]. This charge state must be reached while the ions are inertially confined in their original configuration. Inertial confinement is readily achieved for small molecular ions moving at megavolt kinetic energies when they pass through a thin foil [3]. However, this technique is not well suited as a probe in pump-probe measurements.

For optically driven Coulomb explosion imaging, inertial confinement has been a demanding requirement that has only been satisfied with ~50 fs pulses in experiments involving iodine [4]. In other systems, dynamics of intermediate ionic states distorts the image [5-9]. Few-cycle laser pulses [10] are now generated in a few laboratories. Such pulses should be short enough for distortion-free Coulomb explosion imaging.

Using nuclear motion (a "molecular clock" [11]) to time-resolve the sequential double ionization of D_2 molecules, we show that ~9 fs optical pulses can be used to inertially confine virtually any molecule or molecular ion during its ionization phase. Both calculations and experiments with 9 fs pulses show that the two electron removal $D_2 \rightarrow D_2^{++}$ can be performed within ~5 fs. Furthermore, we present a simulation of Coulomb explosion imaging of D_2 using currently available ~4 fs, $\sim 5\times10^{15}$ W/cm^2 pulses [10].

Also of interest is the fact that we achieve an ionization rate of $\sim 10^{16}$ s^{-1}. The very high ionization rate is due to the rapid increase in pulse intensity combined with a rapidly decreasing ionization potential due to nuclear motion. We make the transition from no ionization to complete ionization in less than two optical cycles. Therefore, we can suppress (or control) processes that occur at larger internuclear separations even for a light molecule such as D_2.

To generate our ~9 femtosecond pulses, the output of a Ti:Sapphire regenerative (810 nm, 40 fs, 250 μJ, 500 Hz repetition rate) amplifier was coupled into a hollow core fibre (250 μm diameter, 100 cm long) filled with 1 atm of argon . The self-phase modulation [10] during propagation of the optical pulses through the hollow fibre broadens the spectral bandwidth from 30 to 200 nm. The pulse was compressed using multiple reflections from a pair of chirped mirrors. The resulting pulses were characterized using SPIDER [12]. As shown in the inset of Fig. 1, we obtained 8.6 fs linearly polarized pulses. 84% of the energy is contained within the main peak and 95% within a 100 fs window. An achromatic quarter wave plate was used to produce circular polarization.

The laser beam was focused inside the high vacuum experimental chamber (10^{-9} mbar background pressure) by an on-axis parabolic mirror (f/2, f = 50 mm) into a collimated beam of deuterium molecules. We estimate the beam diameter at the focus to be ~5 μm and the confocal parameter ~100 μm.

The molecular beam was produced by expanding 25 mbar of D_2 through a 100 μm aperture into the vacuum. The jet was skimmed to produce a beam with a thickness of 40 μm (in the laser propagation direction), a height of 1.5 mm, and a density of ~10^{10} molecules/cm^3 ($P \approx 10^{-7}$ mbar). Since the confocal parameter of the laser beam was greater than the molecular beam's thickness, molecules see only a slight intensity variation along the laser propagation direction. The peak laser intensity was determined by measuring the recoil momentum distribution of D_2^+ ions for circularly polarized pulses [13].

When a femtosecond pulse doubly ionizes D_2, Coulomb repulsion between the deuterium ions converts their initial potential energy to kinetic energy. Coulomb explosion fragments were analyzed using an imaging time-of-flight mass spectrometer [14]. The molecular beam, mass spectrometer axis, and laser beams were mutually orthogonal. Deuterons were detected using a helical delay-line anode time- and position-sensitive detector. From the impact data, the complete velocity vector for each deuteron was determined.

The distribution of kinetic energy per deuteron is shown in Fig. 1 for linearly polarized 8.6 fs and 40 fs pulses. In both cases, the peak intensity is 5×10^{14} W/cm^2. The vertical axis is normalized at 3 eV. For the 40 fs pulse, the energy spectrum is dominated by a peak around 3

eV with a smaller peak observed at ~ 0.7 eV. Those features are signature of laser field induced processes – bond softening and enhanced ionization – discussed below.

In D_2 a laser pulse first creates a molecular ion. With a long (≥ 40 fs) pulse the ion has enough time to undergo field-assisted dissociation [15] (known as bond softening when the field oscillates at optical frequencies [16]) before the second electron is ionized. In the process of bond softening the internuclear separation passes through a region where the ionization rate maximizes (enhanced ionization), exceeding even the rate for infinitely separated atoms by more than an order of magnitude [5,7-9]. Both processes originate in the multiphoton coupling of the Σ_g and Σ_u levels of the ion [7,8]. This coupling is only efficient for molecules parallel to the field leading to fragments that are directed primarily along the laser polarization. The peak at ~ 0.7 eV in Fig. 1 comes from molecular ions that bond soften without further ionization. The peak at ~ 3 eV is a signature of enhanced ionization [7,8].

An energetic fragment channel between 4-10 eV has been observed [11,17-19] with ~ 40 fs pulses. Such high-energy fragments can only come from excitation or double ionization at small internuclear separations. With 40 fs pulses, these fragments are caused by re-collision [11,19] (described below). Compared with enhanced ionization, re-collision is a minor dissociation channel (~ 5%) and is barely observable on the linear scale in Fig. 1.

With our 8.6 fs pulse, however, 4-10 eV energy fragments represent a major dissociation channel (~20%). By measuring the correlated spectrum we confirm that the 4-10 eV ions come from double ionization. As the pulse duration is increased from 8.6 fs to 40 fs, the high-energy peak shifts to lower energies until it merges into the enhanced ionization peak. We now concentrate on the physical origin of this peak.

The observed double ionization can be either sequential or non-sequential. The dominant non-sequential ionization mechanism in strong laser fields is electron re-collision [11]. The first ionized electron is driven by the laser field and in linearly polarized light can inelastically scatter off its parent ion. Known as a re-collision, inelastic scattering is suppressed when the ellipticity increases i.e. the electron will miss the ion core.

Figure 2 compares results obtained with linearly (5×10^{14} W/cm^2) and circularly (1×10^{15} W/cm^2) polarized 10.5 fs pulses. Bond softening (BS) and enhanced ionization (EI)

are present in both spectra. Both spectra also have a peak at about 5 eV that we attribute to sequential double ionization (SI). An additional feature is observed in the linear case – an energetic plateau between 6 – 10 eV (RC). Its polarization sensitivity shows that it is due to electron re-collision. As we shall show below, in the other extreme of very high intensity pulses, the sequential double ionization peak grows and broadens until it dominates all other channels.

Figure 2 (inset) shows the angle dependence of the 0.5-4eV fragments (solid line) and the 4-10 eV fragments (dashed line). Enhanced ionization and bond softening channels are more directional than sequential double ionization. While the angle-resolved data was obtained using an 8.6 fs, 2.8×10^{15} W/cm^2 pulse, the angular dependence is insensitive to the peak laser intensity or whether we include re-collision in the 4-10 eV measurements.

One of our technical achievements is the use of a thin molecular beam [20]. It allows us to expose most of our target molecules to a rapidly increasing but near spatially uniform pulse intensity. Molecules only experience lower intensities in the radial extremes of the focus. Therefore, we can study sequential double ionization when the ionization rates are extremely large. The earlier the first ionization occurs, the faster the intensity will rise, and the sooner the second electron will be removed. This time difference can be measured using a "molecular clock" [11]. The first ionization starts the clock. The removal of the second electron promotes D_2^+ to D_2^{++} where Coulomb repulsion determines the kinetic energy of the deuterons. The deuteron kinetic energy is a measure of the time delay between first and second ionization.

Figure 3 shows the deuteron kinetic energy spectra obtained with circularly polarized light and laser intensities of 1.2×10^{15} W/cm^2 and 2.8×10^{15} W/cm^2. At 2.8 x 10^{15} W/cm^2 sequential double ionization is 15 times more probable than all other channels combined. In agreement with our qualitative prediction, the kinetic energy of deuterons is higher at higher laser intensity. At intermediate intensities (not shown) the kinetic energies are also intermediate.

For a quantitative comparison, we now model the results for the intensities used in Fig. 3. The calculations were performed using the actual time dependent field for the experimental

pulses. We assume that the rates for both stages of the D_2 ionization depend solely upon the corresponding ionization potentials and are described by atomic models [21]. The ionization potentials were calculated using potential energy surfaces for the D_2 ground state and the field-coupled surface for the ground state of the D_2^+.

During the first ionization step, the ground state vibrational nuclear wave function for D_2 was projected onto the D_2^+ potential. The radial distortion due to the coordinate dependence of the ionization rate was taken into account [22]. The resulting wave packet was propagated on the lowest quasi-static time-dependent D_2^+ potential [22] by numerical solution of the time-dependent Schroedinger equation. During the second ionization step, the wave packet was projected onto the Coulombic potential. This procedure yields the deuteron kinetic energy distribution.

In the model, we used circularly polarized light for comparison with the experimental data of Fig. 3. The total kinetic energy distribution was calculated by incoherently summing the weighted kinetic energy distributions obtained for various first and second ionization times within the duration of the pulse. The weighting factors also included the radial intensity distribution in the laser focus. The calculated kinetic energy spectra for intensities of 2.8×10^{15} W/cm^2 and 1.2×10^{15} W/cm^2 are shown in the inset of Fig. 3. In agreement with the experimental data, for higher laser intensity, the sequential double ionization peak shifts to higher energy. This is because the time delay between the first and the second ionization steps decreases.

Though in relatively good agreement with the experiment, the calculated sequential double ionization spectra overestimate the kinetic energy of the deuterons. The discrepancy corresponds to less than 1 fs in time delay. It should be noted that, while the inset of Fig. 2 shows that the ionization rate depends on the molecular orientation [13], the rate used in the model is not orientation dependent. In addition, atomic models often overestimate the molecular ionization rates [23] and the model that we used [21] does not include "over the barrier" ionization [24]. Finally, the calculation neglects the excited quasi-static state of D_2^+[22].

Figure 4 depicts the deuteron kinetic energy spectrum obtained using the most intense (8.6 fs, 2.8×10^{15} W/cm^2) linearly polarized pulse that we can produce. For comparison, calculated kinetic energy distributions for second ionizations that occur one optical cycle (2.7 fs) and two optical cycles (5.4 fs) after the first ionization step are included in Fig. 4. The experimental distribution peaks between the two calculated curves, suggesting that double ionization occurs on the average within 4 fs.

In conclusion, few-cycle pulses will allow nuclear motion to be frozen for almost any molecule. The inset in Fig. 4 depicts the density of the ground state wavefunction of D_2 (solid line), the Coulomb explosion image predicted for a 4 fs, 5.6×10^{15} W/cm^2 circularly polarized pulse (dotted line) and the reconstructed image [25] obtained from the experimental deuteron spectrum of Fig. 4 (dashed line). However, the calculation reveals that ~50% of the shift in the wavefunction's position imaged ~50% is caused by the ionization rate's dependence on the nuclear coordinate. The rest is nuclear motion. While nuclear motion will be slower in heavier molecules, the ionization rate's dependence on the nuclear coordinate will always be an important issue in Coulomb explosion imaging. To obtain accurate molecular structures, its influence will have to be removed.

Experiments with near single cycle pulse will face a new issue. For linear polarization, two electrons would need to occupy the barrier region simultaneously. This will surely impede the ionization process. By comparing linear and circular polarization, we expect to observe a Coulomb blockade in strong field ionization analogous to the Coulomb blockade studied in solid-state devices [26]. We expect that multi-electron ionization with few cycle pulses will require circular polarized light.

Acknowledgements:

The authors appreciate financial support from Canada's Natural Science and Engineering Research Council, Photonics Research Ontario and the Canadian Institute for Photonics Innovation, and Le Fonds Québécois de la Recherche sur la Nature et les Technologies. We acknowledge C. Ellert for his valuable contributions to this work.

References:

[1] A. H. Zewail, J. Phys. Chem. A **104**, 5660 (2000).

[2] Z. Vager, R. Naaman, and E. P. Kanter, Science **244**, 426 (1989).

[3] E. P. Kanter, P.J. Cooney, D. S. Gemmell, K.-O. Groeneveld, W.J. Pietsch, A.J. Ratkowski, Z. Vager, and B.J. Zabransky, Phys. Rev. A **20**, 834 (1979).

[4] D. T. Strickland, Y. Beaudoin, P. Dietrich, and P.B. Corkum, Phys. Rev. Lett. **68**, 2755 (1992).

[5] K. Codling, L. J. Frasinski, and P. A. Hatherly, J. Phys. B **22**, L321 (1989).

[6] M. Schmidt, D. Normand, and C. Cornaggia, Phys. Rev. A **50**, 5037 (1994).

[7] T. Seideman, M. Yu Ivanov, and P. B. Corkum, Phys. Rev. Lett. **75**, 2819 (1995).

[8] T. Zuo, and A. D. Bandrauk, Phys. Rev. A **52**, R2511 (1995).

[9] E. Constant, H. Stapelfeldt, and P. B. Corkum, Phys. Rev. Lett. **76**, 4140 (1996).

[10] M. Nisoli, S. De Silvestri, O. Svelto, R. Szipöcs, K. Ferencz, Ch. Spielman, S. Sartania, and F. Krausz, Opt. Lett. **22**, 522 (1997).

[11] H. Niikura, F. Légaré, R. Hasbani, A.D. Bandrauk, M. Yu Ivanov, D.M. Villeneuve, and P.B. Corkum, Nature **417**, 917 (2002).

[12] C. Iaconis, and I.A. Walmsley, Opt. Lett. **23**, 792 (1998).

[13] I.V. Litvinyuk, K.F. Lee, P. W. Dooley, D. M. Rayner, D. M. Villeneuve, and P. B. Corkum, Phys. Rev. Lett. **90**, 233003 (2003).

[14] P.W. Dooley, I.V. Litvinyuk, K.F. Lee, D. M. Rayner, D.M. Villeneuve, and P.B. Corkum, accepted to Phys. Rev. A.

[15] G.R. Hanson, J. Chem. Phys. **62**, 1161 (1975).

[16] A. Zavriyev, P. H. Bucksbaum, H. G. Muller, and D. W. Schumacher, Phys. Rev. A **42** R5500 (1990).

[17] C. Trump, H. Rottke, and W. Sandner, Phys. Rev. A **60**, 3924 (1999).

[18] A. Staudte, C. L. Cocke, M. H. Prior, A. Belkacem, C. Ray, H. W. Chong, T. E. Glover, R. W. Schoenlein, and U. Saalmann, Phys. Rev. A **65**, 020703(R) (2002).

[19] H. Sakai, J.J. Larsen, I. Wendt-Larsen, J. Olesen, P.B. Corkum, and H. Stapelfeldt, Phys. Rev. A **67**, 063404 (2003)

[20] P.W. Dooley, V.R. Bhardwaj, and P.B. Corkum, Proc. Int. Conf. Lasers '99, p. 8 (1999).

[21] G. L. Yudin, and M. Yu Ivanov, Phys Rev. A **64**, 013409 (2001).

[22] P. Dietrich, M.Yu. Ivanov, F.A. Ilkov, and P. B. Corkum, Phys. Rev. Lett. **77**, 4150 (1996).

[23] S. Hankin, D.M. Villeneuve, P.B. Corkum, and D.M. Rayner, Phys. Rev. Lett. **84**, 5082 (2000).

[24] S. Augst, D. Strickland, D. D. Meyerhofer, S. L. Chin, and J. H. Eberly, Phys. Rev. Lett. **63**, 2212 (1989).

[25] S. Chelkowski, P. B. Corkum, and A. D. Bandrauk, Phys. Rev. Lett. **82**, 3416 (1999).

[26] A. Imamoglu, and Y. Yamamoto, Phys. Rev. Lett. **72**, 210 (1994).

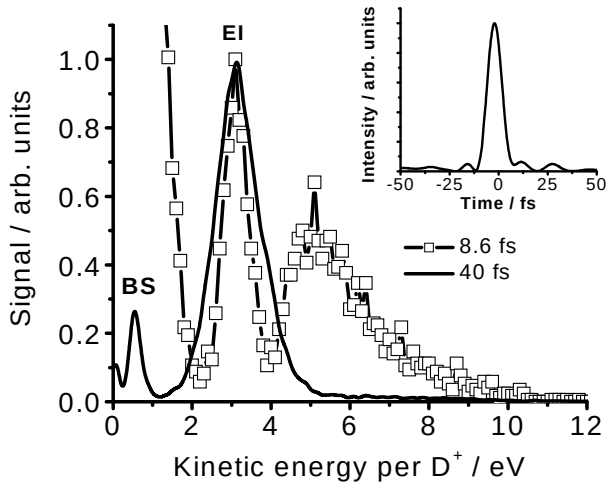

Fig. 1: Deuteron kinetic energy spectra at an intensity of 5×10^{14} W/cm^2 for linearly polarized pulse at durations of (a) 40 fs (solid line) and (b) 8.6 fs (squares). The time-dependent intensity profile for the 8.6 fs pulse is shown in the inset. BS: bond softening, and EI: enhanced ionization.

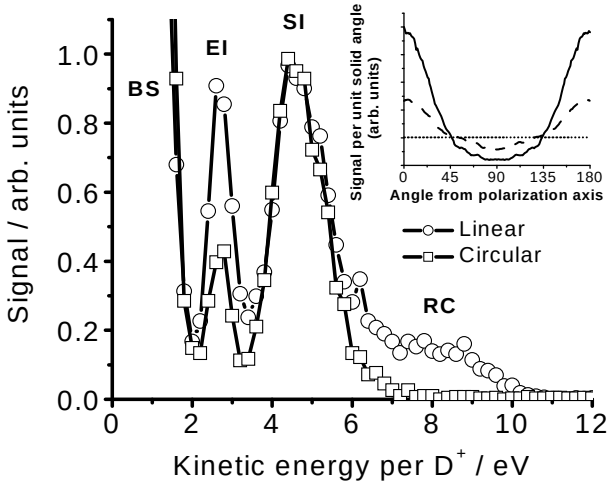

Fig. 2: Deuteron kinetic energy spectra for a 10.5 fs duration pulse with function of polarization. The electric field amplitude is equal in both cases. The intensity in the linear case is 5×10^{14} W/cm^2. Inset: Ion signal as a function of the angle between deuteron momentum and the laser polarization axis for (a) 0.5-4 eV deuterons (solid line), (b) 4-10 eV deuterons (dashed line), (c) an isotropic distribution (dotted line). The inset data were obtained using a linearly polarized, 8.6 fs, 2.8×10^{15} W/cm^2 laser pulse. RC: electron re-collision and SI: sequential double ionization.

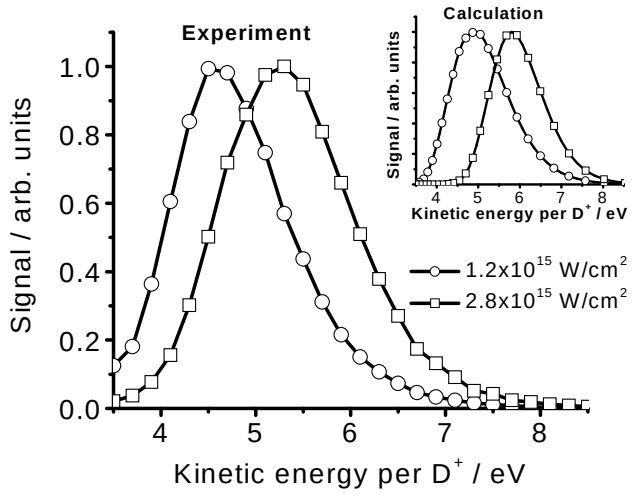

Fig. 3: Deuteron kinetic energy spectra for a 10.5 fs duration, circularly polarized pulse with an intensity of (a) 1.2×10^{15} W/cm^2 (circles) and (b) 2.8×10^{15} W/cm^2 (squares). Inset: Calculated spectra corresponding to (a) (dashed line) and (b) (solid line).

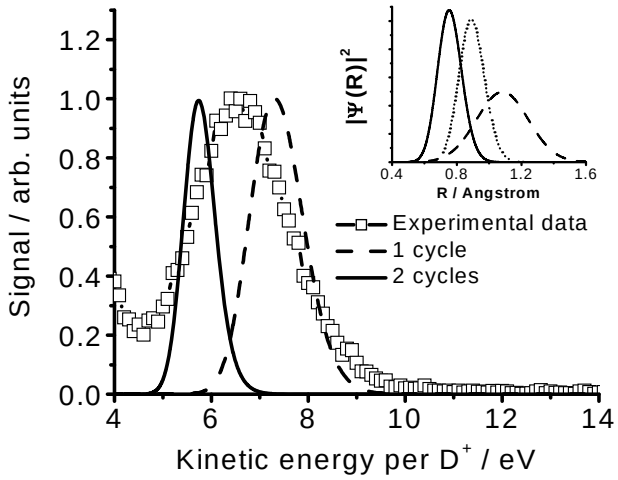

Fig. 4: Deuteron kinetic energy spectra for a linearly polarized, 8.6 fs duration pulse at intensity of 2.8×10^{15} W/cm^2 (squares). Also shown are calculated spectra for time delays of (a) one (dashed line) and (b) two (solid line) optical cycles between the first and second ionization steps. Inset: The density of the D_2 wavefunction for (a) the ground state (solid line), (b) Coulomb explosion image assuming a 4 fs pulse (dotted line), and (c) reconstructed image derived from the experimental spectrum of Fig. 4 (dashed line).

CHAPITRE 4

IMAGERIE DE MOLÉCULES TRIATOMIQUES PAR EXPLOSION COULOMBIENNE LASER

Ce quatrième chapitre étudie l'imagerie de systèmes triatomiques. L'imagerie de molécules diatomiques présente en effet peu d'intérêt pour la chimie, aucun processus de réarrangement n'y étant possible. Pour les triatomiques, l'absorption de photons peut induire des réarrangements du type ABC → ACB. De plus, pour une diatomique, un seul degré de liberté vibrationnel est présent. Pour les triatomiques, des vibrations asymétriques, symétriques et angulaires (angle entre deux liens chimiques) existent.

Pour les diatomiques, l'énergie des fragments lors de l'explosion coulombienne est directement reliée à la distance internucléaire, comme nous l'avons vu dans les trois derniers chapitres. Pour les polyatomiques, la reconstruction de la structure moléculaire n'est possible que si l'on mesure les vitesses tri-dimensionnelles de chacun des fragments atomiques. Expérimentallement, pour mesurer ces vecteurs, nous utilisons la spectroscopie de coincidence.

L'explosion coulombienne a été développée initialement en utilisant des processus de collision avec des feuilles minces (10 nm). Le temps moyen d'interaction dans ce type d'expérience est d'environ 100 attosecondes. Des mesures précises de structures moléculaires ont ainsi été faites. Cependant, il est difficile d'utiliser ces techniques dans des expériences pompe-sonde femtoseconde. C'est pour cette raison que les sources optiques représentent autant d'intérêt.

L'impulsion laser la plus courte générée pouvant provoquée l'explosion coulombienne a une durée d'environ 5 fs. Les impulsions attosecondes ne sont pas encore assez intenses. Ce temps est très court, mais quand même 50 fois plus long que le temps d'interaction lors d'une

collision. *Comment ceci influencera-t-il les mesures d'explosion coulombienne laser?* Nous avons répondu à cette question en étudiant deux triatomiques : D_2O et SO_2.

Ces résultats ont aussi été soumis à Physcical Review Letters pour les mêmes raisons que les travaux sur D_2. Ils sont les tous premiers travaux expérimentaux qui répondent à la question énoncée précédemment. Ma contribution à cet article est similaire à celle du chapitre 3 : génération et caractérisation d'impulsions ultra-brèves ainsi que des simulations numériques traitant l'interaction laser-molécule. Par une collaboration avec F. Krausz et P. Dombi, nous avons amélioré nos impulsions laser, améliorant ainsi nos résultats d'explosion coulombienne. Une contribution importante de mon collègue Kevin F. Lee est à souligner. C'est lui qui a écrit le programme permettant la reconstruction des structures moléculaires à partir des vitesses mesurées à l'aide de la spectroscopie de coincidence. Cette spectroscopie est faite dans la chambre d'interaction laser-molécule, conçue par mes collègues Dr. I.V. Litvinyuk et Dr. P.W. Dooley. Les Drs. S.S. Wesolowski et P.R. Bunker nous ont fourni certains potentiels ab-initio de D_2O, ce qui a nous a permis de confirmer que le potentiel décrivant D_2O^{4+} est coulombien pour la région spatiale qui nous intéresse. Ceci est due à une dynamique moléculaire sur les états de charge intermédiaires lors du processus d'ionisation. J'ai confirmé ceci par des simulations numériques utilisant les potentiels ab-initio, une propagation classique des atomes et un modèle atomique décrivant l'ionisation.

En utilisant des impulsions lasers intenses et ultra-brèves, nous ionisons des molécules jusqu'à l'explosion coulombienne. Nous utilisons le potentiel de Coulomb ou de type ab-initio pour reconstruire des images de la structure moléculaire de D_2O et de SO_2. Ceci est fait en utilisant la corrélation entre les vecteurs de vitesses des fragments explosés. Pour D_2O, un système léger et excessivement rapide, nous observons une déviation d'environ 0.3 Å et de 15^o avec la structure déjà connue. En simulant l'explosion Coulombienne de D_2O pour sa structure d'équilibre, nous montrons que la déviation est due à de la dynamique moléculaire durant l'ionisation. Mesurer des structures moléculaires en 3-D avec une résolution inférieure à la distance de liaison est suffisante pour observer des changements structuraux majeurs comme l'isomérisation.

Laser Coulomb explosion imaging of small molecules

F. Légaré[1,2], Kevin F. Lee[1,3], I.V. Litvinyuk[4], P.W. Dooley[1,3], S.S. Wesolowski[1], P.R. Bunker[1], P. Dombi[5], F. Krausz[5], A.D. Bandrauk[2], D.M. Villeneuve[1], P.B. Corkum[1]

[1]*National Research Council of Canada, 100 Sussex Dr., Ottawa, Ontario, Canada K1A 0R6*

[2]*Département de Chimie, Université de Sherbrooke, Sherbrooke, Québec, Canada J1K 2R1*

[3]*Department of Physics & Astronomy, McMaster University, Hamilton, Ontario, Canada K1S 5P3*

[4]*Department of Physics, Kansas State University, Manhattan, Kansas, 66506, USA*

[5]*Technische Universität Wien, Vienna, Austria*

We use intense few-cycle laser pulses to ionize molecules to the point of Coulomb explosion. We use Coulomb's law or ab-initio potentials to reconstruct the molecular structure of D_2O and SO_2 from the correlated momenta of exploded fragments. For D_2O, a light and fast system, we observed about 0.3Å and 15^o deviation from the known bond length and bond angle. By simulating the Coulomb explosion for equilibrium geometry, we showed that this deviation is mainly caused by ion motion during ionization. Measuring 3-D structure with half bond length resolution is sufficient to observe large-scale rearrangements of small molecules such as isomerization processes.

Coulomb explosion imaging was first demonstrated using small molecular ions moving with ~ 10^6 eV energies passing through a thin foil [1]. All ionization occurred within ~100 attoseconds. The initial structure is reconstructed by measuring the momentum of all fragments after explosion caused by multiple ionization. The reconstruction relies on knowledge of the potential that describes the interaction of the charged particles during the explosion. For simplicity, a Coulomb potential is typically used. This technique can measure the stationary states of small molecules relatively accurately, but is difficult to adapt to dynamic imaging. Lasers are being studied as an alternative to collision ionization because of their greater flexibility for pump-probe experiments [2].

Exploiting the recent development of intense, few-cycle laser pulses [3], we investigate their interaction with small molecules. Even with 5 fs optical pulses, laser ionization will be about 50 times slower then collision. This will make the image less accurate. The question is: how well can we freeze nuclear position during rapid ionization induced with state-of-the-art laser technology? To answer this question, we measured the three-dimensional structures of both D_2O and SO_2 by Coulomb explosion imaging with a few-cycle laser pulse and compared them to the known structures. We simulate the Coulomb explosion of D_2O by using an atomic tunnelling model to describe ionization, and classical mechanics to describe the motion of the fragments. We show that motion occurs during ionization but the image is sufficiently accurate to resolve changes on the length scale of a chemical bond. In comparison to heavy water, our SO_2 images are even closer to the known ground stationary state geometry due to better confinement of the heavier nuclei.

Laser driven Coulomb explosion has already been extensively investigated [4,5]. In most experiments reported so far, the time scale of ionization was comparable with the time scale of molecular dynamics (10-100 fs). When ionization and dissociation occur simultaneously, dissociation occurs on the field-distorted potential energy surfaces of a succession of charge states, making it very complex. With ~50 fs pulses, accurate imaging was only possible for heavy molecules [2] such as iodine. By using few-cycle laser pulses we remove much of this complexity.

Numerical simulations of laser Coulomb explosion of H_2^+ [6] and experiments with D_2 [7] were the only previous studies of the interaction of intense few-cycle laser pulses with molecules. Both suggest the possibility of using intense few-cycle laser pulses as an imaging technique in dynamics experiments. We extend this work to small polyatomic molecules.

We compress the 40 fs pulses from a Ti:sapphire (800 nm, ~500 μJ, 500 Hz) regenerative amplifier–using self-phase-modulation in an argon-filled hollow core fibre followed by dispersion compensation with chirped mirrors. We characterized the pulses using SPIDER [8]. We produced 7 fs pulses but over the duration of the experiment the pulse duration may have increased to ~8 fs due to laser fluctuations. A low density, ~ 40 μm thick molecular beam propagated perpendicular to the 24-cm-long imaging-time-of-flight spectrometer axis [9]. The laser was focused (f=50 mm) perpendicular to both the molecular beam and the spectrometer axis inside a vacuum chamber (10^{-9} mbar background pressure). The tight focus ensured that our interaction volume was small (1000 μm^3) compared to the time-of-flight dimension. Errors due to the size of the interaction volume were negligible.

Our position- and time-sensitive multiple hit ion detector can measure the velocity vectors of up to 16 fragments per laser pulse. As the beam density was low ($<10^{11}$ cm^{-3}), an average of less than one molecule was exploded per laser shot. For a single molecule explosion event, momentum conservation requires that the total momentum is zero. To verify that only triply coincident ions were recorded, we required that the total momentum of all three particles was less than $5x10^{-23}$ kg m/s. We estimate a false coincidence rate of about 3%.

Figure 1 compares D_2O^{4+} explosion ($\rightarrow D^+ + O^{2+} + D^+$) with 8 fs (~$5x10^{15}$ W/cm^2) a 40 fs (~$3x10^{15}$ W/cm^2) linearly polarized laser pulses. While charge states up to 5+ were observed, we selected the D_2O^{4+} channel because of its higher count rate. Lower charge states give lower total kinetic energy. Using a modified ADK theory [10], at $5x10^{15}$ W/cm^2, we estimated respective ionization rates of 10^{16} s^{-1} and 10^{14} s^{-1} for the $D_2O^{2+} \rightarrow D_2O^{3+}$ and $D_2O^{3+} \rightarrow D_2O^{4+}$ charge state transitions.

Instantaneous ionization of ground state D_2O at its equilibrium position to electronic ground state D_2O^{4+} yields a total fragment kinetic energy of ~65 eV. The partition of energy

leaves D^+ with 31 eV and O^{2+} with 3 eV. The angle between the momentum vectors of D^+ is 128°. In Figure 1(a), we observe that both D^+ from the same molecule have similar kinetic energy since the distribution lies on the diagonal of the energy-energy correlation map. For 8 fs laser pulses, the results of Figure 1(a) and Figure 1(b) are much closer to the expected value than they would be with 40 fs pulses. For 8 fs pulses, the D^+ energy peaks at 24 eV, the O^{2+} energy peaks at 2.3 eV the angle between vectors peaks at 123°, and the total kinetic energy distribution peaks at 53 eV compared to 35 eV with 40 fs laser pulses.

The correlation map for 40 fs shown in Figure 1 is characteristic of enhanced ionization [11,12]. It doesn't change as the pulse duration is increased to 100 fs (or more). Coulomb explosion imaging is not as useful in the enhanced ionization regime, since the fragmentation is almost independent of the internal structure. The near absence of enhanced ionization from the 8 fs kinetic energy distribution is consistent with D_2 results [7].

For each event that makes up Fig. 1, the vector momentum of each ion was measured. The inferred atomic positions are directly related to the fragment momentum distribution. However, obtaining a mathematical transformation connecting the correlated velocities with the positions of the atoms for polyatomic molecules is difficult, and remains a subject of current research [13]. Our iterative procedure for reconstructing molecular structure assumes classical motion on an ab-initio or Coulombic potential with zero initial velocity. For each event in the correlated momentum distribution, we find a three-dimensional structure that reproduces the measured fragment velocities. We estimate experimental error due to detector precision (time of flight and detector position) to be about 5^o and 0.02 Å for each individual structure. The term "Coulomb explosion" implies that the Coulomb potential adequately approximates the true potential energy surface of the exploding ion when the charge state is high. We confirm the validity of this approximation by comparison with the ab-initio potential for D_2O^{4+}.

The ab-initio calculation of the potential energy surface of the D_2O^{4+} molecular ion was carried out for 38 geometries covering bond angles from 90^o to 180^o, and bond lengths from 0.85 to 2.0 Å. Energies were computed using an augmented correlation-consistent polarized-valence quadruple-zeta (aug-cc-pVQZ) basis set [14]. Reference electronic wave functions were obtained using the spin-restricted Hartree-Fock (RHF) method, and dynamical

correlation was incorporated using the coupled-cluster method including all single and double excitations as well a perturbative estimate of connected triple excitations (CCSD(T)) [15]. During the correlation procedure, the oxygen 1s core electrons were held frozen.

Figure 2(a) shows a set of structures obtained using 8 fs pulses and the ab-initio potential. Figure 2 (b) and (c) show the bond length (R_{OD}) and the bond angle (θ_{DOD}) distributions for the structures shown in Fig 2(a). For the stationary state geometry of D_2O, R_{OD} = 0.96 Å and θ_{DOD} = 104.5º. When fit to a Gaussian, our radial distribution R_{OD} peaks at 1.24 Å (with a 0.3 Å FWHM) and θ_{DOD} peaks at 117° (58° FWHM). Using the Coulomb potential for reconstruction, R_{OD} peaks at 1.26 Å and $\theta_{DOD} = 117^{o}$.The ab-initio and Coulomb potentials yield nearly identical results for 8 fs laser pulses. In Figures 2 (b) and (c), the dotted curves represent the distributions for the ground stationary state structure of D_2O. For the radial distribution, results similar to D_2 [7] are seen. We observe no dependence of the measured structure on the orientation of the molecule with respect to the polarization axis. We address the substantial broadening of the bond angle distribution below.

The error introduced by the finite duration of the laser pulse can greatly exceed that of the approximate Coulomb potential. For instance, we found that imaging with 40 fs pulses yielded values of R_{OD} = 1.96 Å (0.9 Å FWHM) and θ_{DOD} = 138° (75° FWHM) . These results are consistent with those obtained by Sanderson *et al.* [5]. As in earlier D_2 experiments [10], a few-cycle laser pulse clearly improves our ability to measure molecular structure. Nevertheless, discrepancies remain. For D_2, the measured kinetic energy distribution differed from that expected for an ideal Coulomb explosion because of motion on the intermediate charge states between the time of the first and final ionization and because the ionization potential depends on the internuclear separation. With 8 fs laser pulses, the former effect is more important.

We estimated the role of intermediate charge state dynamics for D_2O by simulating dissociative ionization. We assumed an 8 fs FWHM Gaussian pulse with a peak intensity of $5x10^{15}$ W/cm^2. We described ionization using a tunneling model [10] and followed the nuclear motion by solving the classical equations of motion on the ground state ionic potential. We began with D_2O at rest in its stationary state geometry. We further assumed that the width

of R_{OD} in Fig 2(b) is primarily due to ionization dynamics rather than the size of the initial D_2O vibrational wave function. We simulated nuclear motion on the ground state potential surfaces of each charge state, tracking the probability of ionization as the nuclei moved. When the probability of ionization exceeded a random number, a transition to the next charge state was made. A distribution of nuclear positions was predicted by running 1000 trajectories. Once four electrons were removed, no further ionization was allowed. In this manner, we obtained a total kinetic energy of ~55 eV after the explosion, with an average R_{OD} of ~1.38 Å and θ_{DOD} of ~114°.

The D_2O simulation gives similar but not identical structure to the one reconstructed from the experimental results. The main reason for this difference is that by the time D_2O^{4+} was reached, the ions had accumulated ~3-4 eV of kinetic energy, while our reconstruction assumed initial fragment velocities of zero. In conjunction with our structure retrieval algorithm, the simulated asymptotic fragment velocity distribution yielded values of R_{OD}=1.18 Å and θ_{DOD}=127 °. While the simulated and experimental values are similar, the zero initial velocity assumption gives rise to discrepancies of ~0.2 Å for the bond length and ~15° for the bond angle.

Our model shows that the deviation of R_{OD} from its known value is primarily due to motion on the ground state surfaces of intermediate molecular ions. However, ground state motion cannot account for the width of the θ_{DOD} distribution. We repeated the simulation using the first excited electronic state of D_2O^+ rather than the ground electronic state. The energy difference between these two states is ~2 eV, which is about the energy of one 800 nm photon. Since the potential minimum for the excited state corresponds to a linear molecular geometry, the apparent bond angle will increase with the amount of time the wave packet spends on this potential surface. Using this state for the D_2O^+ surface, we find that the bond length is ~1.40 Å with θ_{DOD} ~129° when D_2O^{4+} is reached. Thus, it appears that for 8 fs pulses, motion on the ground and excited states leads to relatively small (~ 0.4 Å) errors in laser Coulomb explosion imaging of D_2O. However, for the angle, we see a 15° difference between the ground and excited D_2O^+ results. We believe that the broadening of the angular

distribution results from the contribution of several different electronic states to the dynamics. To improve the image further, even shorter pulses are needed.

Recently, intense 4 fs laser pulses were produced using self phase modulation with a two-stage hollow-core fiber configuration [3]. We have simulated Coulomb explosion of D_2O with a 4 fs FWHM Gaussian pulse, neglecting the possibility of Coulomb blockade [7]. The simulation predicts a measured bond length of ~1.14 Å and an angle of ~109^o (D_2O^+ ground state). While these better approximate the stationary state geometry, discrepancies remain due to nuclear motion (which can be very fast in high charge states) during ionization. However, as the importance of this motion decreases, the dependence of the ionization rate on atomic positions becomes more important. In addition, for 4 fs pulses, the Coulomb approximation may be less applicable. Instantaneous transition from D_2O to D_2O^{4+} gives 65 eV if we use the ab-initio potential versus 70 eV for the Coulombic one. For 8 fs pulses, the Coulomb and the ab-initio potentials converge before the wave packet reaches the D_2O^{4+} state. Thus, we found no difference between the two potentials for molecular reconstruction in the 8 fs case.

We now turn our attention to a molecule with heavier nuclei: SO_2. Like D_2O, SO_2 is bent. Figure 3(a) presents the distribution of SO_2 structures that we measured using the 7+ charge state ($SO_2^{7+} \rightarrow O^{2+} + S^{3+} + O^{2+}$) produced using ~8 fs laser pulses. This is the highest charge we observed with reasonable count rate. In Figures 3(b) and 3(c), we show the measured R_{SO} and θ_{OSO} distributions. The total fragment kinetic energy spectrum peaks at ~125 eV (not shown) whereas instantaneous Coulomb explosion would yield a value of ~145 eV. The expected stationary state geometry values for SO_2 are R_{SO} = 1.43 Å and θ_{OSO} = 119.5^o. By assuming a Coulomb potential for the 7+ charge state, we measured mean structural values of R_{SO} = 1.67 Å (0.26 Å FWHM) and θ_{OSO} = 111° (30^o FWHM). Using 50 fs laser pulses, Hishikawa et al. have reported a total fragment kinetic energy distribution peaking at 61.5 eV and values of R_{SO} ~ 3.3 Å and θ_{OSO} ~ 130^o [4]. Although molecules containing heavier nuclei might seem easier to image using laser-induced Coulomb explosion, this is not necessarily so. With heavier nuclei, more electrons must be removed to make the explosion Coulombic. The higher the charge state on which the nuclei move, the more the wavefunction will distort in a given amount of time due to stronger forces.

Unlike D_2O, we found that the measured SO_2 bond angle depends on the molecule's orientation with respect to the laser polarization axis. When the OO axis is parallel to the polarization axis, the measured bond angle is 120^o. When the axis of symmetry of SO_2 (C_{2v} axis) is parallel to the polarization, we measure a bond angle of 100^o. The induced dipole and/or enhanced ionization [11,12] may be responsible for this distortion. Figure 3 contains the results for all orientations.

For both molecules, we observe that the ionization rate ($D_2O \rightarrow D_2O^{4+}$ and $SO_2 \rightarrow SO_2^{7+}$) is strongly dependent on the orientation of the molecules to the laser polarization. The favored orientation is when the OO axis (or DD) is parallel to the polarization axis (approximately one order of magnitude greater rate compared with molecules where the C_{2v} axis is parallel). For molecules whose plane is perpendicular to the polarization axis, the ionization rate is approximately two orders of magnitude lower than the favored axis. Angle dependence ionization rate has been measured for diatomic molecules [16].

While laser Coulomb explosion imaging technology is still improving, there appears to be a fundamental limit to image fidelity. The ionization rate of an atom or a molecule depends on its ionization potential, which varies as a function of the nuclear coordinates. This coordinate dependence will distort the measured probability density describing the nuclear wave function if the ionization rate is not saturated, irrespective of pulse duration. Thus, laser Coulomb explosion imaging is less suitable for measuring stationary state molecular structures than spectroscopic or thin foil techniques [1]. However, the ultimate goal for laser Coulomb explosion imaging is to follow structural changes during photochemical reactions.

We have shown that currently available laser pulses are capable of imaging the structures of small polyatomic molecules containing either heavy or light constituents with sub-bond length resolution. Although we did not initiate and measure dynamics, it is feasible to do so. For example, imaging dramatic changes such as isomerization from trans to cis structure will be possible. Measurements of photochemically induced processes such as proton transfer reactions [17,18] will be particularly interesting. Laser-initiated Coulomb explosion could also be applied to structures of transition states that are highly transient and of great importance to chemistry.

Acknowledgements:

The authors appreciate financial support from Canada's Natural Science and Engineering Research Council, NRC/CNRS collaborative research fund, the Canadian Institute for Photonics Innovation, and Le Fonds Québécois de la Recherche sur la Nature et les Technologies.

References:

[1] E. P. Kanter, P.J. Cooney, D. S. Gemmell, K.-O. Groeneveld, W.J. Pietsch, A.J. Ratkowski, Z. Vager, and B.J. Zabransky, Phys. Rev. A **20** 834 (1979).

[2] H. Stapelfeldt, H. Sakai, E. Constant, and P.B. Corkum, Phys. Rev. A **55**, R3319 (1997).

[3] B. Schenkel, J. Biegert, U. Keller, C. Vozzi, M. Nisoli, G. Sansone, S. Stagira, S. De Silvestri, and O. Svelto, Opt. Lett. **28**, 1987 (2003).

[4] A. Hishikawa, A. Iwamae, K. Hoshina, M. Kono, and K. Yamanouchi, Chem. Phys. Lett. **282**, 283 (1998).

[5] J.H. Sanderson, A. El-Zein, W.A. Bryan, W.R. Newell, A.J. Langley, and P.F. Taday, Phys. Rev. A **59**, R2567 (1999).

[6] S. Chelkowski, P. B. Corkum, and A. D. Bandrauk, Phys. Rev. Lett. **82**, 3416 (1999).

[7] F. Légaré, I. V. Litvinyuk, P.W. Dooley, F. Quéré, A.D. Bandrauk, D.M. Villeneuve, and P.B. Corkum, Phys. Rev. Lett. **91**, 093002 (2003).

[8] C. Iaconis, and I.A. Walmsley, Opt. Lett. **23**, 792 (1998).

[9] P.W. Dooley, I.V. Litvinyuk, Kevin F. Lee, D.M. Rayner, D.M. Villeneuve, and P.B. Corkum, Phys. Rev. A **68**, 023406 (2003).

[10] G. L. Yudin, and M. Yu Ivanov, Phys. Rev. A **64**, 013409 (2001).

[11] T. Seideman, M. Yu Ivanov, and P. B. Corkum, Phys. Rev. Lett. **75**, 2819 (1995).

[12] T. Zuo, and A. D. Bandrauk, Phys. Rev. A **52**, R2511 (1995).

[13] K. Nagaya, and A.D. Bandrauk (Private communication).

[14] T.H. Dunning, J. Chem. Phys. **90**, 1007-1023 (1989); R.A. Kendall, T.H. Dunning, and R.J. Harrison, J. Chem. Phys. **96**, 6796-6806 (1992).

[15] T.D. Crawford and H.F. Schaefer, Rev. Comp. Chem. **14**, 33-136 (2000) and references therein.

[16] I.V. Litvinyuk, Kevin F. Lee, P.W. Dooley, D.M. Rayner, D.M. Villeneuve, and P.B. Corkum, Phys. Rev. Lett. **90**, 233003 (2003).

[17] S. Nagaoka, and U. Nagashima, Chem. Phys. **136**, 153 (1989).

[18] T. Osipov, C. L. Cocke, M. H. Prior, A. Landers, Th. Weber, O. Jagutzi, L. Schmidt, H. Schmidt-Böcking, and R. Dörner, Phys. Rev. Lett. **90**, 233002 (2003).

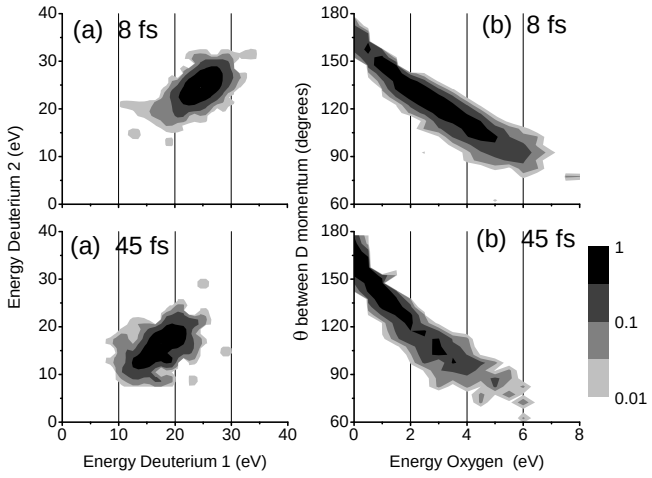

Fig. 1: Comparison of D_2O^{4+} explosion ($\rightarrow D^+ + O^{2+} + D^+$) between an 8 and a 40 fs laser pulses. (a) Energy – energy correlation for D^+. (b) Angle between D^+ momentum.

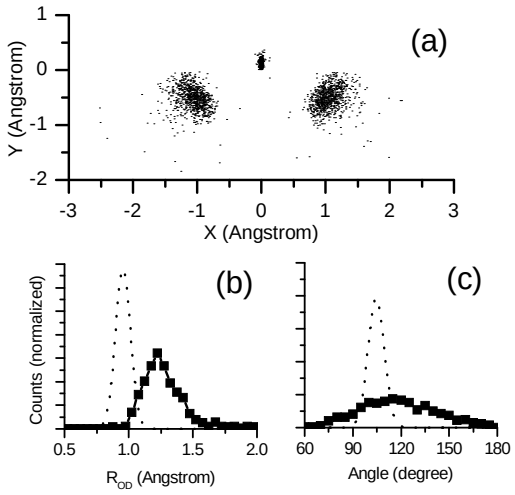

Fig. 2: (a) Structure of D_2O using the 4+ charge states ($D_2O^{4+} \rightarrow D^+ + O^{2+} + D^+$). The reconstruction is achieved by using an ab-initio potential. The center of mass is at x=0, y=0, and the y axis is the bisector of the angle. (b) Radial distribution. (c) Angular distribution. In (b) and (c), the dotted curve represents what we should expect for the v=0 stationary state structure of D_2O.

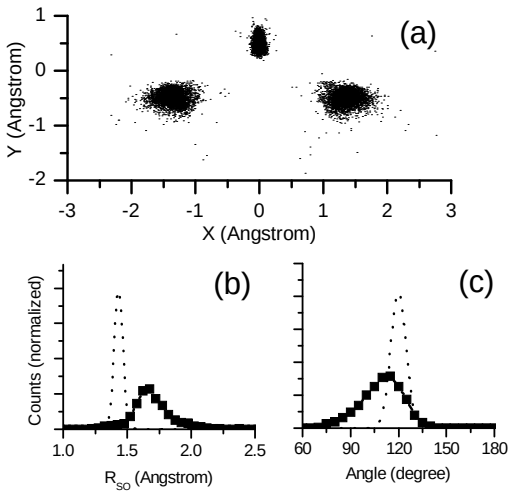

Fig. 3 (a) Structure of SO_2 using the SO_2^{7+} charge states ($SO_2^{7+} \rightarrow O^{2+} + S^{3+} + O^{2+}$). The reconstruction is achieved using the Coulombic potential. The center of mass is at x=0, y=0, and the y axis is the bisector of the angle. (b) Radial distribution. (c) Angular distribution. In (b) and (c), the dotted curve represents what we should expect for the v=0 stationary state structure of SO_2.

CHAPITRE 5

SONDER LA STRUCTURE ET LA DYNAMIQUE MOLÉCULAIRE AVEC DES IMPULSIONS LASERS ULTRA-BRÈVES

Aux chapitres 3 et 4, nous avons mesuré la structure de petites molécules par explosion coulombienne laser. Nous utilisons des impulsions lasers intenses ultra-brèves (sub-10 fs) et la spectroscopie de coincidence. Nous obtenons une résolution spatiale d'environ 0.2 à 0.3 Å. L'explosion coulombienne induite par collision fait beaucoup mieux dû à un temps d'interaction 50 à 100 fois plus court. Par contre, il serait difficile d'utiliser cette technique dans une expérience pompe-sonde. Pour les impulsions lasers, c'est tout à fait différent. La manipulation des impulsions lasers est simple : elle repose sur des techniques optiques bien connues. Il est facile de déphaser temporellement deux impulsions lasers et de contrôler leur délai, ceci est la base d'une expérience pompe-sonde. La résolution temporelle dans ces expériences dépend de la durée des deux impulsions.

Dans une expérience pompe-sonde, l'impulsion laser pompe démarre un processus photochimique, ce qui peut mené à la génération d'un paquet d'onde vibrationnel. Le transfert de population vers un état électronique excité est souvent utilisé. Les transitions électroniques sont généralement comprises dans le spectre ultra-violet. Il est difficile de générer des impulsions lasers ultra-brèves dans cette région spectrale. Comme solution, nous avons décider d'utiliser l'ionisation multiphotonique comme pompe. Notre impulsion laser 8 fs est divisée temporellement en deux. Aux chapitres 1 et 2, nous avons montré que l'ionisation multiphotonique produit un paquet d'onde vibrationnel. En utilisant notre impulsion 8 fs comme pompe, la dynamique est démarrée sous une intervalle de quelques femtosecondes.

Dans les expériences de Zewail, la sonde mesure un signal qui dépend du temps, ce qui mesure la dynamique de la réaction photochimique. Dans nos expériences, nous mesurons les vecteurs vitesses des fragments atomiques obtenus par explosion coulombienne en fonction du délai, ce qui permet de reconstruire l'évolution temporelle de la structure moléculaire. L'article associé à ce chapitre est en préparation et la responsabilité des auteurs sont les mêmes qu'au chapitre 4.

Nous démontrons une nouvelle technique permettant l'imagerie de processus moléculaires ultra-rapides. Cette technique est basée sur la méthode pompe-sonde et utilise des impulsions lasers à quelques cycles optiques (8 fs). Nous appliquons cette technique à l'étude du mouvement des noyaux lorsque D_2^+ est excité vibrationnellement et lorsque SO_2 dissocie via les états de charge SO_2^{2+}/SO_2^{3+}. Dans les deux cas, l'impulsion pompe démarre la dynamique moléculaire en ionisant la molécule non-chargée. L'impulsion sonde, temporellement déphasée, induit l'explosion coulombienne. L'analyse des vecteurs momentums permet de reconstruire la structure moléculaire. Cette méthode permet de suivre le mouvement des atomes dans les molécules avec une résolution temporelle de 5 fs.

Imaging ultra-fast molecular dynamics using few-cycle laser pulses (my favorite)

F. Légaré[1,2], K.F. Lee[1,3], I.V. Litvinyuk[4], P.W. Dooley[1], A.D. Bandrauk[2],
D.M. Villeneuve[1], P.B. Corkum[1]

[1]National Research Council of Canada, Ottawa, Ontario, Canada K1A 0R6

[2]Département de Chimie, Université de Sherbrooke, Sherbrooke, Québec, Canada J1K 2R1

[3]Department of Physics & Astronomy, McMaster University, Hamilton, Ontario, Canada K1S 5P3

[4]Department of Physics, Kansas State University, Manhattan, Kansas, 66506, USA

We demonstrate a novel technique for direct imaging of ultrafast molecular dynamics. The technique is based on pump-probe approach employing few-cycle (8 fs) laser pulses. The technique is applied to directly map nuclear motion in vibrating D_2^+ and dissociating SO_2^{2+}/SO_2^{3+} molecules. In each case, the dynamics is launched by ionizing a neutral molecule with the pump pulse. The time-dependent molecular structure is then interrogated with a delayed probe pulse by analysing the momenta of the Coulomb explosion fragments. The method traces atomic motion with 5 fs time resolution.

Pump-probe spectroscopy using femtosecond lasers is a conventional tool for studying molecular dynamics [1]. The pump pulse initiates motion by population transfer to an excited state, and the probe pulse measures time-dependent signals (correlation between measurement). This technique has been used to measure the dynamics associated with various chemical processes: charge transfer [2], photodissociation [3] and molecular rearrangement [4].

Associated with these processes, there is usually a time-dependent change in the molecular structure. To measure this structure, electron [5,6] and X-ray [7-9] diffraction was proposed. The time resolution of diffraction techniques is limited by pulse duration of their sources (~100 fs). Some ultra-fast molecular processes of great fundamental interest, i.e. as proton transfer [10], will remain beyond the reach of those powerful techniques. Until recently, laser Coulomb explosion imaging was only possible for heavy slow molecules [11] such as iodine. Now, generation of intense sub-10 fs laser pulses is becoming routine in laser laboratories. It was recently shown that few-cycle laser pulses allow Coulomb explosion imaging of any small molecules with sub-Å spatial resolution [12,13]. In this letter, using laser Coulomb explosion as a probe in a pump-probe experiments, we for the first time image evolving molecular structure with 5 fs time resolution.

We demonstrate that by directly observing vibrational motion of D_2^+, one of the fastest molecules. Further, we apply the technique to a more complex case of dissociating SO_2 ions. There we trace the concerted three-body dissociation $SO_2^{3+} \rightarrow O^+ + S^+ + O^+$ and $SO_2^{2+} \rightarrow O^+ + S^+ + O$, and distinguish it from two-body break-up $SO_2^{2+} \rightarrow SO^+ + O^+$. The proposed technique can complement other time-resolved molecular imaging methods by covering the important 0 – 100 fs region in dynamics of small molecules.

In our experiments, a few-cycle pump pulse induces motion by strong field ionization, and the second pulse of the same duration images the molecular structure at different time delays by Coulomb explosion. This technique involves rapidly ionizing a molecule to a highly charged state, causing its fast dissociation. By measuring the momenta of all fragments in a correlated fashion, one can reconstructed the molecular structure [13].

To generate a pair of few-cycle pulses separated by a variable delay we used the same method as described in reference [14]. Briefly, two pieces of fused silica of exactly the same

thickness (cut from the same piece) were aligned in such a way that the central part of a laser beam (the pump) passes through one piece (piece A) and through the corresponding hole in the other piece (piece B), while the outer part of the beam (the probe) passes only through piece B (see Figure 1(a)). Such arrangement allows for a tighter focusing of the probe beam by the same parabolic mirror, allowing probing inside the pump focal volume. When pieces A and B are parallel the time delay is zero and pump and probe pulses precisely overlap in time. By rotating piece B around vertical axis we introduce an extra optical path into the probe beam, thus creating a variable delay of up to 300 fs without seriously affecting beam profile or pulse duration.

Our detection and pulse compression methods are detailed in [12,15]. Briefly, ~8 fs laser pulses are produced by self-phase modulation in an argon-filled hollow core fibre and compression by chirped mirrors [16]. Our detection chamber is a multi-hit, position-sensitive, time of flight spectrometer which provides the velocities, mass, and charge of the fragments [17]. The molecules are injected by a low-density molecular jet, which supplies less then one molecule per laser shot.

Because D_2^+ has a longer equilibrium bond length than D_2, 1.06 Å instead of 0.75 Å, following ionization the molecule will begin to stretch. It takes 12 fs to reach the outer turning point, after which the bond length will continue to oscillate until the wavepacket dephases due to the anharmonicity of the potential. The bond length at the time of explosion can be inferred from the kinetic energy of the fragments that should be higher for smaller nuclear separations. The pump pulse intensity was ~$3x10^{14}$ W/cm^2 and the probe pulse intensity was ~$1x10^{15}$ W/cm^2.

Two kinetic energy spectra of D^+ fragments for 0 and 12 fs delay are shown in Figure 1(b). They correspond to times of the smallest and largest expected bond length. Plotted in Figure 1(c) is the fraction of fragments with kinetic energy greater than 7 eV over the first 75 fs of motion. A clear oscillation of fragment kinetic energy is visible, tracing the ultra-fast dynamics of D_2^+. For precise measurement of $|\Psi(R,t)|^2$ of D_2^+, intense and clean 4 fs laser pulses are needed [ref9].

To verify our interpretation, we calculated the expected behaviour of D_2^+ by projecting the ground state wave function of D_2 onto the D_2^+ X $^2\Sigma_g^+$ surface, solving the time-dependent Schrödinger equation to find average inter-nuclear distance. Projecting the resulting wavepacket onto a Coulombic potential yields the kinetic energy distribution. The theoretical curves are plotted along with the experimental data in Figure 1(b).

For 12 fs, theoretical kinetic energy distribution agrees well with experimental data (Fig. 1(b)). The tail in the experimental curve is due to molecules that were not ionized by the pump pulse and explode directly from neutral D_2. The measured time evolution also agrees well with our calculations (Fig. 1(c)). The ~24 fs vibration period and ~60 fs dephasing time are consistent with our knowledge of the D_2^+ X $^2\Sigma_g^+$ potential. To minimize coupling between X $^2\Sigma_g^+$ and A $^2\Sigma_u^+$ electronic states, the data shown only include molecules that had an angle to the probe polarization axis between 80° to 100°.

For the rest of the paper, we present results for femtosecond time-resolved structures of SO_2 excited by double and triple ionization. Small polyatomic molecules can exhibit interesting chemistry such as molecular rearrangement. For this experiment, the pump intensity was ~1x10^{15} W/cm^2. Such pulse removes up to 3 electrons from SO_2. Using correlation and 3d imaging, we identify five photodissociation channels: *($SO_2^{3+} \rightarrow O^+ + S^+ + O^+$)*; ($SO_2^{3+} \rightarrow SO^{2+} + O^+$); *($SO_2^{2+} \rightarrow SO^+ + O^+$)*; *($SO_2^{2+} \rightarrow S^+ + O^+ + O$)* and ($SO_2^{2+} \rightarrow S^+ + O_2^+$), where major channels have been italicized. Knowing the final charge states, we can image transient structures during dissociation. For example, by looking at three body breakup channels, we can distinguish between concerted and two-step dissociation mechanisms. We image the molecular structure during the first 60 fs and resolved the dynamics for 220 fs. We set our probe pulse intensity at ~5x10^{15} W/cm^2 and we interrogated the dynamics by exploding the molecules via ($SO_2^{7+} \rightarrow O^{2+} + S^{3+} + O^{2+}$).

In Figure 2, we present the total kinetic energy spectra and the oxygen-oxygen energy correlation map for different pump-probe delays, Δt. Approximately half of the counts at nonzero time delays can be attributed to molecules that were not ionized by the pump. These counts have been subtracted from the plots, using $\Delta t=0$ as a reference. Looking at the evolution of the correlation maps with time delay, there is an overall motion along the

diagonal towards lower energy, and there is an off-diagonal motion of the wings that appear 30 fs after ionization, and become well-separated at longer times. The diagonal motion towards lower energy indicates symmetric stretching. Off-diagonal components indicate asymmetry in the molecule.

By looking at the diagonal component at Δt=220 fs, we observe contribution from two dissociation channels ($SO_2^{3+} \rightarrow O^+ + S^+ + O^+$; $SO_2^{2+} \rightarrow O^+ + S^+ + O$). We do this by correlating total kinetic energy with angle between the O^{2+} fragment velocities. This is possible because the molecule has expanded enough at 220 fs that the energy gained from Coulomb explosion is smaller than the kinetic energy the molecule already has from the dissociation process. A lower energy peak at ~22.5 eV at smaller angle with broader angular distribution corresponds to $SO_2^{2+} \rightarrow O^+ + S^+ + O$, and a higher energy peak at ~27.5 eV at larger angle with a narrower angular distribution corresponds to $SO_2^{3+} \rightarrow O^+ + S^+ + O^+$. Both channels are populated nearly equally.

It is known that the decay of $SO_2^{3+} \rightarrow O^+ + S^+ + O^+$ is mostly concerted [18]. For $SO_2^{2+} \rightarrow O^+ + S^+ + O$, the exact decay mechanism remains in question. From our experiments, the predominant peak moving from ~125 eV at Δt = 0 fs to ~25 eV at Δt = 220 fs is always along the diagonal of the correlation map, indicating that the photodissociation of $SO_2^{3+} \rightarrow O^+ + S^+ + O^+$ and $SO_2^{2+} \rightarrow O^+ + S^+ + O$ are dominated by concerted decay.

Asymmetric dissociation by a pump pulse giving a SO^{n+} with an O^{m+} will result in significant energy difference between the two oxygens following the explosion by the probe pulse at long delays. In figure 2, we observe such off-diagonal components. Since the energies of the two oxygen fragments become independent at long times, and by comparison with unexploded fragment energies, we deduce that these wings are part of the $SO_2^{2+} \rightarrow SO^+ + O^+$ sequential dissociation channel. Behind the dynamics observed on figure 2, there is time-dependent structure. Using the same approach that we develop in [13], we will reconstruct the molecular structure for delay up to 60 fs.

For each event that makes up Fig. 2, the vector momentum of each fragment was measured. When the initial kinetic energy is small compared with the energy gained from Coulomb explosion, the inferred atomic positions are directly related to the fragment

momentum distribution. Our iterative procedure for reconstructing molecular structure assumes classical motion on a Coulombic potential $SO_2^{7+} \rightarrow O^{2+} + S^{3+} + O^{2+}$ with zero initial velocities. For each event in the correlated momentum distribution, we find a unique three-dimensional structure that reproduces the measured fragment velocities. For long delays, as the fragments gain kinetic energy during photodissociation, zero initial velocity assumption is no longer valid, and molecular structure reconstruction is not possible.

In order to understand effect of initial velocities (initial kinetic energy), we simulate pump-probe dynamics on SO_2^{3+} and SO_2^{2+}. In our model, SO_2 equilibrium geometry ($r1 = r2 = 1.43$ Å and $\theta = 119.5^o$) is projected vertically to the ion, which photodissociates according to the Coulomb law in a $O^+ + S^+ + O^+$. The dynamics is solved using classical mechanics giving r_1, r_2, velocities and the angle at any time. Starting from a given delay, we continue the dissociation on $O^{2+} + S^{3+} + O^{2+}$ Coulombic potential. We calculate the asymptotic velocities obtained by this explosion. We use these velocities as inputs to our structure reconstruction program. For $\Delta t \geq 45$ fs, the velocities acquired by dynamics on SO_2^{3+} are too large and we cannot measure the bond distance with sub-Å resolution. Probing with a higher final charge state, such as $SO_2^{10+} \rightarrow O^{3+} + S^{4+} + O^{3+}$ improves only slightly the quality of the image. The measured count rate for this channel was too low to be practical. Dynamics of $SO_2^{2+} \rightarrow SO^+ + O^+$ is slower due to weaker Coulomb repulsion and we are able to image the structure for the first 60 fs.

Figure 3 presents the reconstructed structures in the form of r_1-r_2 correlation map. It shows diagonal and off-diagonal densities corresponding to symmetric and asymmetric breakup. The star on the $\Delta t = 0$ fs map shows the known structure of neutral SO_2 molecule. The offset between our measurement and the known structure is due to molecular dynamics during the multiple ionization of SO_2 to the final Coulombic charge state $SO_2^{7+} \rightarrow O^{2+} + S^{3+} + O^{2+}$. Because of this, we can expect a 0.2 Å of error on our bond distance measurement [13].

For the first 15 fs, only symmetric stretch is observed for all photodissociation channels. For symmetric stretch, the structure is reliable for only the first 30 fs. During this time, we see a symmetric elongation of both bond distances from 1.65 Å to 2.8 Å. According to our simulation, at $\Delta t = 60$ fs, the bond distance error exceeds 1 Å. However, based on the

measurement, we reliably identify the nature of the decay, as being concerted and symmetric. For asymmetric stretch, we obtain reliable imaging up to 60 fs. At $\Delta t = 30$ fs, we observe bond distance of $<r_1>\sim 1.8$ Å and $<r_2>\sim 2.6$ Å which become ~2.2 Å and ~3.2 Å at $\Delta t = 60$ fs.

The reconstruction of the bond angle is much more sensitive to initial velocities and its values are not reliable for non-zero delays. However, time-dependent angle between oxygen fragment velocities contains information about bond angle dynamics. This angle does not change much, varying from ~120° at $\Delta t = 0$ fs to 113° at $\Delta t = 220$ fs for $O^+ + S^+ + O^+$ channel, and from ~120° to 108° for $O^+ + S^+ + O$ channel. These relatively small changes suggest that the molecule does not bend significantly during dissociation through these two channels.

For $SO_2^{2+} \rightarrow SO^+ + O^+$ channel, the angle between oxygen fragment velocities decreases to ~70^o during the first 135 fs. This change directly correlates with O^{2+} fragment energy difference. During the first ~75 fs, the decreasing bond angle corresponds to increasing oxygen energy difference (from ~0 eV to ~20 eV). The energy difference then decreases to ~5 eV as this angle approaches 70^o at 135 fs delay. Simple classical simulation of $SO_2^{2+} \rightarrow SO^+ + O^+$ dynamics assuming Coulomb interaction shows the decrease of the bond angle as SO^+ fragment rotates after the dissociation. Up to 135 fs, the simple model and the experiments agree showing the same correlation of the angle between oxygen fragment velocities and oxygen energy difference. After that, the energy difference increases to ~35 eV and the velocity angle increases up to ~140^o. The nature of the motion after 135 fs is unclear and further simulations using are needed.

In [12,13], it was shown how the nature of the interaction between intense few-cycle laser pulses and molecules limits resolution of laser Coulomb explosion imaging (sub-Å). In addition, while imaging molecular dynamics another limitation arises from velocities acquired by the fragments during the photochemical reaction. This limits imaging to structures characterized by slow moving constituents. In our case, because we look at dissociating molecular ions, imaging range is limited to 60 fs. Dissociation in neutral charge state and molecular rearrangement are characterized by slower motion of atomic constituents, making this limitation less critical.

To investigate coherent ultra-fast molecular dynamics, population transfer by the pump has to occur on a really short time scale compared to vibrational motion. We have shown that strong field ionization with few-cycle laser pulses can do it. To study neutral charge state, intense few-cycle UV laser pulses are needed. Using self-phase modulation [19] and cross-phase modulation [20], sub-10 fs UV laser pulses are available. Combining such pulses with laser Coulomb explosion imaging, making a sequence of snapshots picturing evolving molecular structure is possible for small molecules with less than 5 fs between consecutive frames.

This method can also be used for studying statistical dynamics processes including measuring the structure of a transition state. In this case, the duration of the pump laser is less critical because of the statistical behavior of such processes. With state-of-the-art laser technology combined with coincidence spectroscopy, imaging of molecular structure with half bond length precision and a time resolution of 5 fs is achievable.

[1] A. H. Zewail, J. Phys. Chem. A **104**, 5660 (2000).

[2] I. B. Martini; E.R. Barthel, and B.J. Schwartz, Science **293**, 462 (2001).

[3] J. A. Davies, J. E. LeClaire, R. E. Continetti, and C.C. Hayden, J. Chem. Phys. **111**, 1 (1999).

[4] T. Saito, and T. Kobayashi, J. Phys. Chem. A **106**, 9436 (2002).

[5] B. J. Siwick, J. R. Dwyer, R. E. Jordan, and R. J. D. Miller, Science **302**, 1382 (2003).

[6] H. Ihee, V. A. Lobastov, U. M. Gomez, B. M. Goodson, R. Srinivasan, C.-Yu Ruan, and A. H. Zewail, Science **291**, 458 (2001).

[7] C. Rischel, A. Rousse, I. Uschmann, P.-A. Albouy, J.-P. Geindre, P. Audebert, J.-C. Gauthier, E. Fröster, J,-L. Martin, A. Antonetti, Nature **390**, 490 (1997).

[8] C. Rose-Petruck, R. Jimenez, T. Guo, A. Cavalleri, C. W. Siders, F. Rksi, J. A. Squier, B. C. Walker, K. R. Wilson, and C. P. J. Barty, Nature **398**, 310 (2002).

[9] F. Schotte, M. Lim, T. A. Jackson, A. V. Smirnov, J. Soman, J. S. Olson, G. N. Phillips Jr., M. Wulff, and P. A. Anfinrud, **300**, 1944 (2003).

[10] S. Lochbrunner, T. Schultz, M. Schmitt, J. P. Shaffer, M. Z. Zgierski, and Albert Stolow, J. Chem. Phys. **114**, 2519 (2001).

[11] H. Stapelfeldt, H. Sakai, E. Constant, and P.B. Corkum, Phys. Rev. A **55**, R3319 (1997).

[12] F. Légaré, I. V. Litvinyuk, P.W. Dooley, F. Quéré, A.D. Bandrauk, D.M. Villeneuve, and P.B. Corkum, Phys. Rev. Lett. **91**, 093002 (2003).

[13] F. Légaré, K.F. Lee, I. V. Litvinyuk, P.W. Dooley, S. S. Wesolowski, P. R. Bunker, P. Dombi, F. Krausz, A.D. Bandrauk, D.M. Villeneuve, and P.B. Corkum, (submitted).

[14] P. M. Paul, E. S. Toma, P. Breger, G. Mullot, F. Aug, Ph. Balcou, H.G. Muller, and P. Agostini, Science **292**, 1689 (2001).

[15] P.W. Dooley, I.V. Litvinyuk, Kevin F. Lee, D.M. Rayner, D.M. Villeneuve, and P.B. Corkum, Phys. Rev. A **68**, 023406 (2003).

[16] M. Nisoli, S. De Silvestri, O. Svelto, R. Szipöcs, K. Ferencz, Ch. Spielman, S. Sartania, and F. Krausz, Opt. Lett. **22**, 522 (1997).

[17] A. Hishikawa, A. Iwamae, K. Hoshina, M. Kono, and K. Yamanouchi, Chem. Phys. Lett. **282**, 283 (1998).

[18] S. Hsieh, and J. H. D. Eland, J. Phys. B **30**, 4515 (1997).

[19] O. Dhr, E. T. J. Nibbering, G. Korn, G. Tempea, and F. Krausz, Opt. Lett. **24**, 34 (1999).
[20] N. Zhavoronkov, and G. Korn, Phys. Rev. Lett. **88**, 203901 (2002).

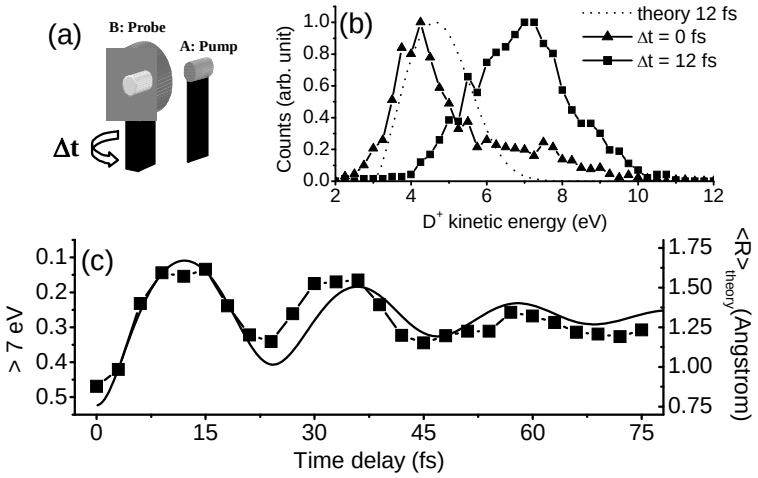

Fig. 1: (a) Pump-probe setup. (b) D^+ kinetic energy (KE) spectra for delay of 0 fs (square) and 12 fs (triangle). Dotted curve is the expected kinetic energy spectra for 12 fs of delay. (c) Ratio of fragments with more then 7 eV of KE over total (square). Time-dependent average internuclear distance as a function of time on D_2^+ $X\ ^2\Sigma_g^+$ (solid line).

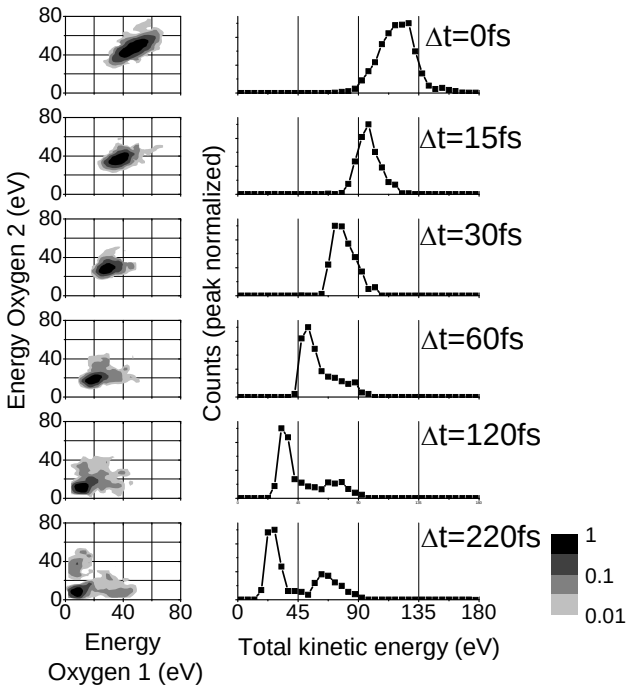

Fig. 2: Right: total kinetic energy spectra as a function of time delay. Left: O^{2+} energy-energy correlation. Final charge state is $SO_2^{7+} \rightarrow O^{2+} + S^{3+} + O^{2+}$.

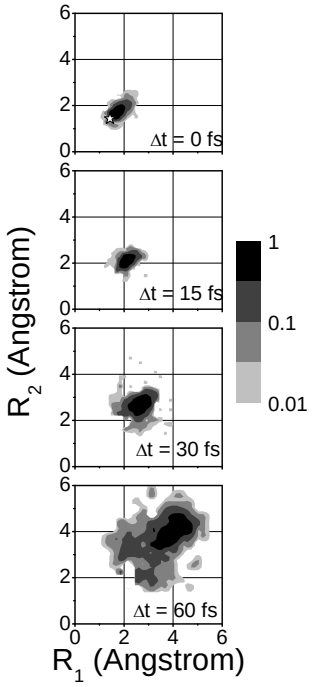

Fig. 3: R_{SO} (1) vs R_{SO} (2) as a function of time delay. Final charge state for reconstruction is $SO_2^{7+} \rightarrow O^{2+} + S^{3+} + O^{2+}$.

CHAPITRE 6

CONTRÔLE DU TRANSFERT DE POPULATION DANS UN SYSTÈME DÉGÉNÉRÉ PAR EFFET STARK NON RÉSONANT

L'article associé à ce chapitre (François Légaré, Physical Review A **68**, 063403 (2003)) a été écrit en marge de mon projet de thèse; c'est pourquoi il constitue mon dernier chapitre. En fait, cette recherche est liée à mes travaux de maîtrise. Au cours de celle-ci, j'ai travaillé sur les transferts de population dans les systèmes quantiques où les niveaux d'énergie sont non-dégénérés. Écrire un code numérique traitant le cas dégénéré n'était donc pas difficile pour moi. Cependant, durant ma maîtrise, malgré une réflexion sur ce sujet, aucun schéma de transferts ne m'était venu à l'esprit.

Les idées derrière cet article me sont venues lors de ma participation à une école d'été (Summer School on Coherent Control, France, octobre 2002). Les présentations du Dr. Bruce Shore et du Dr. K. Bergmann m'ont fait prendre conscience que la seule façon de contrôler les transferts de populations dans les systèmes dégénérés est de briser la dégénérescence initialement, plus précisément par l'effet Stark. J'ai pensé à deux schémas de transfert.

À mon retour, j'ai écrit les programmes qui m'ont permis de vérifier mes hypothèses. J'ai présenté ces résultats aux Drs A.D. Bandrauk, M. Yu Ivanov et P.B. Corkum et ceux-ci m'ont encouragé à publier mes résultas. En novembre 2002, un article traitant ce sujet est parue dans Physical Review A. Cependant, aucun schéma n'était présenté. Il solutionnait le problème par contrôle optimal. Par algèbre de Lie, il détermine si le contrôle est possible selon la matrice halmitonienne. Mes schémas simples étaient donc un ajout important à leurs travaux. J'ai soumis cet article à Physical Review A pour une raison principale; cette revue est lue

autant par les physiciens que par les chimistes et ces travaux intéressent les deux communautés.

Deux schémas simples permettant un transfert sélectif de population lorsque l'état final est doublement dégénéré sont présentés. Chacun des états dégénérés est couplé à l'état fondamental via une résonance à un photon. Les schémas utilisent la combinaison de deux impulsions lasers. La première impulsion lève la dégénérescence entre les niveaux par effet Stark. La fréquence de la deuxième impulsion est adaptée temporellement aux nouvelles énergies. Ces deux schémas sont illustrés par simulation de l'équation de Schrödinger dépendante du temps pour un système à quatre niveaux. Le transfert efficace de population est expliqué à l'aide des états habillés. En conclusion, certaines applications moléculaires sont proposées.[P.S.]

[P.S.] L'équation 5 contient une erreur. On doit additionner la composante due au dipôle induit.

Control of population transfer in degenerate systems by nonresonant Stark shifts

François Légaré*

Laboratoire de Chimie Théorique, Université de Sherbrooke, PQ, Canada, J1K 2R1

and National Research Council of Canada, Ottawa, Ontario, Canada K1A 0R6

*FAX: (613)-993-3437. Email address: francois.legare@nrc.ca

Abstract

Two simple schemes are presented for the selective population transfer in systems where the target state is degenerate with a second level. Both states are coupled with the ground state via a one photon resonance. The schemes use a combination of two laser pulses. The first pulse breaks the degeneracy of the levels by inducing a Stark shift. The second pulse is chirped across the new levels. The idea is illustrated by numerical simulations of the time-dependent Schrödinger equation for a four-level system. The efficient population transfer is explained using a dressed state representation. In conclusion, applications for molecules are suggested.

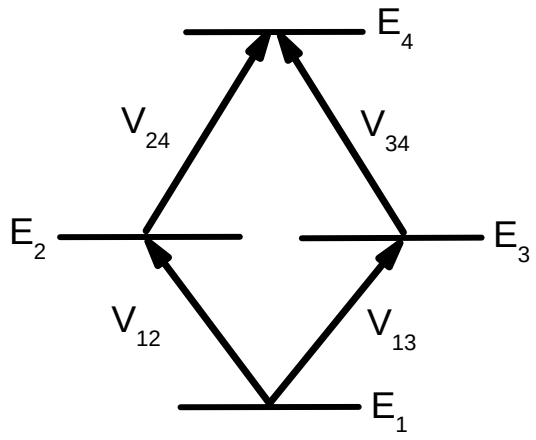

FIG. 1: Four-level system associated with Eq. (2). $V_{ij} = \mu_{ij}\mathcal{E}(t)$ and $\mu_{23}=0$.

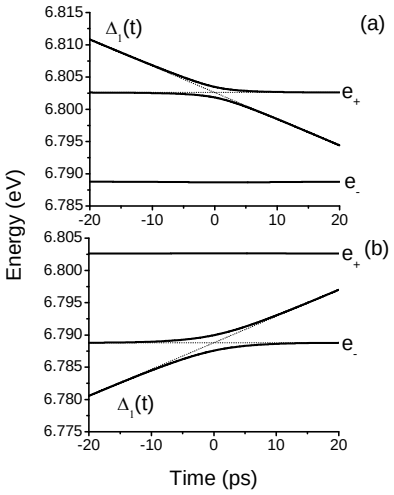

FIG. 2. Dressed state representation of scheme 1. (a) Population inversion to $|e_+\rangle$ ($\approx|E_2\rangle$). (b) Population inversion to $|e_-\rangle$ ($\approx|E_3\rangle$).

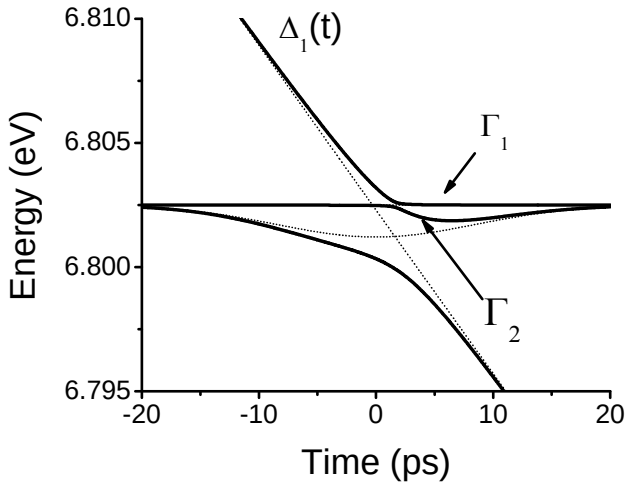

FIG. 3. Dressed state representation of scheme 2. By launching $\cos^2(\theta/2)$ of the population into the pathway Γ_1 and the rest into Γ_2 , one can use the phase difference [Eq. (14)] to make on efficient population inversion to level 2 or 3.

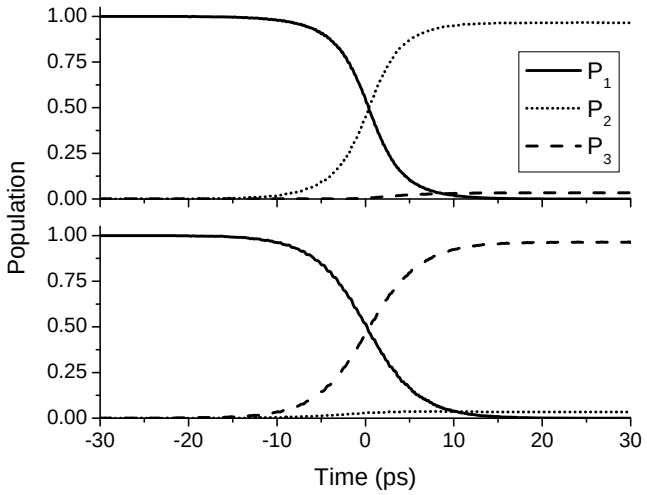

FIG. 4. Time-dependent population transfer for scheme 1. (a). See Fig. 2(a). (b) See Fig. 2(b).

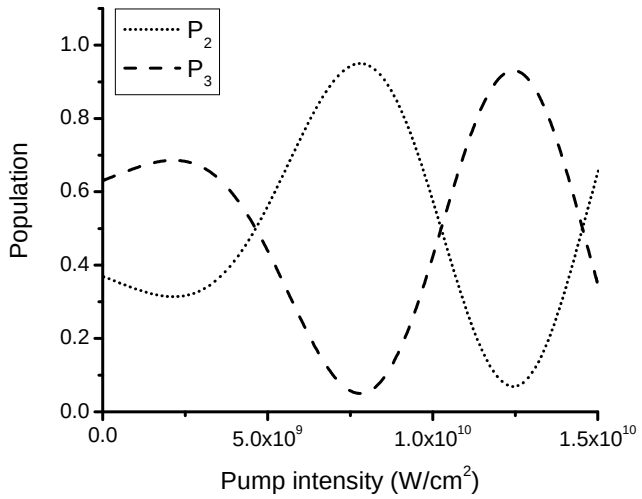

FIG. 5. Final population in level 2 and 3 for scheme 2. The *x* axis is the intensity of the nonresonant laser pulse.

CONCLUSION ET PERSPECTIVES

Au chapitre 1, nous avons démontré qu'il est possible de faire des mesures attosecondes sans pour autant utiliser des impulsions attosecondes. Ceci est possible lorsque deux paquets d'onde sont corrélés, que l'un d'entre eux est contrôlé avec une précision attoseconde et que la corrélation est produite sous une échelle temporelle attoseconde. L'ionisation en présence d'impulsions lasers infra-rouges offre ces conditions. Pour une molécule, un paquet d'onde vibrationnel et électronique sont corrélés lors de l'ionisation. Près de 50 % de la population électronique éjectée dans le continuum revient à la source avec un délai d'environ 2/3 la période optique. Au chapitre 2, nous avons sondé la propagation vibrationnelle de D_2^+ en utilisant la collision inélastique des deux paquets. Lors de la collision, des processus élastiques et de recombinaison peuvent aussi avoir lieu.

Pour des molécules plus complexes, ils seraient difficile d'utiliser cette méthode pour mesurer la structure moléculaire.

Pour la majorité des molécules, 2/3 de la période optiqueest si court qu'aucune dynamique sera observée.

BIBLIOGRAPHIE

[1] S. Nagaoka et U. Nagashima, Chem. Phys. **136**, 153 (1989).

[2] A.H. Zewail, Nobel Lecture, p. 274 (1999).

[3] I.B. Martini; E.R. Barthel et B.J. Schwartz, Science **293**, 462 (2001).

[4] J.A. Davies, J.E. LeClaire, R.E. Continetti et C.C. Hayden, J. Chem. Phys. **111,** 1-4 (1999).

[5] T. Saito et T. Kobayashi, J. Phys. Chem. A **106**, 9436 (2002).

[6] S. Lochbrunner, T. Schultz, M. Schmitt, J.P. Shaffer, M.Z. Zgierski et A. Stolow, J. Chem. Phys. **114**, 2519 (2001).

[7] C. Davisson et L.H. Germer, Phys. Rev. **30**, 705 (1927).

[8] M.F. Perutz, Science **140**, 863 (1963).

[9] Z. Vager, R. Naaman, et E.P. Kanter, Science **244**, 426 (1989).

[10] B.J. Siwick, J.R. Dwyer, R.E. Jordan et R.J.D. Miller, Science **302**, 1382 (2003).

[11] H. Ihee, V.A. Lobastov, U.M. Gomez, B.M. Goodson, R. Srinivasan, C.-Yu Ruan, et A.H. Zewail, Science **291**, 458 (2001).

[12] C. Rischel, A. Rousse, I. Uschmann, P.-A. Albouy, J.-P. Geindre, P. Audebert, J.-C. Gauthier, E. Fröster, J.-L. Martin, A. Antonetti, Nature **390**, 490 (1997).

[13] C. Rose-Petruck, R. Jimenez, T. Guo, A. Cavalleri, C.W. Siders, F. Rksi, J.A. Squier, B.C. Walker, K.R. Wilson et C.P.J. Barty, Nature **398**, 310 (2002).

[14] F. Schotte, M. Lim, T.A. Jackson, A.V. Smirnov, J. Soman, J.S. Olson, G.N. Philips, M. Wulff et P.A. Anfinrud, Science **300**, 1944 (2003).

[15] P.H. Bucksbaum et R. Merlin, Solid State Commun. **111**, 535 (1999).

[16] P.G. O'Shea et H.P. Freund, Science **292**, 1853 (2001).

[17] T. Osipov, C.L. Cocke, M.H. Prior, A. Landers, Th. Weber, O. Jagutzi, L. Schmidt, H. Schmidt-Böcking et R. Dörner, Phys. Rev. Lett. **90**, 233002 (2003).

[18] D. Zajfman, T. Graber, E.P. Kanter et Z. Vager, Phys. Rev. A **46**, 194 (1992).

[19] Z. Vager, E.P. Kanter, G. Both, P.J. Cooney, A. Faibis, W. Koenig, B.J. Zabransky et D. Zajfman, Phys. Rev. Lett. **57**, 2793 (1986).

[20] D. Strickland et G. Mourou, Opt. Comm. **56**, 219 (1985).

[21] M.V. Ammosov, N.B. Delone et V.P. Krainov, Sov. Phys. JETP **64**, 1191 (1986).

[22] M. Ferray, A L'Huillier, X.F Li, L.A. Lompré, G. Mainfray et C. Manus, J. Phys. B **21**, L31 (1988).

[23] D.N. Fittinghoff, P.R. Bolton, B. Chang et K.C. Kulander, Phys. Rev. Lett. **69**, 2642 (1992).

[24] U. Mohideen, M.H. Sher, H.W.K. Tom, G.D. Aumiller, O.R. Wood, R.R. Freeman, J. Boker et P.H. Bucksbaum, Phys. Rev. Lett. **71**, 509 (1993).

[25] P.B. Corkum, Phys. Rev. Lett. **71**, 1994 (1993).

[26] P. Dietrich, N.H. Burnett, M. Yu Ivanov et P.B Corkum, Phys. Rev. A **50**, 3585 (1994).

[27] P.B. Corkum, N.H. Burnett et M.Yu Ivanov, Opt. Lett. **19**, 1870 (1994).

[28**]** M. Drescher, M. Hentschel, R. Kienberger, G. Tempea, C. Spielmann, G.A. Reider, P.B. Corkum et F. Krausz, Science **291**, 1923 (2001).

[29] The Economist, 26 février 2004.

[30] A. Zavriyev, P.H. Bucksbaum, H.G. Muller et D.W. Schumacher, Phys. Rev. A **42**, R5500 (1990).

[31] K. Codling, L.J. Frasinski et P.A. Hatherly, J. Phys. B **22**, L321 (1989).

[32] A.D. Bandrauk et M.L. Sink, J. Chem. Phys. **74**, 1110 (1981).

[33] T. Seideman, M. Yu Ivanov et P.B. Corkum, Phys. Rev. Lett. **75**, 2819 (1995).

[34] T. Zuo et A. D. Bandrauk, Phys. Rev. A **52**, R2511 (1995).

[35] P. Dietrich, M. Yu Ivanov, F.A. Ilkov et P.B. Corkum, Phys. Rev. Lett. **77**, 4150 (1996).

[36] H. Stapelfeldt, H. Sakai, E. Constant et P.B. Corkum, Phys. Rev. A **55**, R3319 (1997).

[37] S. Chelkowski, P. B. Corkum et A. D. Bandrauk, Phys. Rev. Lett. **82**, 3416 (1999).

[38] A. D. Bandrauk et S. Chelkowski, Phys. Rev. Lett. **87**, 273004 (2001)

[39] M. Nisoli, S. De Silvestri et O. Svelto, Appl. Phys. Lett. **68**, 2793, (1996).

[40] M. Nisoli, S. De Silvestri, O. Svelto, R. Szipöcs, K. Ferencz, Ch. Spielman, S. Sartania et F. Krausz, Opt. Lett. **22**, 522 (1997).

[41] H. Niikura, F. Légaré, R. Hasbani, A.D. Bandrauk, M. Yu Ivanov, D.M. Villeneuve et P.B. Corkum, Nature **417**, 917 (2002).

[42] H. Niikura, F. Légaré, R. Hasbani, M. Yu Ivanov, D.M. Villeneuve et P.B. Corkum, Nature **421**, 826 (2003).

[43] F. Légaré, I. V. Litvinyuk, P.W. Dooley, F. Quéré, A.D. Bandrauk, D.M. Villeneuve, and P.B. Corkum, Phys. Rev. Lett. **91**, 093002 (2003).

[44] F. Légaré, K.F. Lee, I.V. Litvinyuk, P.W. Dooley, S.S. Wesolowski, P.R. Bunker, P. Dombi, F. Krausz, A.D. Bandrauk, D.M. Villeneuve et P.B. Corkum, Soumis à Phys. Rev. Lett. (2004).

[45] J. Allen et J.H. Eberly, Optical Resonance and Two-Level Atoms, Wiley, New York, 1975.

[46] F.T. Hioe et C.E. Carroll, J. Opt. Soc. Am. B, **3**, 497 (1984).

[47] C.E. Carroll et F.T. Hioe, Phys. Rev. A **36**, 724 (1987).

[48] J.R. Kuklinski, U. Gaubatz, F.T. Hioe et K. Bergmann, Phys. Rev. A **40**, 6741 (1989).

[49] F. Légaré, S. Chelkowski et A.D. Bandrauk, J. Raman Spectrosc. **31**, 15 (2000).

[50] S. Chelkowski, A.D. Bandrauk et P.B. Corkum, Phys. Rev. Lett. **65**, 2355 (1990).

[51] S. Chelkowski et G. Gibson, Phys. Rev. A **52**, R3417 (1995).

[52] S. Chelkowski et A.D. Bandrauk, J. Raman Spectroscop. **28**, 459 (1997).

[53] S. Schiemann, A. Kuhn, S. Steuerwald et K. Bergmann, Phys. Rev. Lett. **71**, 3637 (1993).

[54] J. Karczmarek, J. Wright, P. Corkum et M. Yu Ivanov, Phys. Rev. Lett. **82**, 3420 (1999).

[55] D.M. Villeneuve, S.A. Aseyev, P. Dietrich, M. Spanner, M. Yu Ivanov et P.B. Corkum, Phys. Rev. Lett. **85**, 542 (2000).

[56] F. Légaré, S. Chelkowski et A.D. Bandrauk, Chem. Phys. Lett. **329**, 469 (2000).

[57] K. Bergmann, H. Theuer et B.W. Shore, Rev. Mod. Phys. **70**, 1003 (1998).

[58] L.V. Hau, S.E. Harris, Z. Dutton et C.H. Behroozi, Nature **397**, 594 (1999).

[59] A.M. Weiner et D. E. Leaird, Opt. Let. **15**, 51 (1990).

[60] T. Brixner et G. Gerber, Opt. Lett. **26**, 557 (2001).

[61] R. S. Judson et H. Rabitz, Phys. Rev. Lett. **68**, 1500 (1992).

[62] A. Assion, T. Baumert, M. Bergt, T. Brixner, B. Kiefer, V. Seyfried, M. Strehle et G. Gerber, Sience **282**, 919 (1998).

[63] R.J. Levis, G.M. Menkir et H. Rabitz, Science **292**, 709 (2001).

[64] S.P. Shah, D.J. Tannor et S.A. Rice, Phys. Rev. A **66**, 033405 (2002).

[65] F. Légaré, Phys. Rev. A **68**, 063403 (2003).

1 Introduction

By controlling the time dependent electric field of a laser pulse (amplitude and phase), one can control various processes in molecules [1, 2]. One of the routes relies on controlling population transfer using appropriate interference between quantum pathways. The efficiency of the control is determined by the ability to make this population transfer effective and selective. The simplest example for population inversion is the two level system. By amplitude control, called a π pulse, complete population inversion is achievable [3]. Another scheme relies on chirp (the time derivitative of the phase) where complete population transfer can be achieved by adiabatic passage, sweeping the frequency slowly across a resonance. This technique has been used for vibrational excitation of heteronuclear molecules [4, 5] and electronic excitation [6]. Recently, Rickes et al. have proposed to replace phase modulation by an ac Stark shift [7].

For homonuclear molecules, where one-photon absorption within the same electronic state is forbidden by symmetry, the Raman effect has been used for population transfer between ro-vibrational states. The three level Λ system is the basic model for such a laser control scheme. Two different approaches have been proposed for population inversion in Λ systems, STIRAP [8] (Stimulated Raman Adiabatic Passage) and CARP [9, 10] (Chirped Adiabatic Raman Passage). The first is resonant whereas the second can be resonant or non-resonant. STIRAP is based on a counterintuitive sequence of two laser pulses (with pump pulse preceding the stokes pulse), whereas CARP is achieved by slowly sweeping the frequency difference of a combination of two laser pulses across the anharmonicity of a ro-vibrational ladder. Recently, this idea has been used (and predicted) for the dissociation of diatomics by climbing the J, M_J ladder [11] and aligning excited vibrational states [12, 13].

Current understanding of all these techniques of population inversion using coherent laser source applies to systems with non-degenerate quantum states, and with spacing between the final states large compared to the Rabi frequencies. In this paper, we consider the case of a degenerate V systems and the possibility of controlling into which of the two degenerate upper states the population will be transferred. Recently, Shah et al. have shown that controllability in such system is not possible [14] if there is no additional level. If the system has at least four levels and:

$$\frac{\mu_{12}}{\mu_{24}} \neq \frac{\mu_{13}}{\mu_{34}}, \tag{1}$$

then the control is possible. μ_{ij} are the transition dipole moments between states i and j. This system is represented in Fig. 1. In this paper, two simple schemes based on chirp and induced Stark shifts are presented. Full population inversion from level 1 to level 2 (or 3) will be demon-

strated by numerical simulation of the 4 level time-dependent Schroedinger equation and the efficiency of the process is explained using the dressed state representation [15, 16]. The key idea is that the fourth level can break the degeneracy of the levels. Strong non-resonant fields allow the energy shift to be large.

2 Description of the system and dressed state representation

The time-dependent Schroedinger equation for the system illustrated in Fig. 1 is written as follow:

$$i\hbar\frac{\partial}{\partial t}\begin{bmatrix} a_1(t) \\ a_2(t) \\ a_3(t) \\ a_4(t) \end{bmatrix} = \begin{bmatrix} E_1 & V_{12}(t) & V_{13}(t) & 0 \\ V_{12}(t) & E_2 & 0 & V_{24}(t) \\ V_{13}(t) & 0 & E_3 & V_{34}(t) \\ 0 & V_{24}(t) & V_{34}(t) & E_4 \end{bmatrix} \begin{bmatrix} a_1(t) \\ a_2(t) \\ a_3(t) \\ a_4(t) \end{bmatrix}, \tag{2}$$

with $V_{ij} = \mu_{ij}\mathcal{E}(t)$. μ_{ij} are the dipole matrix elements. The time dependent coefficients $a_i(t)$ are calculated using the Split Operator technique [17]. The time steps used in the integration of Eq. (2) are 1 a.u. which correspond to 0.0242 fs. The level 4 may represent a manifold of states with energies close to each other in comparison with the spacing between the level 2, 3 and the manifold. In our model, $E_1 = 0$, $E_2 = E_3 = 0.25$ a.u. and $E_4 = 0.55$ a.u. (1 a.u. = 27.21 eV).

The electric field used for population inversion to level 2 (or 3) is the combination of an intense non-resonant laser pulse which Stark shifts the energy of the levels and a resonant laser pulse with the frequency chirped across the new Stark-shifted energies. The electric field is written as follows:

$$\mathcal{E}(t) = \mathcal{E}_{nr}(t)\cos\left(\omega_{nr}t\right) + \mathcal{E}_r(t)\cos\left(\omega_r t + \frac{1}{2}\beta t^2\right), \tag{3}$$

nr stands for the non-resonant and r for the resonant laser pulse. $\mathcal{E}_{nr,r}(t)$ are the electric field envelope. The frequency of the non-resonant laser pulse, ω_{nr}, corresponds to wavelength of 800 nm (Titanium sapphire). β is the chirp rate of the resonant pulse.

Before presenting results on exact numerical simulations, let describe the physics of the proposed control schemes. First, the effect of the non-resonant laser pulse on the system can be included using perturbation theory. For levels 1 and 4, the energies are:

$$e_1 = E_1 - \frac{\mathcal{E}_{nr}^2}{4}\sum_{\pm}\left(\frac{\mu_{13}^2}{E_3 - E_1 \pm \hbar\omega_{nr}} + \frac{\mu_{12}^2}{E_2 - E_1 \pm \hbar\omega_{nr}}\right), \tag{4}$$

$$e_4 = E_4 - \frac{\mathcal{E}_{nr}^2}{4} \sum_{\pm} \left(\frac{\mu_{24}^2}{E_4 - E_2 \pm \hbar\omega_{nr}} + \frac{\mu_{34}^2}{E_4 - E_3 \pm \hbar\omega_{nr}} \right). \tag{5}$$

For levels 2 and 3, the non resonant coupling to the levels 1 and 4 yields the following energies:

$$e_i = E_i - \frac{\mathcal{E}_{nr}^2}{4} \alpha_{ii}, \tag{6}$$

with:

$$\alpha_{ii} = \sum_{\pm} \left(\frac{-\mu_{i1}^2}{E_i - E_1 \pm \hbar\omega_{nr}} + \frac{\mu_{i4}^2}{E_4 - E_i \pm \hbar\omega_{nr}} \right). \tag{7}$$

Second, resonant Raman coupling between shifted levels has to be included exactly. The matrix element for such coupling is, since $E_2 = E_3 = E_{int}$:

$$V_{23} = -\frac{\mathcal{E}_{nr}^2}{4} \sum_{\pm} \left(\frac{\mu_{24}\mu_{34}}{E_4 - E_{int} \pm \hbar\omega_{nr}} - \frac{\mu_{12}\mu_{13}}{E_{int} - E_1 \pm \hbar\omega_{nr}} \right) = -\frac{\mathcal{E}_{nr}^2}{4} \alpha_{23}. \tag{8}$$

Thus, the matrix in Eq.(2) can be reduced to a 3x3 matrix for levels 1-3, with non-resonant level 4 adiabatically eliminated:

$$\begin{aligned} i\hbar \frac{\partial}{\partial t} \begin{bmatrix} a_1(t) \\ a_2(t) \\ a_3(t) \end{bmatrix} &= \left(\begin{bmatrix} E_1 & V_{12}(t) & V_{13}(t) \\ V_{12}(t) & E_2 & 0 \\ V_{13}(t) & 0 & E_3 \end{bmatrix} - \frac{\mathcal{E}_{nr}(t)^2}{4} \begin{bmatrix} \alpha_{11} & 0 & 0 \\ 0 & \alpha_{22} & \alpha_{23} \\ 0 & \alpha_{23} & \alpha_{33} \end{bmatrix} \right) \begin{bmatrix} a_1(t) \\ a_2(t) \\ a_3(t) \end{bmatrix} \\ &= \begin{bmatrix} e_1 & V_{12}(t) & V_{13}(t) \\ V_{12}(t) & e_2 & V_{23}(t) \\ V_{13}(t) & V_{23}(t) & e_3 \end{bmatrix} \begin{bmatrix} a_1(t) \\ a_2(t) \\ a_3(t) \end{bmatrix}. \end{aligned} \tag{9}$$

In Eq.(9), the resonant couplings are in the first matrix, and the non-resonant Stark shifts and Raman coupling are in the second matrix. The Raman coupling $V_{23}(t)$ gives two new Stark shifted states. These energies are:

$$e_{\pm} = \frac{e_2 + e_3}{2} \pm \sqrt{(e_2 - e_3)^2 + 4V_{23}^2}. \tag{10}$$

The eigenvectors associated with e_+ and e_- are:

$$|e_+\rangle = \cos(\theta/2)|e_2\rangle + \sin(\theta/2)|e_3\rangle, \tag{11}$$

$$|e_-\rangle = -\sin(\theta/2)|e_2\rangle + \cos(\theta/2)|e_3\rangle, \tag{12}$$

with:

$$\tan\theta = 2\frac{\alpha_{23}}{\alpha_{22}-\alpha_{33}} \quad (13)$$

The field free eigenvectors $|E_i\rangle$ are close to the Stark shifted states $|e_i\rangle$ because of the nature of the non-resonant coupling. Note that $\tan\theta$ is *independent of the non-resonant field and is not changed after the field is turned off.* In order to understand our control scheme, we use the dressed state representation. The dressed state matrix in the rotating wave approximation is:

$$\begin{bmatrix} \Delta_1(t) & \frac{1}{2}\Omega_{1-}(t) & \frac{1}{2}\Omega_{1+}(t) \\ \frac{1}{2}\Omega_{1-}(t) & e_- & 0 \\ \frac{1}{2}\Omega_{1+}(t) & 0 & e_+ \end{bmatrix}, \quad (14)$$

with $\Omega_{1\pm} = \mu_{1\pm}\mathcal{E}_r(t)$, $\Delta_1(t) = e_1 + \hbar\omega_r(t)$ and $\omega_r(t) = \omega_r + \beta t$. $\mu_{1\pm}$ are calculated using Eqs. (10) to (12). The diagonalization of the matrix gives the time dependent dressed states. Two schemes for efficient population transfer to these levels will be presented.

2.1 Scheme 1

The first scheme applies when $|\alpha_{33} - \alpha_{22}| \gg |\alpha_{23}|$. When such condition applies, the angle θ is close to zero and the Stark-shifted eigenvectors $|e_+\rangle$ and $|e_-\rangle$ are close to the field free states $|E_2\rangle$ and $|E_3\rangle$. Since θ is independent of the non-resonant field intensity, it is better to use higher non-resonant field in order to increase the energy splitting between $|e_+\rangle$ and $|e_-\rangle$ and thus matke it easier for the resonant field to distinguish the two Stark-shifted states energitically. Larger splitting also allows one to increase the chirp rate (and the resonant field) whole maintaining the adiabatic passage. Turning off the non-resonant field afterwards does not change the population transferred into the field-free degenerate states.

The dressed state representation associated with this scheme is presented in Fig.2 (a) and (b). In Fig.2 (a), the inversion of the population is from level 1 to level $|e_+\rangle$ ($\approx |E_2\rangle$) and in Fig.2 (b) from level 1 to level $|e_-\rangle$ ($\approx |E_3\rangle$). The non-resonant laser pulse for this control scheme has a plateau envelope and the resonant pulse has a Gaussian envelope of 20 ps (FWHM) in the intensity profile. If the angle θ is far from zero, then this control scheme cannot be uses. For example, if $|\alpha_{33} - \alpha_{22}| \ll |\alpha_{23}|$, then $|\theta| \approx \frac{\pi}{2}$ and the new states $|e_+\rangle$ and $|e_-\rangle$ are an equal superposition of the original states 2 and 3. Then, in order to achieve control, a different scheme can be used.

2.2 Scheme 2

The second scheme is completely general when condition of Eq. (1) applies. The example that will be demonstrated in this paper is for $|\alpha_{33} - \alpha_{22}| \ll |\alpha_{23}|$. Nevertheless, the general condition for complete population transfer to any target state will be given. Note that in the limit $|\alpha_{33} - \alpha_{22}| \ll |\alpha_{23}|$, $|e_+\rangle$ and $|e_-\rangle$ are almost equal superpositions of $|E_2\rangle$ and $|E_3\rangle$.

Compared with the first scheme, instead of sweeping only across $|e_+\rangle$ or $|e_-\rangle$, the frequency of the resonant field is swept across both states. The non-resonant pulse has now a Gaussian envelope of 20 ps (FWHM) in the intensity profile, the same as the resonant pulse. In Fig. 3, the dressed state representation for this scheme is shown. Population starts in the level $|E_1\rangle$, and the adiabatic evolution of the corresponding dressed state is shown as path Γ_1. However, if the chirp rate is not too slow, a non-adiabatic transition at the avoided crossing makes a part of the population follow the path Γ_2. The phase difference between these two pathways [16, 18] controls population transfer at the end of the pulse. The phase difference is given by the following equation:

$$\Delta\phi = \int_{t_1}^{\infty} \mid \Gamma_2 - \Gamma_1 \mid dt. \tag{15}$$

The time t_1 is the time where the avoided crossing occurs. The condition for complete control can be established by rewriting the field free eigenvectors as a linear combination of $|e_+\rangle$ and $|e_-\rangle$.

$$|E_2\rangle \approx \cos\frac{\theta}{2}|e_+\rangle - \sin\frac{\theta}{2}|e_-\rangle, \tag{16}$$

$$|E_3\rangle \approx \cos\frac{\theta}{2}|e_+\rangle + \sin\frac{\theta}{2}|e_-\rangle. \tag{17}$$

To control the population, one can launch $\cos^2\frac{\theta}{2}$ into Γ_1 and $\sin^2\frac{\theta}{2}$ into Γ_2, which can be done by tuning the chirp rate (or the field) of the resonant laser pulse. Then, for the phase difference $\Delta\phi = \pi$ one would only populate $|E_2\rangle$, and for $\Delta\phi = 2\pi$ all population will end up in $|E_3\rangle$. The phase difference $\Delta\phi$ is controlled by the intensity or the duration of the non-resonant laser pulse.

3 Results and discussion

3.1 Scheme 1

Without the presence of level 4, it has been demonstrated that the population ratio between level 2 and 3 is given by $\frac{P_2}{P_3} = \frac{{\mu_{12}}^2}{\mu_{13}^2}$ [14, 19]. Adding the fourth level (or a manifold of levels)

allows to control the population transfer. Consider first the case when the condition for scheme 1 are satisfied. The dipole matrix elements are: $\mu_{12} = \mu_{13} = 1$, $\mu_{24} = 2$ and $\mu_{34} = 10$. The dressed state representation is shown in Fig.2 (a) and (b). The intensity of the non-resonant pulse (plateau envelope) is $1 \times 10^{11} W/cm^2$, $2 \times 10^8 W/cm^2$ for the resonant pulse (Gaussian intensity profile with 20 ps FWHM) and the chirp rate $\mid \beta \mid$ is $4.11 \times 10^{-4} eV/ps$. Because $\alpha_{33} - \alpha_{22}$ is much greater than the Raman matrix element $2\alpha_{23}$, $|e_-\rangle \approx |E_3\rangle$ and $|e_+\rangle \approx |E_2\rangle$. Then, by sweeping the resonant frequency across $|e_+\rangle$ or $|e_-\rangle$, efficient population transfer either to level 2 or 3 can be achieved.

In Fig. 4, the results related to Fig. 2 are presented. Virtually full population inversion to any target state (2 or 3) is achieved in Fig.(4). The residual population in level 2 (or 3) for Fig. 4(a) (or (b)) is given by $P_{2(3)} = sin^2\left(\frac{\theta}{2}\right)$ with θ given by Eq. (13). In our case, $\theta = -0.373$ rad and $P_{2(3)} = 3.44 \times 10^{-2}$. The numerical simulation gives $P_3 = 3.51 \times 10^{-2}$ for Fig. 4(a) and $P_2 = 3.42 \times 10^{-2}$ for Fig. 4(b), close to our analytical prediction. Note that the Rabi frequency of the resonant pulse has to be small compared with $|e_+ - e_-|$. With the condition enumerated in the previous paragraph, the ratio between $|e_+ - e_-|$ and the Rabi frequency is approximately 10. Since θ is independent of the intensity of the non-resonant laser pulse, high intensity should be used so large Rabi frequency for the resonant laser pulse can also be used in order to sweep rapidly the frequency of the resonant laser pulse [16], making the process as fast as possible while still satisfying the adiabatic condition.

3.2 Scheme 2

In the case of scheme 2, the dressed state representation is shown in Fig. 3. The dipole matrix elements are: $\mu_{24} = \mu_{34} = 5$, $\mu_{12} = 0.8$ and $\mu_{13} = 1$ and the intensity of the non-resonant pulse (Gaussian intensity profile with 20 ps FWHM) is a control parameter. Tuning the intensity of this pulse changes the phase difference (Eq. (14)) between the two pathways in Fig. 3 and tuning the chirp rate (or the field) of the resonant laser pulse makes the right superposition of the amplitudes launch into pathways Γ_1 and Γ_2. The intensity of the resonant laser pulse is $2 \times 10^8 W/cm^2$ (Gaussian intensity profile with 20 ps FWHM) and the chirp rate β is $-6.61 \times 10^{-4} eV/ps$. Because $\mu_{24} = \mu_{34}$, $|\alpha_{33} - \alpha_{22}|$ is small compared to the Raman coupling $2|\alpha_{23}|$, the angle θ (Eq. (12)) is approximately equal to $-\frac{\pi}{2}$. Then, the eigenvectors given by Eqs. (10) and (11) are: $|e_+\rangle \approx \frac{|E_2\rangle - |E_3\rangle}{\sqrt{2}}$ and $|e_-\rangle \approx \frac{|E_2\rangle + |E_3\rangle}{\sqrt{2}}$. If μ_{12} converge to μ_{13}, then $|e_+\rangle$ approaches more and more a dark state [20] and the control becomes difficult to achieve, see Eq. (1). In our case, the controllability condition is satisfied since $\mu_{12} \neq \mu_{13}$. In the *real world*, the non-equality condition will be always satisfied because two degenerate states have different quantum

numbers, making for example the Clebsh-Gordan coefficients different. Then, by making an appropriate coherent superposition of $|e_-\rangle$ and $|e_+\rangle$, population can be transferred to either level 2 or level 3. In Fig. 5, the numerical results associated with the scheme of Fig.3 are presented. They confirm the validity of the control scheme.

4 Conclusion

From numerical solutions of the time-dependent Schroedinger equation for a four state system, it is shown that population inversion in the presence of degeneracy can be controlled using laser induced Stark shifts. Two schemes have been presented. Both schemes use a combination of two laser pulses, one non-resonant (intense) and another resonant. The intense pulse breaks the degeneracy of the system and the second one is swept (chirped) across the new energies. Completely general formulation requires only the knowledge of the Stark matrix of couplings to the non-resonant laser field: α_{22}, α_{33} and α_{23}. The two cases studied in this paper are $|\alpha_{23}| \ll |\alpha_{33} - \alpha_{22}|$ (Scheme 1) and $|\alpha_{23}| \gg |\alpha_{33} - \alpha_{22}|$ (Scheme 2). Scheme 1 is only efficient when condition (1) applies. The scheme 2 is completely general and the condition for complete inversion to any target state is defined using Eqs.(15) to (17).

The first scheme uses the difference between the coupling of the degenerate states to a manifold of states (the fourth level). Because of the different coupling, these degenerate states move differently in the presence of the intense laser field. By sweeping the resonant frequency across one of the new Stark-shifted states, efficient population inversion can be achieved for any of the two target states.

The second scheme uses the phase difference between the two pathways created by the non-resonant laser pulse. By sweeping the frequency of the resonant photon across these two pathways and by launching $\cos^2\frac{\theta}{2}$ into Γ_1 and $\sin^2\frac{\theta}{2}$ into Γ_2, efficient population inversion can be obtained by tuning the phase difference using the intensity of the non-resonant laser pulse as the control variable.

Coherent control of population inversion in degenerate system is of interest in photochemistry [21]. Often, fragmentation channels are degenerate [22] and using only resonant laser pulses yields population ratios associated with the dipole moment ratio [14, 19]. In the present model, discrete states are used as compared to multiple or quasidegenerate continua in real systems. The first scheme which uses only Stark shift should be easier to implement experimentally. The scheme 2 is strongly phase dependent, and one can expect that it would be more difficult to implement in practice, especially for systems with continua where couplings are energy de-

pendent. On the other hand, the scheme 2 will be efficient in atomic systems, where a similar interference scheme has been used to control the atomic population inversion [18]. Extension to molecular degenerate systems will require further numerical simulations for establishing the limitation of this control scheme which is based on differentiating the level via their Stark shifts, which is essential for controlling population transfer in system where the target states are degenerate.

Acknowledgements

F.L thanks NSERC and FQRNT for grants supporting the present research. Also, F.L. thanks Dr. A.D. Bandrauk at Université de Sherbrooke, B. Sussman, Dr. M. Yu. Ivanov and Dr. P.B. Corkum at NRC Ottawa for stimulating discussions.

References

[1] M. Shapiro, P. Brumer, Rep. Prog. Phys. **66**, 859 (2003).

[2] A.D. Bandrauk, Y. Fujimura, R.J. Gordon, Laser Control and Manipulation of Molecules, ACS symposium 821 (Washington, 2003)

[3] J. Allen, J.H. Eberly, Optical Resonance and Two-Level Atoms (Wiley, New York, 1975).

[4] S. Chelkowski, A.D. Bandrauk, P.B. Corkum, Phys. Rev. Lett. **65**, 2355 (1990).

[5] V.D. Kleiman, S.M. Arrivo, J.S. Mellinger, E.J. Heilweil, Chem. Phys. **233** 207 (1998).

[6] J.C. Cao, C.J. Bardeen, K.R. Wilson, Phys. Rev. Lett. **80**, 1406 (1998).

[7] T. Rickes, L.P. Yatsenko, S. Steuerwald, T. Halfmann, B.W. Shore, K. Bergmann, Phys. Rev. A **113**, 534 (2000).

[8] K. Bergmann, H. Theuer, B.W. Shore, Rev. Mod. Phys. **70**, 1003 (1998).

[9] S. Chelkowski, G. Gibson, Phys. Rev. A **52**, R3417 (1995).

[10] S. Chelkowski, A.D. Bandrauk, J. Raman Spectrosc. **28**, 459 (1997).

[11] D.M. Villeneuve, S.A. Aseyev, P. Dietrich, M. Spanner, M. Yu Ivanov, P.B. Corkum, Phys. Rev. Lett. **85**, 542 (2000).

[12] F. Légaré, S. Chelkowski, A.D. Bandrauk, Chem. Phys. Lett. **329**, 469 (2000).

[13] A.D. Bandrauk, S. Chelkowski, F. Légaré, Recent Research Developments in Raman Spectroscopy, p. 83-104 (Transworld Research Network, India, 2002).

[14] S.P. Shah, D.J. Tannor, S.A. Rice, Phys. Rev. A **66**, 033405 (2002).

[15] A.D. Bandrauk, Molecules in Laser Fields (Marcel Dekker, New York, 1994).

[16] F. Légaré, S. Chelkowski, A.D. Bandrauk, J. Ramam Spectrosc. **31**, 15 (2000).

[17] A.D. Bandrauk, H. Shen, J. Chem. Phys. **99**, 1185 (1993).

[18] D.J. Maas, C.W. Rella, P. Antoine, E.S. Toma, L.D. Noordam, Phys. Rev. A **59**, 1374 (1999).

[19] M.N. Kobrak, S.A. Rice, Phys. Rev. A **57**, 2885 (1998).

[20] P. Král, M. Shapiro, Phys. Rev. A **65**, 043413 (2002).

[21] Z. Chen, M. Shapiro, P. Brumer, Phys. Rev. A **52**, 2225 (1995).

[22] S.S. Brown, R.B. Metz, H. Laine Berghout, F. Fleming Crim, J. Chem. Phys. **105**, 6293 (1996).